Alma Mater Studiorum – Università di Bologna

DOTTORATO DI RICERCA IN

Chimica

Ciclo XXVII

Settore Concorsuale di afferenza: 03/A2

Settore Scientifico disciplinare: CHIM/02

ELECTROCHEMICAL IMAGING OF LIVING CELL METABOLISM: INVESTIGATION ON WARBURG EFFECT IN CANCER

Presentata da: ***Alice Soldà***

Coordinatore Dottorato

Prof. Aldo Roda

Relatori

Dr.ssa Stefania Rapino

Prof. Francesco Paolucci

Dr. Marco Giorgio

Esame Finale Anno 2015

"La conoscenza scientifica non gode di un accesso immediato alla realtà di cui parla.
Non è come aprire gli occhi e constatare che si è fatto giorno."

Albert Einstein

Acknowledgment

First and foremost I want to thank my supervisor, Dr. Stefania Rapino. It has been an honor to be her first Ph.D. student. She introduced me in this amazing field of Bioelectrochemistry. I appreciated all her contributions, her presence and the great ideas: she made my PhD experience productive and stimulating. The joy and enthusiasm she has for her research was contagious and motivational for me, even during tough times in the PhD pursuit. I am also thankful for the excellent example she has provided as a successful woman, friend and professor.

I gratefully acknowledge Prof. Francesco Paolucci (University of Bologna) who gave me the chance to take up my PhD career at University of Bologna and for his precious advises. I am especially grateful for the Italian Chemistry Society (Electrochemistry Division), which made us know during the SCI meeting in Lecce (2011), and the fun group of EMFM Bologna members.

I gratefully acknowledge Prof. Pier Giuseppe Pelicci and Dr. Marco Giorgio (European Institute of Oncology -IEO-) who gave me the great opportunity to work at IEO Campus. I have really appreciated the inspirational discussions with them regarding all the biological claims. I want to thank all the members of the group, which have contributed immensely to my personal and professional time at the Campus. They have been a source of friendship as well as good advice and collaboration. I am especially grateful to Dr. Alessandra Bigi, who made significant contribution in some experiments. The kinetics studies of oncogene expression discussed in this dissertation would not have been possible without the remarkable skills of Dr. Sara Barozzi, who performed the microinjection. I would also like to thank also all the people that work in the Campus Facilities, in particular the Imaging Unit and the Cell Biology/Tissue Culture Unit.

I have appreciated the collaboration and the impressive mathematical skills of Dr. Evangelos Bakalis (Università di Bologna), who designed the new theoretical model by which I treated and discussed the kinetics of enzymatic activity, and I would like to thanks also Prof. Francesco Zerbetto for the helpful and inspirational discussion regarding these experiments.

In regards to the AFM analysis, I thank Prof. Massimo Marcaccio (University of Bologna), which assist me during the measurements and shared with me some of his expert knowledge.

Finally, I gratefully acknowledge the funding sources that made my PhD work possible. I was founded by the triennal FIRC fellowships “Guglielmo Lucatello e Gino Mazzega”.

Preface

Cancer affects all the humankind. It is one of the most leading causes of death worldwide, with approximately 14.1 million new cases and 8.2 million cancer related death in 2012. This trend is projected to rise by about 75% over the next two decades. [World Cancer report 2014]

About 30% of cancer deaths are due to behavioural and dietary risks. Viral or bacterial infections are responsible for up to 20% of cancer deaths, but chronic infections and ageing remain the major risk factors. It is clear that cancer is a generic term for a multiplicity of different diseases that can affect any part of the body. It arises from normal cells that mutate in tumor cell and grow beyond usual boundaries, invading adjoining parts of other organs; the latter process is referred to as metastasis. Metastases are the major cause of death from cancer.

Identification of hexogenous causes, screening protocols, high-risk groups, means of diagnosis, and effective therapies vary across tumor types. An understanding of cancer biology behind each of them is critical to rationally develop designed target therapy and in order to offer effective preventive options. Cancer mortality can be reduced if cases are detected and adequately treated at an early stage. For this reason, it is crucial to improve the early diagnosis and develop new accessible and affordable screening methods for specific target therapies. Emerging evidences demonstrated that there are thousands of point mutations, translocations, amplifications and deletions that may contribute to cancer development, and that the mutational range can differ even among histopathologically identical tumors. Furthermore, it is becoming clear that many oncogenic signalling pathways converge to adapt cancer cell metabolism in order to support their high growth rate and their survival. ***In view of these fundamental discoveries alterations to cellular metabolism should be considered a crucial hallmark of cancer.*** The knowledge of cancer cell metabolism will help to design more efficient treatment strategies both to slow down tumor progression and to improve the response to therapy, resulting in positive clinical outcomes[12].

Emerging evidences indicate that most of the ***cancer cells have an increased glycolytic rate and a detriment of oxidative phosphorylation to support abnormal cell proliferation; this phenomenon is known as aerobic glycolysis or Warburg effect. This switching toward glycolysis implies that cancer tissues metabolize approximately tenfold more glucose to lactate in a given time and the amount of lactate released from cancer tissues is much more greater than the amount from***

normal ones. Therefore, the investigation of the metabolic differences between normal and cancer cells is very important in cancer research with great potential impact on clinical applications.

The aim of this PhD project was to investigate the cellular metabolic alterations at single cell level, by monitoring glucose and lactate, in order to provide a better insight in cancer research.

For this purpose, electrochemical techniques have been applied. The field of electrochemistry is in constant progress and can substantially impact on the future of medical devices. Indeed, there are already several clinical applications that assert the validity of the electrochemical approach in medicine and in medical devices. ***Ad hoc modified enzyme-based electrode biosensors used as probes for Scanning Electrochemical Microscopy (SECM) were employed in this work. Advancements in this technology and its applications in the non-invasive study of cellular metabolism at single cell level were demonstrated.***

The work is mainly divided in three parts:

Part I. Designs, Principles and Methods (chapters 1-7). The first part of the thesis provides a general overview and introduction about the basic knowledge of the project topic. The main aspects about the cellular metabolism and electrochemistry are briefly presented, underlining the importance of *Warburg effect* in cancer research and the potentiality of Scanning Electrochemical Microscopy as a new possible approach for clinical application. In this part the specific issue of the biosensor manufacturing, which are used in combination with SECM for real-time metabolites detection, are addressed. Moreover, the practical protocols for the enzyme-immobilization methods, which were optimized in this work, and their full characterization have been deeply described.

Part II. Case Studies (chapters 8-11). In this part are reported the main in *in vitro* studies that have been done using the optimized enzyme-based electrode biosensors for metabolic investigation on normal and cancer cells. The aim of this second part is not only to show the results obtained during this work, but also to demonstrate the great potential of this technique in real medical and biological fields.

Part III. Conclusions and Future Directions (chapter 12). The last chapter concerns a brief summary of the obtained results, describing the main advantages and disadvantages of the technique. Future technical upgrades to improve the analytical setup are suggested and new biological challenges are proposed.

CONTENTS

PART II CASE STUDIES

APPENDIX

PART I

PRINCIPLES, DESIGNS, AND METHODS

Chapter 1

Cellular Metabolism and Cancer

Abstract

Cellular metabolism is a set of biochemical reactions that take place within the cell. These reactions are turned on and off or sped up and slowed down according to the cell's immediate needs. At any given time, the numerous pathways involved in building up and breaking down cellular components are balanced in a coordinated mode. Reactions involved in energy production are coordinated as well and unbalance in energetic metabolism is typical of many disease states, including cancer. Emerging evidences indicate that cancer cells have an increased glycolytic rate and a detriment of oxidative phosphorylation to support abnormal proliferation.

Key words Energy, Metabolism, Oxidative Phosphorylation, Aerobic Glycolysis, Cancer, Target Therapies

1.1 Background and Historical Overview of Energy Metabolism

1.1.1 Introduction

"In 1986 explorers set out to reach the North Pole by dogsled from Ellesmere Island at latitude 83° north. Their objective was to make the journey without resupply along the way and thus to re-enact the famous expedition by Admiral Robert Peary in 1909. Each of the modern explorers' sleds was huge – 16 feet (5 m) long, and loaded with 1400 pounds (630 kg) of material. Of the two-thirds of a ton on each sled, most was food for people and dogs. Most of the weight of the food, moreover, was required to meet energy needs […] Two people's needs for energy were to be met by the supplies on each sled. The sleds needed to be pulled and pushed over numerous ice ridges 20-60 feet high on the way to the pole. Even during the progress over level ice fields, the

way for the sleds' runners had to be cleared by the explorers often. A trek to the North Pole by dogsled would be immeasurably easier if there were no need for food energy for people and dogs. The need for energy is equally consequential in the natural world. Every species regularly risk their lives to obtain energy, or die because they did not obtain enough. Why do we need energy?" (*Cit. Animal Physiology, 3rd Ed*. 2012)[1].

1.1.2 Energy

All-living organisms are very organized systems. The assembling molecules that compose living organisms are routinely exchanged with molecules present in the external environment, and their assembly is more important than the molecule structures. The second law of thermodynamics, one of the greatest achievements of intellectual history, provides a basic interpretation about the nature of organized systems[1].

"The second law of thermodynamics states that no process is possible in which the sole result is the absorption of heat from a reservoir and its complete conversion into work." It can be also expressed in terms of entropy. *"The entropy of an isolated system increases in the course of a spontaneous change:* $\Delta S_{tot} > 0$*"*[2].

One of its corollaries is the following: order can be conserved or enhanced within the same system only if the latter is not isolated. Therefore, once *energy* gets inside a system, order has to be conserved or even increased.

A broader and simpler definition, often used in biology, is that *energy is the capacity to maintain order*[1]. Without an energy input, the blood might not flow through the circulatory system and the molecule assemblies within cells and tissues would become more disorganized and full of structural defects, losing their biochemical and functional properties. Furthermore, ionic species and electrons would be randomly distributed across the cell membrane, and this electrical randomization might highly interfere with the main cellular functionalities. The living organisms would even die if they loose their inner organization, because order is essential for life[1].

The external chemical energy, such as food and sun, are used by all organisms to carry out the three essential needs: *i)* ***biosynthesis*** of macromolecules (carbohydrates, proteins, lipids and nucleic acids), *ii)* ***maintenance*** of the all processes for supporting the integrity of the main physical functionalities in

living systems (e.g. circulation, respiration, nervous coordination, gut motility and tissue repair), and *iii)* ***generation of external work***, seen as the mechanical forces by which living organisms act on the surrounding environment (e.g. muscle contraction)[1].

1.1.3 Metabolism

Cell metabolism is the entirety of the biochemical reactions through which every living cell acquires energy, channels it into useful functions, and dissipates it[1]. All these thousand reactions are part of particular metabolic pathways that are organized by the presence of enzymes and coenzymes[3]. Enzymes act as selective catalysts, decreasing the activation energies, accelerating the reaction rate and enhancing the specificity of the metabolic pathways, to digest and synthesize any kind of molecule present in living systems[3]. They also turn the reactions in response to environmental changes. Most of the enzymes are proteins that may employ organic and inorganic cofactors to assist the catalysis. Coenzymes act as temporary group-transfer intermediates, carrying different functional groups between the reactions. One central coenzyme is adenosine triphosphate (ATP), composed by an adenine ring, a ribose sugar and three-phosphate groups[3].

ATP

Usually, a cellular system is far away from the equilibrium and it has a relative high *Gibbs free Energy*, hence, it is able to do work[4]. The energy ($\Delta G°$) released by cleaving a phosphate unit from ATP to ADP at standard condition is equal to *-30.5 kJ/mol = -7.3 kcal/mol*[5]. Living cells maintain the ATP concentration fivefold higher than the ADP one. This displacement from equilibrium means that the cell has a large amount of energy stored and that can come out from the hydrolysis of ATP[4].

NAD^+/NADH

Other important coenzymes are nicotinamide adenine dinucleotide (NAD^+) and nicotinamide adenine dinucleotide phosphate ($NADP^+$) that act as hydrogen acceptors. They mainly act in combination with dehydrogenase, enzymes that oxidase substrates and reduce NAD^+ into NADH (see catabolic reactions) or $NADP^+$ into NADPH form (see anabolic reactions). As a consequence they are employed as hydrogen donors for any kind of reductases[6]. Metabolism consists of two subsets of processes: *catabolic processes* that break down large organic molecules and oxidize food molecules to provide energy, and *anabolic processes* that use the energy

released by catabolism to synthesize complex molecules that include all the constituents of living cells, such as membranes, chromosomes, enzymes, antibodies, neurotransmitters and hormones[1]. ATP acts as a bridge between catabolism and anabolism[3].

Catabolism

Catabolism involves three basic stages[4]: *stage 1*. Digestion of large organic molecules (proteins, polysaccharides and lipids) into their smaller components (amino acids, simple sugars as glucose, fatty acids and glycerol), this happen outside the cells. *Stage 2.* Absorption of these components by cells and their conversion in acetyl coenzyme A (acetyl CoA) accompanied by a production of a limited amount of ATP and NADH. The major breakdown route is glycolysis, an 11-steps enzymatic reaction, where sugars, such as glucose and fructose, are converted into pyruvate and some molecules of ATP are generated. *Stage 3*. Into the mitochondria Acetyl CoA is oxidised by using oxygen as electron acceptor into water and carbon dioxide, through the Krebs Cycle, also known as the tricarboxylic acid cycle (TCA cycle). The electrons, coming out from TCA cycle, flux through electron transport chain, creating a proton gradient that drives the ATP synthesis, which is stored by reducing the coenzyme NAD^+ into NADH.

Anabolism

Anabolism involves three basic stages as well[4]: *stage 1*. Precursors production (e.g. amino acids, monosaccharides and nucleotides). *Stage 2.* Activation of these precursors into reactive forms using the high chemical energy released when ATP is turned in ADP. *Stage 3*. Assembly of these precursors into complex molecules (e.g. peptides, proteins, polysaccharides, lipids and nucleic acids). Different enzymatic pathways constitute these processes and are often allocated in different part of the cell, but at the same time they are in some way intimately linked to allow organisms to grow and reproduce, maintain their structures and respond to the external stimuli.

1.1.4 Energy Processing

A ***quantitative*** understanding of the rules, which regulate this kind of energy conversion, is crucial for a qualitative and quantitative characterization of the relative advantages linked to the different modes of energy processing. *Metabolic rate* is the way in which all living organisms transform nutrients into both thermal energy and biological work, required for providing life. These transformations involve the interconversion of two forms of chemical

energy: the redox potential difference between the donor and acceptor couples in the electron transport chain and the ADP phosphorylation potential[7]. The coupling between the electron transfer chain and ADP phosphorylation could involve electrons, in case of *oxidative phosphorylation* (OxPhos), and chemical groups in *glycolytic* processes.

OxPhos

"*OxPhos is a mode of energy processing where cell carries out the ADP phosphorylation during the* ***oxygen-dependent*** *transmission of electrons down the respiratory chain. This reaction produces NADH, which fuels OxPhos to maximize ATP production with* ***minimal production of lactate***"[7].

The respiratory chain or electron transfer chain consists of four multimeric enzyme complexes (Complex I, II, III, IV) positioned along the mitochondrial membrane. Electrons from the reduced forms of NADH and FADH enter in the chain and reduce complex I and II, respectively. *Coenzyme Q10* (or ubiquinone) is an electron carrier present in the inner mitochondrial membrane that accepts an electron from either complex I or II and donates it to complex III. *Cytochrome c*, another electron carrier, present in the mitochondrial intermembrane space, accepts an electron from complex III and donates it to complex IV. The latter one donates electrons to molecular oxygen, which results in the formation of water. During the electron flow, complex I, III and IV pump the protons from the mitochondrial internal matrix toward the intermembrane space generating an electrochemical gradient across the mitochondrial inner membrane. Finally complex V employs the energy of the electrochemical gradient to generate ATP from ADP[8]. This pathway is a high efficient way of releasing energy; 38 molecules of ATP for every glucose molecule used, in comparison to alternative fermentation processes such as anaerobic glycolysis, which produces only 2 molecules of ATP per glucose[9].

Glycolysis

In general glycolysis (lysis of glucose) first requires the conversion of glucose to pyruvate and then to lactate. In most cells glycolysis is inhibited by the presence of oxygen, which allows the mitochondria to oxide pyruvate to water and carbon dioxide. This inhibition was termed the '*Pasteur effect'*, after Louis Pasteur demonstrated that glucose flux was reduced by O_2 presence in fermentative organisms. He first observed that aerating yeasted broth causes yeast cell growth to increase, while conversely, fermentation rate decreases[10].

Anaerobic Glycolysis

"*Anaerobic glycolysis (glycolysis **suppressed by oxygen**) describes another mode of energy generation when oxygen is supply limited. In this process, cells direct the pyruvate generated by glycolysis away from the mitochondrial OxPhos pathway. This is achieved by **generating lactate**. This process does not occur within the mitochondria, but in the liquid protoplasm of the cell. This generation of lactate allows glycolysis to continue, but results in a lowered ATP production rate. The rate-limiting factors for net ATP production are the efficiencies of glucose delivery and lactate removal*"[7].

The amount of ATP production is small, around 5% of total ATP generated from OxPhos, but at the same time the speed of the reaction is very fast, around 100 times more than OxPhos.

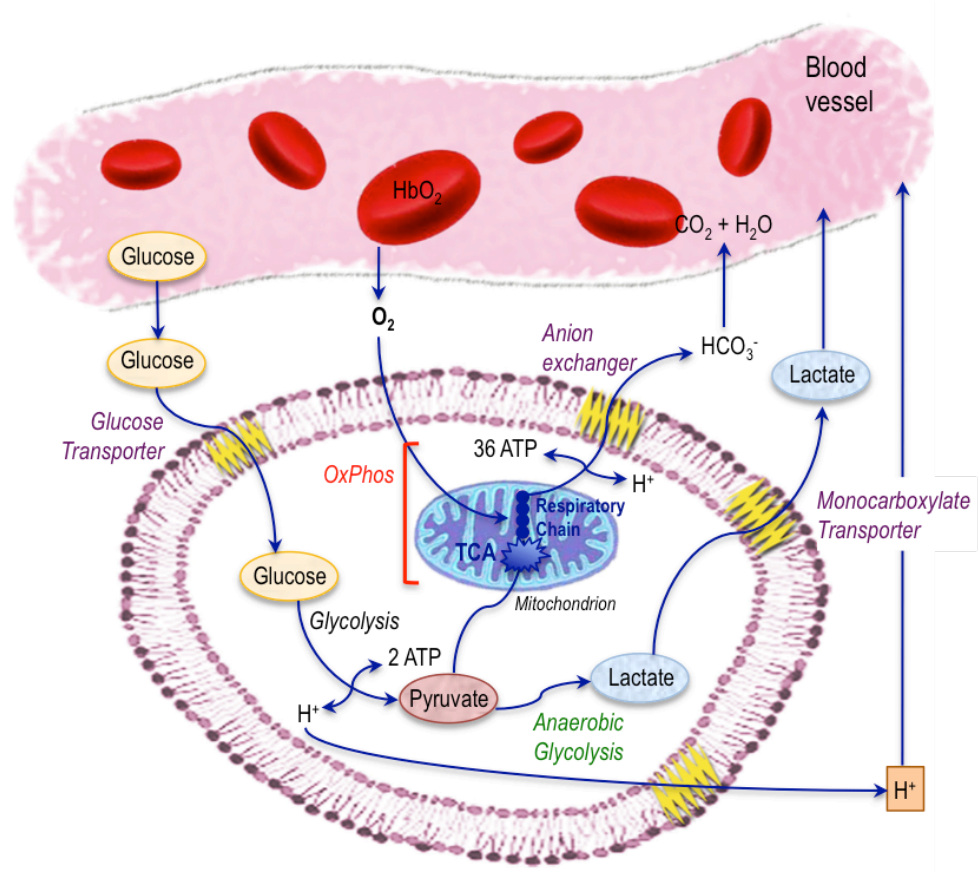

Figure 1. *Glucose Metabolism in living cells*. Blood delivers glucose and oxygen (on haemoglobin) to tissue, where they reach cells by diffusion. Glucose is taken up inside the cell by the use of specific transporters, and it is metabolized in pyruvate by glycolysis, generating 2 ATP per glucose. In the presence of O_2, the pyruvate enters in the mitochondria and is oxidized to CO_2 and H_2O, generating 36 ATP per glucose. In absence of O_2, pyruvate is reduced to lactate, which is exported out of the cell. Both processes produce H^+, which cause acidification of the extracellular space (adapted from *Nature Reviews Cancer*, 2004)[9].

Aerobic Glycolysis

"*Aerobic glycolysis (glycolysis not suppressed by oxygen) refers to the conversion of glucose to pyruvate and then to lactate regardless of whether oxygen is present or not. This process is also localized in the liquid cytoplasm. This property is shared by normal proliferative tissue*"[7].

It is worth to underline that the terms aerobic and anaerobic glycolysis are imprecise, although they have been used extensively in the literature. Both type of glycolysis follow substantially the same pathway, the terms aerobic and anaerobic are used to emphasize the difference with respect to their dependence on oxygen.

All cells use both pathways to generate energy, but they preferentially rely on OxPhos, switching to glycolysis only in case of oxygen depletion. Marathon runners and other athletes benefit from this shift. However, increased aerobic glycolysis is uniquely observed in most cancer cells[7].

1.2 Altered Metabolism in Cancer

1.2.1 Introduction

The link between altered metabolism and cancer is not new: since the early period of cancer biology research, many metabolic alterations as a common feature of tumor tissues were described[11] (e.g. the *Warburg Effect*; discussed in Chapter 2). Over the past 25 years, the progress in cancer research has revealed that the main characteristics of cancer cells phenotypes resulted from numerous and heterogeneous mutations, which alter critical regulatory processes (signalling pathways). Now it is becoming clear that many oncogenic signalling pathways converge to adapt cancer cell metabolism in order to support their high growth rate and their survival in the tumor environment. DNA sequencing data suggest that the mutations in genes controlling metabolism and leading to carcinogenesis are even more numerous and heterogeneous than previously thought. Some of these metabolic alterations seem to be strongly linked to malignant tumors[11]. In view of these fundamental discoveries, alterations to cellular metabolism should be considered a crucial hallmark of cancer.

Clinical data about tumor metabolic profiles will be highly required in future to determine which metabolic alterations are prevalent in specific types of cancer. This knowledge will help to design more efficient treatment strategies

both to slow down tumor progression and to improve the response to therapy, resulting in positive clinical outcomes[12].

1.2.2 *Metabolic Adaptations to the Micro-environment*

In addition to the genetic changes, the altered tumor microenvironment has a major role in altering many metabolic signalling pathways of cancer cells. Tumors vasculature is structurally and functionally abnormal; there is spatial and temporal heterogeneity in oxygenation, pH and unusual concentrations of glucose and many other metabolites, such as glutamine and lactate [11].

These extreme stressful conditions cause several cellular feedbacks that might contribute to alter the metabolic phenotype of tumors and can influence their progression[11]. For example normal cells commonly do not take up nutrients from the environment unless stimulated by grow factors, while cancer cell overcome this growth factor dependence by acquiring genetic mutations and functionally reprogramming metabolic signalling pathways to meet needs during the process of tumor progression[12].

Many of these transformed cells achieve the majority of the required energy from aerobic glycolysis, converting most of the incoming glucose to lactate rather than metabolize it by OxPhos into the mitochondria[11]. Despite ATP production by glycolysis can be more rapid than by OxPhos, it is much less efficient in terms of ATP generated per unit of glucose consumed. This shift explains why cancer cells show an abnormal high rate of glucose uptake in order to meet the three crucial requirements: *i)* larger energy production, *ii)* sufficient macromolecular biosynthesis, seen as building blocks synthesis and *iii)* maintenance of redox balance[11]. The reasons why cancer cells prefer a less efficient metabolism, at least in term of ATP productions, is still unknown and an argument of discussion. However, two possible explanations are suggested: *i)* a consequence of mitochondrial damages or *ii)* an adaptive response to tumor hypoxia. Nowadays there are many studies that belie the first hypothesis, rather demonstrating the key role of mitochondria function in tumors[13]. Concerning these studies, it was observed that even in glycolytic tumors OxPhos is not completely shut down. It is clear from clinical data, as well as *in vitro* and *in vivo* experimental studies, that cancer cells are capable of using alternative fuel sources, such as amino acids, fatty acids and even lactate to proliferate, leaving glucose for energy production[11].

Hypoxia

Regarding the second hypothesis, even if it was observed that hypoxia might influence several molecular pathways involved in cellular metabolism, many cancer cells appear to use glycolytic metabolism even before exposure to hypoxic conditions. For example, lung cancer cells exhibit aerobic glycolysis even when they are exposed to oxygen during cancer progression[14]. Thus, although tumor hypoxia is clearly important for many aspects of cancer biology, causing an increase of the glycolytic capacity and a decrease of the mitochondrial respiration, the available evidence suggests that it is a late-occurring event that may not be a major contributor in the glycolytic switching of cancer cells. Only extreme hypoxia ($[O_2] < 0.02\%$) causes endoplasmic reticulum (ER) stress and activates the unfolding protein response, which provides a further adaptive mechanism that allows cancer cells to survive under these adverse metabolic conditions[11-14].

1.2.3 *Importance of Studying Cancer Metabolism*

For all these reasons it is worth to underline that the relationship between tumor microenvironment and cancer cell metabolism is not a simple cause-and-effect one, in which metabolism is a self-correcting system where a set of enzymes enables the cell to respond to changing bioenergetics demands. Instead, there is a complex, dynamic and regulated relationship between metabolism and cancer microenvironment[14].

Metabolites concentrations are governed by their supply by the vasculature and the demand of the tissue. Metabolism is programmed every time to meet the requirements for cell proliferation or to meet the specific needs of each differentiated tissue; as a consequence these changes have profound effect on the environment surrounding the cells. Metabolic adaptations are needed to give cells the ability to drive cell nutrient uptake and coordinately to regulate metabolic pathways in order to support an altered proliferation[14].

This aspect emphasizes the importance of studying metabolic regulation both *in vitro* and *in vivo* using appropriate model systems, as well as the need for more sophisticated measurements of cell metabolism and microenvironment of human tumors. Efforts to model human metabolism and select rational target combinations are on going. Complementing these models with a more complete understanding of biochemical pathway in cancer cells will help to determine the best targets for possible intervention[13].

1.3 Approaches for Targeting Cancer Cell Metabolism

1.3.1 Introduction

As before mentioned, cancer cells exhibit alterations of a number of metabolic pathways in order to support their high rates of proliferation. This provides the cells with the ability to continually generate ATP, to support cell survival, and crucial biosynthetic precursors for cell growth. Since most of cancer cells are dependent on these metabolic changes, altered pathways represent a very attractive therapeutic target[13]. The common assumption that a therapeutic window obtained by using particular anticancer drugs, which can act on these alterations, is due to the more rapid proliferation of cancer cells is not necessarily true. Cancer cells have a cell cycle time that is estimated to be 30-40 hours and may proliferate as frequently as every 10 hours under optimal tissue culture conditions, but most cancer cells proliferate more slowly *in vivo*[13]. Metabolism is a complex network of reactions and there are several different metabolic programmes among all cancer cells; every type of cancer follows a specific altered route. This may explain why chemotherapies acting on metabolism are efficacious in some cancers but not in others, despite the need for all cancer cell to synthesize the same macromolecules[13]. It is worth to underline that the same pathways are required in normal proliferating cells. Therefore, a better understanding of how metabolism is altered in specific cancer will provide an insight into which enzymes represent promising targets, in order to identify drugs that can successfully act on these metabolic enzymes and have minimal effects on normal tissues[11]. Recent advances in metabolite profiling methodologies are providing new tools for understanding molecular fluxes through pathways; furthermore, an increased utilization of techniques, such as ^{13}C Magnetic Resonance Spectroscopy, can allow direct visualization of how metabolism is altered in patients, as a result of new therapies. This technique include the use of dynamic nuclear polarization to generate hyperpolarized ^{13}C-labbeled metabolites to track metabolism in tumors *in vivo*[15]; it will be especially important for studying how cell metabolism is influenced by the tumor microenvironment and for selecting the right drugs targeting cancer cell metabolism for specific patients.

1.3.2 Existing Approaches

Structural information and basic knowledge of some target enzyme already exist for many potential drugs. However, improve this number and improve the human metabolism models with the relative biochemistry comprehension remains a challenge for the development of successful therapies[13]. Despite a renewed interest in exploring metabolic enzymes as targets for cancer therapy, very few molecules are currently used in clinical trials. However, new compounds showed encouraging results in preclinical models and they will probably enter in clinical trials in the next few years[12]. These new drugs have the potential to limit the macromolecular synthesis needed for cell growth, limiting pathways important for supplying nutrients and preventing an adaptive response to cell stress.

Targeting Glucose

For example, one of the principal nutrients for living cells is glucose. Many of the studies exploring glucose utilization of cancer cells illustrate the need for pharmacological agents to inhibit glucose uptake. Various agents have been shown to block glucose uptake by cancer cells, but so far a specific glucose transport inhibitors has not reported. It may be difficult to act directly on the main glucose transporter (GLUT1) without having a negative effect on normal tissues; however, there are some passive glucose transporters that are not expressed in normal cells, but are present at high level in cancer cells, that could be used as possible therapeutic targets[13].

Targeting Lactate

Lactate is excreted mainly from cancer cells[11]. The inhibition of lactate production and lactate transport out of the cells are two strategies that directly target the Warburg effect (see Chapter 2) in cancer: *1)* The family of monocarboxylate transporters (MCTs) comprises the major proteins that are responsible for lactate export in cancer cells: targeting those transporters using small molecules inhibits the proliferation of cells that rely on aerobic glycolysis. *2)* Lactate dehydrogenase (LDH) is the enzyme that interconverts pyruvate and NADH into lactate and NAD^+, respectively. When LDHA, the form of LDH that is over-expressed in many cancer cells and absent in normal ones, is knocked down, cancer cell proliferation is severely impaired both *in vitro* and *in vivo*. Furthermore, LDHA inhibitors slow the growth of tumors in mice and can induce tumor regressions, indicating that this enzyme, as well as MCTs inhibitors, are promising therapeutic targets for cancer therapy[13].

Targeting Glutamine

In some cancer cells glutamine was observed to be an alternative fuel source. This one is the major source of nitrogen for nucleotide and amino acid synthesis, but many cancer cells metabolize an excess of glutamine to supply their high level of proliferation. Glutamine also has an important role in replenishing intermediates of the Krebs Cycle that are depleted by biosynthetic reactions. It was observed that the growth of cancer cells could be selectively inhibited by targeting the activity of: *i)* glutaminase, the enzyme that convert glutamine to glutamate and is required for proliferating, and *ii)* α-ketoglutarate, which is found to be at abnormal levels in some human cancers. It was demonstrated that blocking glutamine entry could slow in particular the growth of fibroblasts and breast cancer cells[13].

1.3.4 *Perspectives of Personalized Therapies*

Personalized cancer therapy is a treatment strategy founded on the idea that each person is a unique metabolic entity. Personalization of metabolic therapies as broad-based cancer treatment strategy will require a fine-tuning process based on the understanding of individual human physiology[12].

Despite the promises of personalized metabolism cancer treatments, it is worth to underline that many of these drugs acting on metabolism are not already available in clinic or have produced disappointing results when tested in clinical trials, indicating that there are many challenges that must be addressed to advance this field[13-16].

The most recent personalized approach is based on the sequencing of tumor DNA, which reveals the specific genomic alterations that have implications for cancer treatment. Genetic factors of the patients can be associated with drug metabolism, drug response and drug toxicity. Cancer molecular profiles, cancer sites and other patient characteristics are potentially used for determining optimum individualized therapy options[12-16].

However, many experts agree that personalized cancer medicine, defined here as a treatment based on the molecular characteristics of a cancer from an individual patient, has great potential in the therapy of many cancers. Therefore, it is crucial to have new imaging technologies and approaches that can measure the specific metabolic response upon drug administration in order to guide the selection of the most beneficial treatment[12].

References

[1] Hill RW, Wyse GA, Anderson M, *Animal Physiology,* 3rd Ed. (Chapter 7), © Sinauer Associates Inc. Publishers (2012)

[2] Atkins P, De Paula J, *Physical Chemistry,* 7th Ed. (Chapter 4), Oxford University Press, (2002)

[3] Smith AL, *Oxford Dictionary of Biochemistry and Molecular Biology*, pp. 508. Oxford University Press (1997)

[4] Ferguson SJ, Nicholls D, *Bioenergetics3,* 3rd Ed. Academic Press (2002)

[5] Jencks WP, Fasman GD, *Handbook of Biochemistry and Molecular Biology*, 3rd Ed. Physical and Chemical Data, Vol. 1, pp. 296-304, CRC Press (1976)

[6] Pollak N, Dölle C, Ziegler M, The power of reduce: pyridine nucleotides – small molecules with a multitude of functions. *Biochem. J.* 402, pp. 205-218 (2007)

[7] Demetrius LA, Coy JF, Tuszynski JA, Cancer proliferation and therapy: the Warburg effect and quantum metabolism. *Theoretical Biology and Medical Modelling.* 7:2 (2010)

[8] Apte SP, Sarangarajan R, *Cellular Respiration and Carcinogenesis*. Humana Press c/o Springer Science (2009)

[9] Gatenby RA, Gillies RJ, Why do cancers have high aerobic glycolysis? *Nature Reviews Cancer*. 4, pp. 891-899 (2004)

[10] Racker E, History of the Pasteur effect and its pathobiology. *Mol. Cell. Biochem*. 5, pp. 17-23 (1974)

[11] Cairns RA, Harris IS, Mak TW, Regulation of cancer cell metabolism. *Nature Reviews Cancer*. 11, pp. 85-95 (2011)

[12] Vander Heiden MG, Exploiting tumor metabolism: challenges for clinical translation. *The Journal of Clinical Investigation*. 123:9, pp. 3648-3651 (2013)

[13] Vander Heiden MG, Targeting cancer metabolism: a therapeutic window opens. *Nature Reviews Cancer*. 10, pp. 671-684 (2011)

[14] Vander Heiden MG, Cantley LC, Thompson CB, Understanding the Warburg effect: the metabolic requirements of cell proliferation. *Science.* 324:5930, pp. 1029-1033 (2009)

[15] Kurhanewicz J, Bok R, Nelson SJ, Vigneron DB, Current and Potential Applications of Clinical 13C MR Spectroscopy. *J Nucl. Med*. 49:3, pp. 341-344 (2008)

[16] Seyfried TN, Flores RE, Poff AN, D'Agostino DP, Cancer as a metabolic disease: implications for novel therapeutics. *Carcinogenesis*. 35:3, pp. 515-527 (2014)

Chapter 2

The Warburg Effect: Historical Background and Current Views

Abstract

Otto Warburg pioneered quantitative investigations of cancer cell metabolism and respiration. Warburg and co-workers showed in 1920s that cancer cells are characterized by metabolic alterations, involving a shift from the generation of ATP through *oxidative phosphorilation* to ATP generation through *glycolysis*, even under normal oxygen concentration. This phenomenon today is known as aerobic glycolysis or *Warburg effect*. This switching toward glycolysis implies that cancer tissue metabolizes approximately ten fold more glucose to lactate in a given time than normal tissue and the amount of lactate released from cancer tissues becomes two orders of magnitude greater than the amount of normal ones.

Key words Warburg Effect, Glucose, Lactate, Positron Emission Tomography (PET)

2.1 History of the Warburg Effect

2.1.1. Warburg's Life

Otto Heinrich Warburg was one of the first true interdisciplinary scientists[1]. Warburg, spent his entire career in Germany, completed his Chemistry Ph.D. dissertation in 1906 and he concluded his studies in Medicine in 1911, obtaining a *Habilitation* in physiology in 1913. One year later he was appointed head of the Department on Physiology of the Kaiser Wilhelm Institute (which later became the Max Planck Institute) for Biology. During the First World War, Warburg volunteered for military service, but he was convinced from Albert Einstein to fulfil his patriotic duty doing research rather than serving at the front. In 1931 he was awarded the Nobel Prize in Physiology or Medicine for his

discovery of the respiratory chain enzyme *cytochrome c* oxidase. Warburg was allowed to continue working during the Nazi period plausibly because he was working on cancer, a disease that Hitler morbidly feared. He enjoyed working with his hands until his death in 1970, at the age of 87 years. Warburg was a firm ***believer in quantitative methods in biology research***; he is famous principally for his ***quantitative physical-chemical approaches*** to investigate the rapid growth of cancer cells, however, he was also the first one to use thin tissue slices for physiology research, he improved manometric techniques to measure changes in pressure accompanying cell and tissue processes, and he is credited as the inventor of the single-beam spectrophotometer[1].

2.1.2 From the Earliest Studies to the Actual Warburg Effect

In his early studies on sea urchin eggs, Warburg observed a rapid increase in O_2 consumption and a subsequent rapid cell division upon fertilization, hence he postulated that cancer tissues might also take up more O_2 than normal tissue[1-2a]. To address this hypothesis, Warburg used his improved manometric techniqu[2b] to measure O_2 and glucose consumption in thin tissue slices, measuring also the CO_2 emission, which is equivalent to lactate production[1].

$$CH_3CHOHCOOH + HCO_3^- \rightarrow CH_3CHOHCOO^- + H_2O + CO_2$$

Warburg and co-workers discovered that Flexner-Jobling rat liver carcinoma does not take up more O_2, but that, even in the presence of O_2, such tissue produces lactate. This indicates that in tumor cells most of the pyruvate is directed away from mitochondria to produce lactate through the action of the lactate dehydrogenase enzyme (LDH), bypassing the pyruvate utilization in the Krebs Cycle in order to generate ATP to meet the cell's energy demands[1]. Lactate production, for normal cells, is typically restricted to anaerobic conditions when oxygen levels are low, however, cancer cells preferentially direct glucose towards lactate production even when oxygen is plentiful[3].

This phenomenon is called *aerobic gycolysis* or, from his discoverer, the ***Warburg Effect*** [4].

This glycolytic production of ATP under aerobic conditions was found to be a characteristic of most cancer cells and, in addition, the most glycolytic tumor cells were also found to be the most aggressive ones[4-5]. Furthermore, Warburg and co-workers determined how O_2 affects this aerobic glycolysis, defining a

molar ratio, known as the *Meyerhof quotient* that takes into account the amount of O_2 required to convert one glucose molecule to lactate under aerobic and anaerobic conditions[1-5]. They observed that the quotient is more or less equivalent for both cancer and normal tissues, meaning that the O_2 consumption of cancer tissues should be the same as that of normal ones[1]. Since the increased production of lactate by cancer cells is not nullified by higher O_2 consumption, and lactate is widely recognized as an indicator of respiratory insufficiency in biological systems, Warburg was strongly convinced that the respiration must be altered in cancer tissues. He also assumed that aerobic glycolysis was a universal property of cancer cells due to the defects in mitochondrial respiration and he suggested that cancer might be caused by impaired mitochondrial metabolism[1].

In contrast to these findings, recent studies have demonstrated that tumor mitochondria are fairly functional regarding the respiration and ATP synthesis. They show normal respiratory control ratios and normal oxidation abilities owning to the respiratory substrates. Warburg himself misinterpreted his own early observations. In fact, his *in vitro* findings show that, in the same time interval normal and cancer cells metabolize glucose in different ways:

Normal cell metabolize 1 molecule of glucose → 36 molecules of ATP
Cancer cell (in ***presence of O_2***) metabolize: 1 molecule of glucose → 36 molecules of ATP + 10 molecule of glucose → 20 molecules of lactate = 20 molecules of ATP Tot: 11 molecule of glucose → 56 molecules of ATP + 20 molecules of lactate
Cancer cell (in ***absence of O_2***) metabolize Tot: 13 molecule of glucose → 26 molecules of ATP + 26 molecules of lactate

These data are in agreement with the proper functioning of mitochondria[6].

Moreover, in recent past, many studies on cancer cells have documented preferably oncogenic nuclear and mitochondrial DNA mutations in proteins involved in respiration, rather than mitochondrial defects[4]. Hence, in a critical analysis of Warburg's theory, Sidney Weinhouse concluded: ''*no substantial evidence has been found that would indicate a respiratory defect, either in the machinery of electron transport, or in the coupling of respiration with ATP formation, or in the unique presence or absence of mitochondrial enzymes or cofactors involved in electron transport*"[7].

Nowadays, the Warburg effect is generally used to explain the alterations in signalling pathways that govern glucose uptake and lactate release, which are also involved in the regulation of mitochondrial activity. Independently of mitochondrial defects or damages, most cancer cells do display high rate of glycolysis, aerobic or anaerobic, and this property is now widely used for tumors visualisation and monitoring in clinic.

Recently the field of cancer biology, pharmacology and clinical oncology have seen a rapid increase of new technologies that allow the study of genes and proteins expression from cell extracts and from intact cells in culture[8]. However, it is necessary to study and investigate on cancer cells in their physiological environmental without altering and stressing them[9].

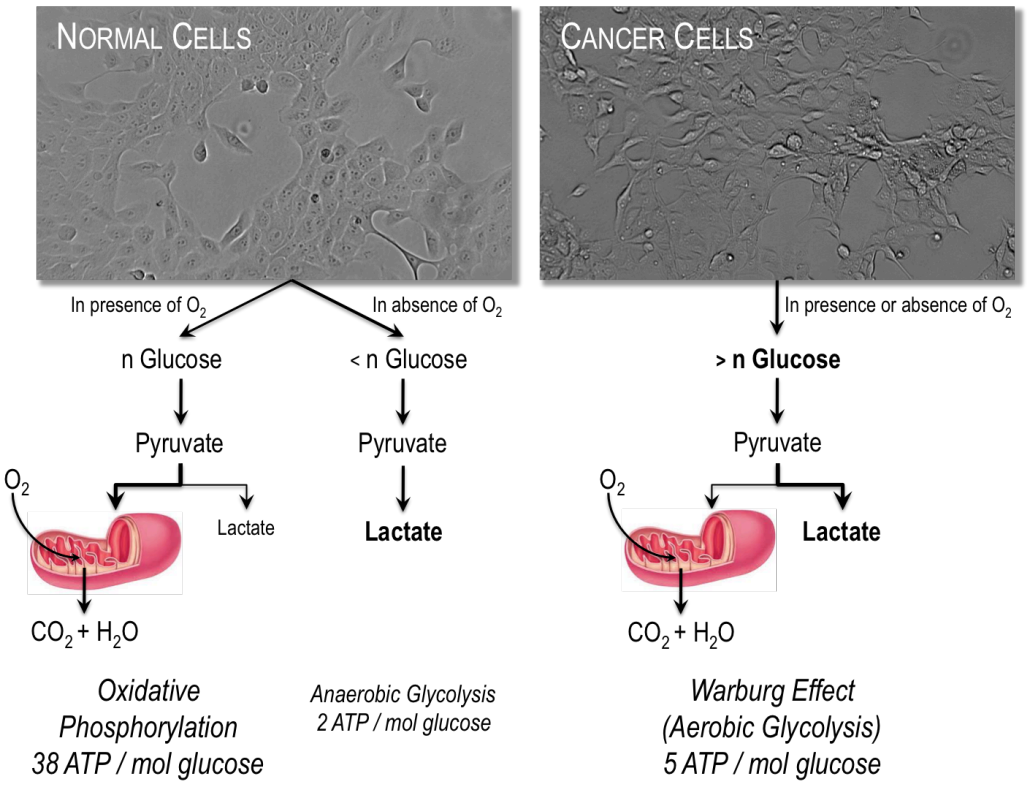

Figure 1. Schematic representation of the main differences among oxidative phosphorylation, anaerobic glycolysis and aerobic glycolysis, the last also called the *Warburg effect*. Warburg observed that cancer cells tend to convert most glucose to lactate regardless of the presence of O_2. Differently normal cells in presence of O_2, channel the pyruvate into the mitochondria, where it is oxidized to CO_2 and H_2O, generating ATP to meet cell's energy demands. This upregulation of lactate release allows glycolysis to continue, by the cycling of NADH back to NAD^+, but results in a decreased ATP production[10].

2.2 Translating the Warburg Effect to the Clinic

2.2.1 FDG-PET Imaging

The employment the *Warburg effect* in combination with tracers was found a good strategy to develop a non-invasive imaging tool[8].

Currently one of the most powerful diagnostic technology widely used in oncology for cancer detection is FDG-PET (2-deoxy-2-[^{18}F]fluoro-D-glucose positron emission tomography) that can be used both for staging the tumor and for monitoring the therapy response. This is a highly sensitive, non-invasive molecular imaging technique, introduced for the first time 50 years ago in hospitals, that exploits cancer cells' preferential utilization of aerobic glycolysis, instead of oxidative phosphorylation[10]. This technique is based on the employment of a molecule similar to glucose, fluorodeoxyglucose (FDG) as a radiolabelled tracer, which is injected in non-pharmacological doses into the patient. Fluorine-18 (^{18}F) is a fluorine radioisotope that is an important source of positrons (it decays to stable Oxygen-18) and it is characterized by a short half-life (around 20 - 30 minutes)[8].

This molecule after the *in vivo* injection is taken up and trapped in cells by phosphorylation, but is not subject to further metabolism and once phosphorylated is unable to diffuse out of cells. Therefore, it accumulates at a rate proportional to glucose utilization, providing a way to assess glucose uptake rates in cells. Tumor tissues, which take up more glucose than surrounding tissues, can be non-invasively visualized in cancer patients by FDG-PET. ^{18}F undergoes positive beta decay, a type of radioactive decay in which a proton inside the atomic nucleus is transformed into a neutron emitting a positron and electron neutrino [$^{18}F \rightarrow {}^{18}O + e^{+} + \nu_e$]. The emitted positron collides and annihilates with a nearby electron releasing two gamma rays with an approximately 180-degree relative angle[8]. The PET scanning machinery detects these two gamma rays and using computational software calculates the 3D origin inside the body. The positron annihilation event could recognize areas of abnormal metabolic behaviour of cancer *in vivo* and it can localize the precise site of cancer cells, with a spatial resolution around 0.5 cm (Figure 2).

Clinical PET is approved for many investigations, such as staging of cancers, differentiation between residual tumor and scarring, diagnosis of suspected

recurrences, monitoring response to therapy, prognosis and radiotherapy treatment planning in many typologies of cancers (not all)[11]. Despite its widespread use in clinical oncology, some cancers remain difficult to be imaged by FDG-PET, such as hepatocellular carcinoma, prostate and pancreatic cancer. It is possible that these tumor types do not exhibit the Warburg effect metabolic phenotype or there is a low density of cancer cells in these kinds of tumor tissues[11].

PET scanning can also monitor uptake of other nutrients (e.g. glutamine and glutamate). However, the uptake of those nutrients is not specific to cancer cells. A better understanding of how increased nutrient uptake supports different stages of tumor progression will be important to exploit metabolism for therapeutic benefit[12].

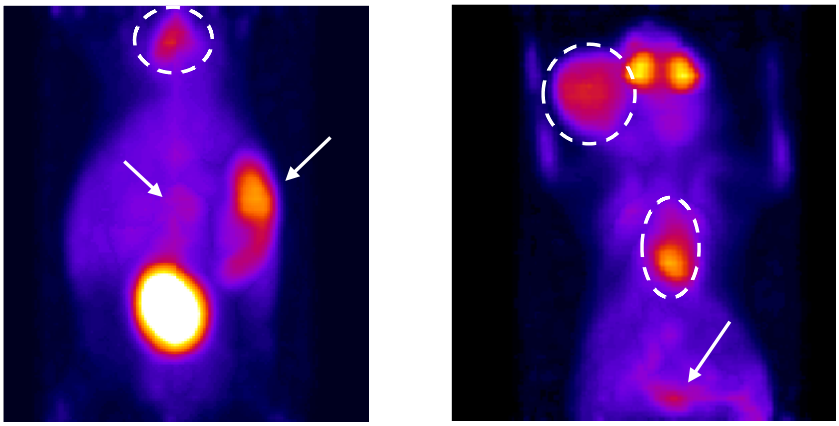

Figure 2. Small-animal FDG-PET imaging. MicroPET imaging of two mice 1h after intravenous injection of FDG. Increased fluorescent signal indicates area of FDG accumulation that marks high glucose consumption. On the left, the arrows indicate the spleen and the heart that often scores positive due to high energetic demand of the myocardium, the circle indicates the thymus whereas the saturation of the signal in the bladder is due to the high physiological urinary excretion of the tracer. On the right, the arrow indicates an empty bladder and the circles mark a thymoma and infiltrated lymph nodes. Notably, the spatial resolution of FDG-PET analysis are does not reach more than half cm.

References

[1] Koppenol WH, Bounds PL, Dang CH, Otto Warburg's contributions to current concepts of cancer metabolism. *Nature Reviews Cancer*. 11, pp. 325-337 (2011)

[2] (a) Warburg O, Notizen zur entwickelungsphysiologie des seeigeleies. *Arch. F. d. ges. Physiol.* 160, pp. 324-332 (1915) (b) Warburg O, Verbesserte methode zur messung der atmung und glykolyse. *Biochem. Zeitschr.* 152, pp. 51-63 (1924)

[3] Warburg O, On the origin of cancer cells. *Science*. 123:3191, pp. 309-314 (1956)

[4] Gogvadze V, Zhivotovsky B, Orrenius S, The Warburg effect and mitochondrial stability in cancer cells. *Molecular Aspect of Medicine*. 31, pp. 60-74 (2010)

[5] Warburg O, Posener K, Negelein E, Über den Stoffwechesel der Carcinomzelle. *Biochem. Zeitschr*. 152, pp. 309-344 (1924)

[6] Koppenol WH, Bounds PL, The Warburg effect and metabolic efficiency: re-crunching the numbers. Science E-Letter (2009).

[7] Weinhouse S, The Warburg hypothesis fifty years later. Z. Krebsforsch. *Klin. Onkol. Cancer Res. Clin. Onc*. 87, pp. 115-126 (1976)

[8] Gambghir SS, Molecular imaging of cancer with positron emission tomography. *Nature Reviews Cancer*. 2, pp. 683-693 (2002)

[9] Cairns RA, Harris IS, Mak TW, Regulation of cancer cell metabolism, *Nature Reviews Cancer*. 11, pp. 85-95 (2011)

[10] Vander Heiden MG, Understanding the Warburg effect: the metabolic requirements of cell proliferation. *Science.* 324:5930, pp. 1029-1033 (2009)

[11] Almuhaideb A, Papathanasiou N, Bomanji J, ^{18}F-FDG PET/CT imaging in oncology. *Ann. Saudi. Med*. 31:1, pp. 3-13 (2011)

[12] Christofk HR, Bensinger SJ, New aspects of the Warburg effect in cancer cell biology. *Seminars in Cell & Developmental Biology*. 23, pp. 352-361 (2012)

Chapter 3

Electrochemistry in Biology and Medicine

Abstract

"The topic of this chapter is devoted to the subject matter of electrochemistry in the service of, and how it relates to, medicine. In the on going process of "globalization," we are witnessing not only the tendency of commercial unification of the globe, but also the rapidly emerging interdisciplinarity among different scientific and technical disciplines, as well. The word "nanotechnology" is the underlying thread in this technological melding process.
With the advent of relativity and quantum mechanics in the early part of the twentieth century, and the development of molecular biology in the second half, it is now accepted that mathematics, physics, chemistry, and biology constitute different parts of the same broader scientific discipline. Such interdependency, and subsequent confluence, of different disciplines are becoming one of the hallmarks of the twenty-first century." (Cit. *The Electrochemical Society Interface*) Electrochemistry and its constant progress can substantially impact on the future of medical devices. Indeed there are several applications that assert the validity of the electrochemical power in medicine and in medical devices, beyond its well-known employment in analytical applications.

Key words Electrochemistry, Biology, Medical Applications, Electrochemical Techniques

3.1 Bioelectrochemistry

3.1.1 History

The beginnings of electrochemical study in biological systems are closely related to the names of *Luigi Galvani* (1737-1798), who first coined the term *animal electricity* to describe that the impetus behind muscle movements was electrical energy carried by a fluid, and *Alessandro Volta* (1745-1827), which, embracing this new field, discovered the electrochemical series and the law of the electromotive force (*efm*) of the galvanic cell. In view of these findings Volta invented the voltaic pile, an early electric battery[1].

The first modern work in this field is attributed to *Julius Bernstein* (1839-1917), a German physiologist, who is recognized for his correct "membrane hypothesis". This hypothesis describes the resting and action potentials of nerve and muscle as diffusion potentials of K^+ ions through the cell membrane, from cytoplasm (high concentration) to extracellular solution (low concentration). He pioneered the experimentations of nerve conduction of impulses and transmission of the information in the nervous system.

Among all the prominent electrochemists who have contributed to this field, *John Bockris* (1923-2013) has to be mentioned, for his findings regarding biological substances with characteristics of semiconductors.

They are just some leading examples, but the domain of physical electrochemistry, a discipline having broad applications to many areas of technology, has grown considerably over the past century. Thanks to many contributors all over the world, electrochemistry gained a solid theoretical background, it is supported by a strong technological development, and it maintains close connections with medical disciplines[2].

3.1.2 Main Concepts

Scientists use electrochemistry for studying oxidation (loss of electrons) and reduction (gain of electrons) processes that a material of single molecules undergoes during an electrical stimulation. These observations give information about the concentrations, the kinetics, the reaction mechanisms and the chemical status of the species under investigation, both free in the solution or linked onto the electrode surface. Electrochemical techniques can be used for several purposes and offer a different perspective in respect to spectroscopy or other optical techniques.

In an electrochemical experiment one can mainly measure the potential (E), the current (i), the charge (Q) and the time (t).

In most electrochemical techniques a three-electrodes configuration is used comprising: the working electrode (WE), the reference electrode (RE) and the counter (or auxiliary) electrode (CE). All of them are immersed in an electrolytic solution that permits the electrical conduction between the electrodes and connected to a potentiostat. The latter can control the working potentials and measure the resulting current or the opposite, such as in potentiometric techniques[3].

It is worth to underline that the working electrode, where the electrochemical reactions take place, is usually made of an inert material, such as platinum or glassy carbon. The first one is suitable because it does not corrode, it catalyses proton reduction, useful for H_2O_2 detection, with a high intrinsic exchange current density, and it has an excellent reproducibility of the potential. Instead, the second one combines glassy and ceramic properties with those of graphite; it has a high temperature resistance, low density, low electrical and thermal resistance, extreme resistance to chemical attack and it is impermeable to gases and liquids[3].

The potential of WE is measured versus the reference. Typical reference electrodes are saturated calomel electrode [SCE; E = +0.241 V vs SHE] and silver/silver chloride [Ag/AgCl 3M KCl; E = +0.197 V vs SHE], which have stable and well-known electrode potentials[3]. Since potential is a measurement of the voltages difference between two electrodes, the fixed value of the reference electrode provides a way to control the potential of the working electrode. The counter electrode is typically a wire of an inert material, such as platinum. Various electrochemical techniques, including cyclic voltammetry, chrono-amperometry and pulsed approaches can be performed through the combined measurement of potential, current, charge and time.

In paragraph 3.2 brief descriptions and relevant parameters of the electrochemical techniques employed in the present work are provided.

3.1.3 Bioelectro-chemistry in Medicine

Medicine is an applied field of science that has always exploited technologies and techniques coming from several areas of interest. Innovations in the synthesis of new medications, improvement on diagnosis technologies and on mechanical implantations, among many of others, improve human health and increase the life span of individuals[4].

The goal of medicine is to treat patients in the best way possible, and it requires a great deal of research from a wide variety of fields. As medical treatments and technologies evolve, electrochemistry is playing an increasingly role in the development of medical treatments and devices. Blood, saliva, urine and other biological fluids, which contain ions, hormones, enzymes, proteins etc., act as electrolytes, providing a conductive environment that promotes the electrochemical exchange of electrons. This exchange of electrons between the

redox active molecules within the cells is at the base of the functioning of many vital biological processes. The real-time monitoring of these processes, using electrochemical devices, gives a great and unique improvement on the comprehension of the involved mechanisms[5].

3.1.4 Some Applications

Nowadays many electrochemical devices and methods, listed below, are used in biology and in medicine[4-6], and new approaches are under study.

- Electrochemical biosensors are used for monitoring cellular dynamics, such as cellular redox environment, exocytosis and cellular adhesion. For these purposes many devices have been developed, such as interdigitated electrode arrays, nanopillars, nano- or micro-electrodes and microchip based biological systems, which are important for the development of point-of-care testing, monitoring and for medical research and drug development. Among these cancer biomarker sensors, glucose sensors and DNA arrays for multiple gene analysis have to be mentioned.
- Electrode/self-assembled monolayer (SAM) has been widely used to explore fundamental aspects of electron exchange mechanism between electrodes and redox active biomolecules, such as proteins. These devices, with nanoscopically tunable physical properties, provide a unique powerful system for fundamental electron transfer studies and nanotechnological applications.
- Surface modification of implants, namely surface bio-functionalization or coating of different substrates for medical devices such as drug eluting stents, orthopaedic and dental implants (e.g. bone-binding metals).
- Applications of nanoelectrochemistry and nanoelectrodes for studying the transport of electrons through the cell membrane, the ion channels, the transporters in pore-suspending membranes and neurotransmitters.
- Nanowire-based electronic devices emerged as a powerful platform for ultra-sensitive, rapid, direct electrical detection and quantification of biological and chemical species in solution. These devices can be used for sensing proteins, DNA, viruses and cells, down to the ultimate level of a single molecule. These ones are promising building blocks for nanoscale bioelectronic interfaces with living cells and tissues, since they have the potential to form strongly coupled interfaces with cell membrane.

- DNA microarrays offer a high throughput method for simultaneously evaluating large numbers of genes. Electrochemical-based DNA arrays provide many advantages over radioisotope- or fluorophore-based detection systems.
- Electrochemical Scanning Probe techniques used in the investigation of immobilized biomolecules: due to the high spatial resolution of the Scanning Electrochemical Microscope (SECM), this technology has been suggested as a readout method for locally immobilized, micro-meter-sized biological recognition elements, including a variety of DNA arrays with different formats and detection modes.
- Employment of biomimetic membranes for studying the functions of single proteins, such as ions channels and transporters, and smaller lipophilic biomolecules. They are common in pharmaceuticals, as well as for the investigation of phase stability, protein-membrane interactions, and membrane processes. They are also useful to design membrane-based biosensors and devices for assaying membrane-based processes.

3.2 Main Electrochemical Techniques Employed in this Work

3.2.1 Cyclic Voltammetry

Cyclic Voltammetry (CV) is one of the most common electroanalytical techniques for its ability to characterize electrochemical systems with high sensitivity. CV experiments could be used for several applications, such as determination of the reversible or non-reversible behaviour of the redox couple, the number of electrons involved, the formal potentials, the rate constants, the formation constants, the reaction mechanisms and the diffusion coefficient of the redox species. In CV experiment, the potential is ramped linearly versus time. The scan starts from an initial potential toward either high potential or low potential depending on the initial polarity, and then it scans back. The resulting current is recorded as function of potential. The following diagram shows a typical potential waveform applied as function of time. One can run single-cycle or multi-cycle CV; the repetition of the potential waveform can also allow the build-up of reaction products at the electrode surface, such as electropolymerization of a polymer[7].

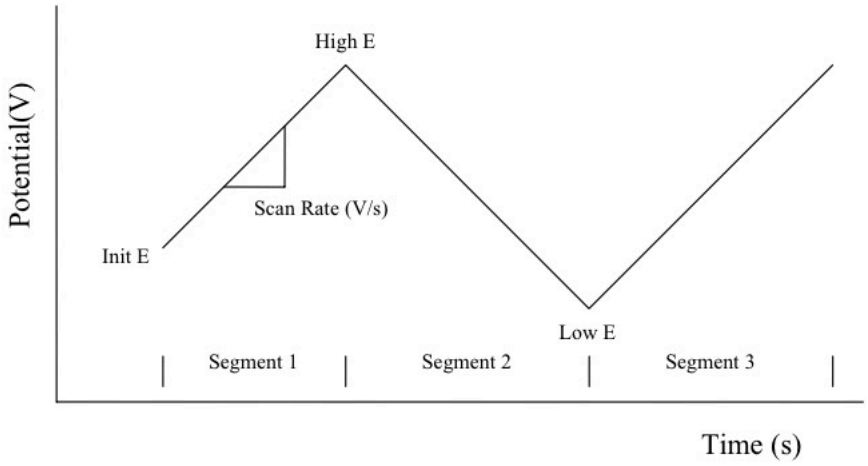

3.2.2 Chrono-Amperometry

Chronoamperometry (CA) is another common electroanalytical technique, useful for determining diffusion coefficients and for investigating kinetics and mechanisms of the reactions. In CA, the potential is stepped from an initial potential toward either high E or low E depending on the initial polarity, and then it will step back. The following diagram shows the potential waveform applied in time. The CA response requires a supporting electrolyte to insure the absence of ion migration and no other competitive reactions. From CA other useful value can be calculated: the active area of the electrode, which in many cases does not correspond to the geometric area, due to the roughness factor that increases the active area of the electrode. In multiple CA, slow heterogeneous electron transfers exhibit a strong dependence on time width of the potential step and slow diffusion of the species at the electrode can affect the shape of the resulting current if the pulse width is not enough large[7].

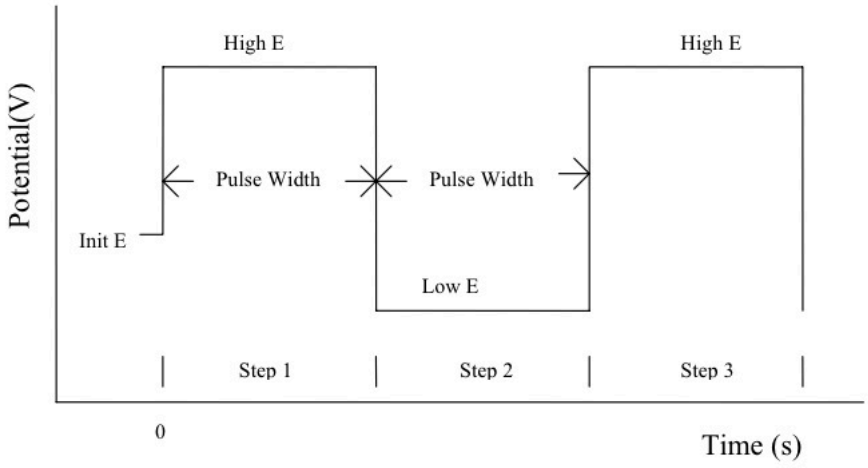

3.2.3 Amperometric i-t Curve

In Amperometric *i-t* Curve, a constant potential is applied and the current, also due to the faradaic processes occurring at the electrode, is recorded in function of time. The following diagram shows the potential waveform applied as the function of time and the sample scheme[7].

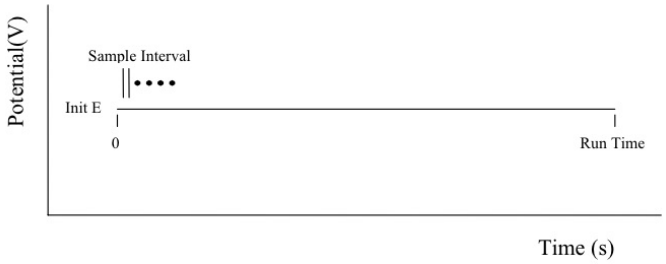

3.2.4 Differential Pulse Amperometry

In Differential Pulse Amperometry (DPA), two flexible potential pulses are applied after a cleaning step, which could be used for electrode conditioning The current is sampled at the end of each pulse step and is recorded as a function of time. This mode is very useful to monitor two different redox species in solution. In the experimental set up employed in the present work, only the difference of the two current samples in consecutive step is displayed, but the two single data sets are available. The time step is chosen in order to have a good compromise between *i)* longer sample intervals with better signal averages and decreased noises and *ii)* less species depletion due to the tip reaction for shorter time steps. The following diagram shows the potential waveform applied as function of time and the current sampling scheme[7].

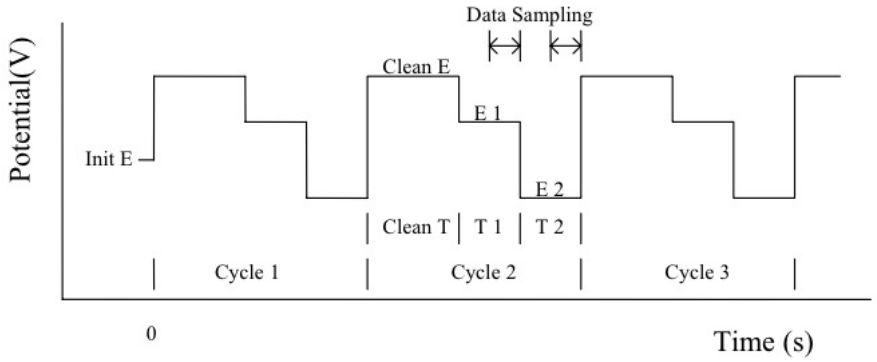

3.2.5 Scanning Electro-chemical Microscope

The scanning electrochemical microscope (SECM) can examine chemistry at high resolution in proximity of interfaces. It is based on the use of small electrodes scanned in close proximity of a surface with high precision. SECM can be employed to obtain chemical reactivity images of surfaces and also in quantitative measurements of reaction rates. For the all details see *Chapter 4*.

References

[1] Munro J. *Pioneers of Electricity; or, short lives of the great electricians*. The Religious Tract Society, London (1902)

[2] The Electrochemical Society *Interface* (Fall, 2003)

[3] Zoski CG, *Handbook of Electrochemistry*. Elsevier (2006)

[4] Schlesinger M, *Applications of electrochemistry in medicine. Modern aspect of electrochemistry*. Vol. 56. Springer Science (2013)

[5] Shedlovsky T. *Electrochemistry in biology and medicine*. John Wiley & Sons Inc., New York (1955)

[6] Eliaz N, *Applications of electrochemistry and nanotechnology in biology and medicine*. 1st Ed. Springer Science (2011)

[7] CH Instruments User's Manual (Model 920D Scanning Electrochemical Microscope), Chapter 4.

Chapter 4

Scanning Electrochemical Microscopy

Abstract

Scanning Electrochemical Microscopy (SECM) is a scanning probe technique that employs micro-nano electrode probes, which is moved in the proximity of the sample surface recording an amperometric signal. The signals obtained depend on the topography and reactivity of the sample. The SECM response is sensitive to the presence of conducting materials and electroactive species. For this reason, SECM is useful for high-resolution imaging of heterogeneous and homogeneous reactions on surfaces, in order to characterize them and measure the local kinetics. In this chapter an historical background, the basic principles and the instrumentation used to obtain images and surface reaction-kinetic information are briefly discussed. This technique has been proved to be useful for a broad range of interdisciplinary applications, such as biological system, sensors and probing reactions at the liquid/liquid surface.

Key words Scanning Electrochemical Microscopy, UMEs, Approach Curves, SECM Imaging, Biological System

4.1 Introduction and Principles of SECM

4.1.1 Background

Scanning Electrochemical Microscopy (SECM) is a member of the Scanning Probe Microscope, which appeared for the first time in 1989[1]. SECM employs an ultramicroelectrode (UME) as probe to scan in close proximity to a surface of interest. The electrochemical response provides quantitative information of interfacial physiochemical processes[2]. SECM UMEs, with a radius *a* in the range of tens of nm to 25 μm,[3] can induce chemical changes and collect electrochemical information while approaching or scanning the substrate. The probe is held by a support and it can be moved in an electrolytic solution in close vicinity of interfaces. For this reason SECM is a powerful tool for

studying structures and processes in micrometer- and submicrometer-sized system. It can be used to analyze electron, ion and molecule transfer at solid substrates of different types (e.g. glass, metal, polymer and biological material),, liquid/liquid or liquid/air interfaces (e.g. mercury, oil) to investigate their nature and properties[4]. The movement of the tip is actuated by using a three dimensional positioner composed by three stepper motors for coarse positioning and a XYZ piezo block for finer displacement. This set up gives a spatial resolution of 1.6 nm and allows a maximum travelling distance of 2.5 cm[2-4]. The precise positioning capability (micrometer and nanometer scale) makes SECM a high spatial resolution imaging technique and offers the possibility to precisely reposition the tip. An interesting advantage of the repositioning is the capability of mapping and recording the topography of the surface and subsequently scanning the same area at constant height in order to obtain the contributions of both surface topography and reactivity to the probe current. Moreover, the nature of the probe and the way it interacts with the substrate determine which information can be obtained during SECM experiment. There are several operational modes of SECM[2-4]: *i)* the tip generation-substrate collection mode (TG/SC), where the probe is used to electrochemically generate a reactant that is detected at the substrate, which acts as a second working electrode; *ii)* the substrate generation-tip collection mode (SG/TC), where the species are generated at the substrate and the tip collects current changes. This method is useful in studies of reactions and concentration profiles at substrate surfaces; *iii)* the feedback mode, the most used operational mode, where the probe current due to a redox mediator in solution is monitored. In this case the UME current is perturbed by the presence of the substrate: it can be a *negative* feedback if there is a hindering of the electroactive species diffusion to the probe, causing a decrease current in respect to the one recorded in bulk or a *positive* feedback where the current, upon oxidation or reduction at the UME, is regenerated to the original state by the substrate (*paragraph 4.1.4 and 4.1.5*). Nowadays, there are several applications of SECM in biophysical and biochemical fields, even at single cell and subcellular levels. Those include measurements of flows through membranes[5], investigation of local transport properties and kinetic parameters of intracellular enzymatic redox processes[6], which are essential for cellular respiration, metabolism and protein synthesis.

4.1.2 Overview on BioSECM Setup

For this work, SECM measurements were performed using an experimental setup coupling a 910B SECM (CH Instruments Inc., Austin, TX) and a Nikon ECLIPSE 200 inverted microscope. The position system of 910B CHInstrument was removed from the original stage and mounted on the plate of the inverted microscope. The modifications for the optical/electrochemical microscope coupling were accomplished *in house* in our workshop. This setup is very helpful to assist the UME movement along the axis during approach, scan curves and imaging, in order to minimize the opportunities of UME damaging. Furthermore, the optical microscope is used to assess the morphology of the substrate, in our case, living cells and the scan area. The positioning system is controlled by a computer, which is used also for data acquisition. Figure 1 shows the entire apparatus.

A bipotentiostat controls the potential (range ±10 V) of the tip and/or the substrate versus the reference electrode and it is able of measuring a broad range of current responses (range ±10A): with sensitivity from pA (or even sub-pA) currents to much higher currents, recorded at macroscopic substrates[4]. The BioSECM apparatus instrument is mounted on a vibration-free table inside a Faraday cage to isolate it from environmental vibrations and electromagnetic noise. This kind of insulation is fundamental for high-resolution (nm-scale) and low-current measurements (pA and sub-pA).

The experiments were carried out in a 3.5 cm Petri dish, usually used for cell cultures, located on the inverted microscope plate holder and constituting the electrochemical cell by itself. The SECM probes (from CHI) are 10 μm Pt ultra-microelectrodes with RG = 10 (see *paragraph 4.1.3*). The tips were cleaned prior to use with alumina (0.05 mm) or diamond paper and sonicated for some minutes in a bath sonicator. The cell (Petri dish containing electrolytic solution and used for the cell culturing) was also equipped with a platinum wire as a counter electrode and an Ag/AgCl (3M KCl) as a reference electrode. In this work, all the potentials are referred to the Ag/AgCl (3M KCl).

Reference & Counter Electrodes

Software

The CHI900 software allows extensive experimental control and analysis of acquired data, but for data elaborations, computation of integrals and statistics OriginPro7.5 was utilized. The post processing of the bi-dimensional images was performed using the software "MIRA", written by Prof. G. Wittstock[7].

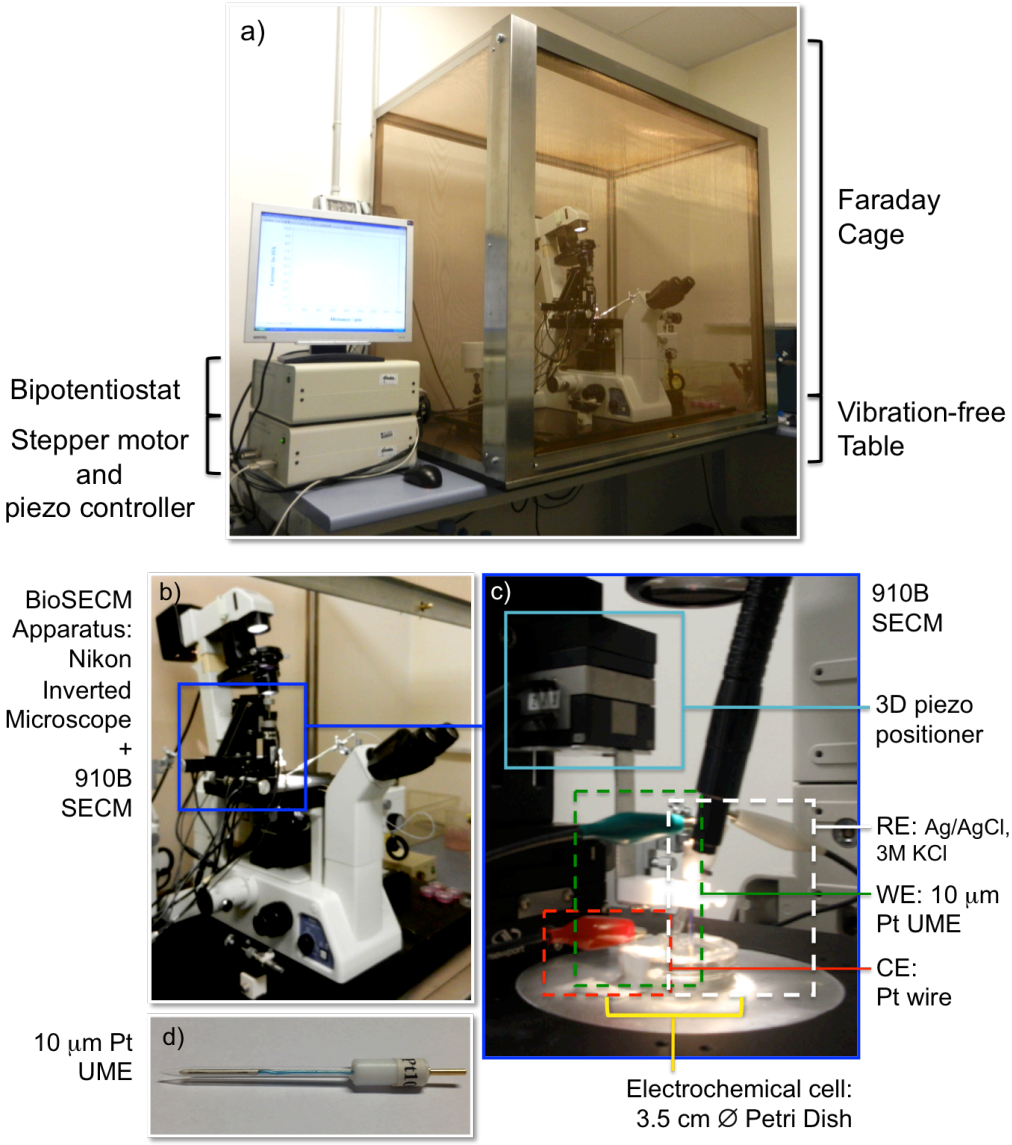

Figure 1. BioSECM Setup. A) SECM is mounted on the stage of a Nikon ECLIPSE 200 Inverted Microscope, on a vibration-free table inside a Faraday cage. B) Picture of the BioSECM apparatus. C) Part of the Scanning Electrochemical Microscope Components. Stepper motors and 3D piezo positioner (blue square) control the movement of the probe: 10 μm Pt UME (D), that act as WE. In the electrochemical cell (3.5cm ∅ Petri dish) are allocated also the CE and the RE (Counter and Reference electrodes).

4.1.3 Ultramicro-electrodes (UMEs)

One of the fundamental part of the instrumentation is the probe, a micrometer-sized UME sharpened to allow closer approach to the substrate surface[4].

The probe is 10 μm Pt wire sealed in a glass capillary under vacuum and connected with silver epoxy to a larger copper or silver wire to permit the contact with the potentiostat. The two important features of the UME geometry are: the radius of the conductive core -***a***- and the total tip radius (also comprehensive of the glass support thickness) -***r***-[4]. In order to use an electrode

as SECM probe the dimensionless parameter **RG,** equal to ***r/a***, has to be enough small: typical UME used in this work has an RG of 10 (Figure 2b)[2].

Once the electrode is immersed in a solution containing a redox mediator (R), at concentration *c*, and a supporting electrolyte, which decreases the solution resistance and insures that the transport of R to the electrode occurs by diffusion, a proper potential can be applied. Consequently, if the electrode is positioned in bulk solution (the probe is far away from the substrate, that means at distance greater than several active UME diameters) the R species is reduced or oxidised at the electrode, resulting in a current flow (Figure 2a).

Figure 2c displays a typical UME voltammogram at scan rate of 10 mV/s. The current, under these conditions, is driven by hemispherical diffusion of the redox mediator to the electrode surface and it reaches a steady state controlled also by the rate of mass transfer of R. For a conductive disk electrode of radius *a* in a insulating support (like our probe), the diffusion-controlled current under the steady state has been evaluated by the method of the Bessel expansion and is expressed by:

$$i_{T,\infty} = 4nFc^{*}Da$$

where *D* is the diffusion coefficient of the redox mediator, *F* is the Faraday constant (96485 s·A/mol) and *n* is the number of the electrons transferred during the reaction. ∞ means the bulk situation with a long distance between the probe and the substrate[9].

Advantages

The use of ultramicroelectrodes offers several advantages: first of all, because the flux of the species to the small electrode disk is quite large by diffusion[2], the current is immune to convective effects, and also independent from the radius of the insulating support. UME reaches steady state in a relatively short time, in our case fractions of a second, and, as a consequence, SECM scanning probe can be treated as a steady-state system. Moreover, due to the small currents that characterize the SECM experiments with ultramicroelectrode working electrodes (generally from nA to pA), the ohmic potential drops in solution and the charging current in double-layer are negligible[2]. Finally, thanks to their very small size, they allow experiments in microscopic domains, dimensions of the same order of living cell systems (typical cell dimensions: 20 ÷ 100 μm).

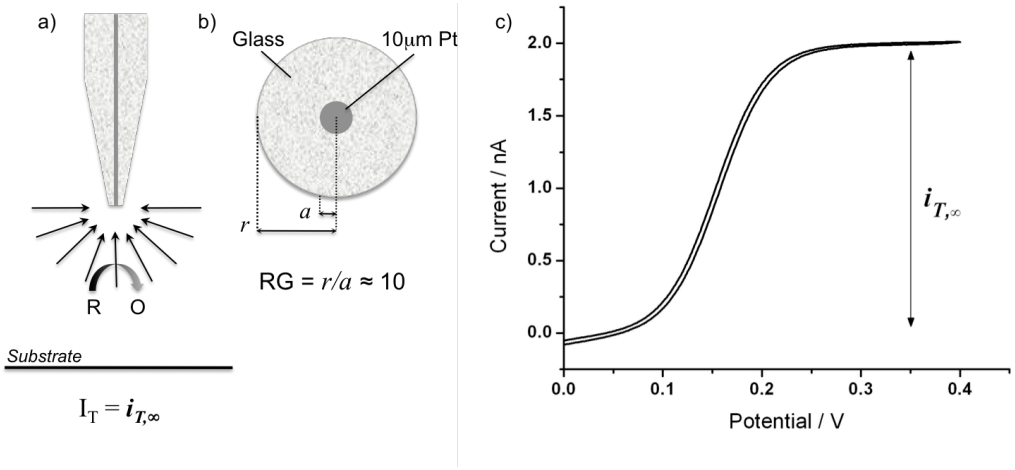

Figure 2. a) Electrode behaviour in bulk solution: the redox mediator reaches the tip by hemispherical diffusion. b) Frontal outline of the tip of a 10μm Pt UME. c) Typical cyclic voltammogram for a 10μm Pt UME in PBS (pH 7.4) containing 1mM of FcMeOH.
E = 0÷0.4 V versus Ag/AgCl 3M KCl. Scan rate = 10 mV/s.

4.1.4 Feedback Mode

In a feedback-mode SECM experiment the tip UME is placed in a solution containing an oxidized (or reduced) form of a redox mediator and is moved along z-axis, since it reaches the proximity of the substrate. Once applied a potential, the reduction or oxidation of the mediator at the tip surface produces a steady-state current ($i_{T,\infty}$). The recorded approaching current changes when the electrode is close enough to the substrate, depending on its characteristics: if the substrate is an insulating material, like a piece of glass or a plastic Petri dish, the diffusion of the redox mediator at the electrode surface is hindered and the current decreases in respect to $i_{T,\infty}$. The closer the tip gets to the substrate, the smaller i_T becomes[2] (i_T is the probe current recorded during the measurement). In an ideal system, when the distance between the substrate and the UME approaches zero, even the recorded current is zero. This mechanism is called *negative feedback* (Figure 3b).

Negative Feedback

Positive Feedback

When the substrate is an electrically conductive material, like a gold or a platinum electrode, the diffusion of the redox mediator to the probe is still hindered by the substrate, but there is also the regeneration of the redox centre. This species generated at the substrate diffuses to the tip and leads to an increase of current compared to $i_{T,\infty}$[2]. This mechanism is called *positive feedback* (Figure 3a). When the distance between the substrate and the tip approaches zero, i_T becomes very high owing to the electron-tunnelling regime[2].

Approach Curves (ACs)

Steady-state current-distance curves are called *approach curves* (ACs) (Figure 3), since the probe is moved along the z direction through the solution. The plot is reported in dimensionless form by plotting $I_T = i_T / i_{T,\infty}$ versus $L = d/a$. By fitting these experimental current-distance curves to theoretical equations it is mandatory to determine the zero separation point ($L = 0$), which in turn allows one to establish the distance scale essential for any quantitative SECM measurement. Analytical expressions were numerically calculated by Mirkin and Bard in function of several RG values[10]. The following theoretical equation fits within 1% the experimental current-distance curves for conductive substrates, over L interval from 0.04 to 10 and RG values between 1.1 to 10:

$$I_T^C(L) = \frac{i_T}{i_{T,\infty}} = k_1 + \frac{k_2}{L} + k_3 \exp\left(\frac{k_4}{L}\right)$$

where $L = d/a$ and k_1, k_2, k_3, and k_4 are parameters listed in Table 1. While, for an insulating substrate, the accuracy of the following equation is around 1% for $L \geq 2$ when RG = 1.11 and $L \geq 0.2$ for any other RG values present in Table 2:

$$I_T^{INS}(L) = \frac{i_T}{i_{T,\infty}} = \frac{1}{\left[k_1 + \frac{k_2}{L} + k_3 \exp\left(\frac{k_4}{L}\right)\right]}$$

Table 1. RG dependence on k_1, k_2, k_3, and k_4 for ACs under hindered diffusion control[4].

RG	k_1	k_2	k_3	k_4	% Error	Validity Range
1002	0.13219	3.37167	0.8218	-2.34719	<1%	0.3-20
100	0.27997	3.05419	0.68612	-2.7596	<1%	0.4-20
50.9	0.30512	2.6208	0.66724	-2.6698	<1%	0.4-20
20.1	0.35541	2.02259	0.62832	-2.55622	<1%	0.4-20
15.2	0.37377	1.85113	0.61385	-2.49554	<1%	0.4-20
10.2	0.40472	1.60185	0.58819	-2.37294	<1%	0.4-20
8.13	0.42676	1.46081	0.56874	-2.28548	<1%	0.4-20
5.09	0.48678	1.17706	0.51241	-2.07873	<1%	0.4-20
3.04	0.60478	0.80683	0.39569	-1.89455	<0.2%	0.2-20
2.03	0.76179	0.60983	0.23866	-2.03267	<0.15%	0.2-20
1.51	0.90404	0.42761	0.09743	-3.23064	<0.7%	0.2-20
1.11	-1.46539	0.27293	2.45648	8.995E-7	<1%	2-20

Table 2. RG dependence on k_1, k_2, k_3, and k_4 for ACs under positive feedback control[4].

RG	k_1	k_2	k_3	k_4	% Error	Validity Range
1002	0.7314	0.77957	0.26298	-1.29077	<0.2%	0.1-200
10.2	0.72627	0.76651	0.26015	-1.41332	<0.3%	0.1-200
5.1	0.72035	0.75128	0.26651	-1.62091	<0.5%	0.1-20
1.51	0.63349	0.67476	0.36509	-1.42897	<0.2%	0.1-200
10	0.68	0.78377	0.3315	-1.0672	<0.7%	0.05-20

Since approach curves involve only dimensionless variables, they do not depend upon the concetration or diffusion coefficient of the redox mediator. The AC shapes depend upon RG, since the sheath around the conductive part of the electrode blocks the diffusion of the redox mediator as well. Therefore, it might be difficult to fit approach curves obtained with coated UMEs, such enzyme-based biosensor (*Chapter 5*), because the real value of "*a*" is unknown.

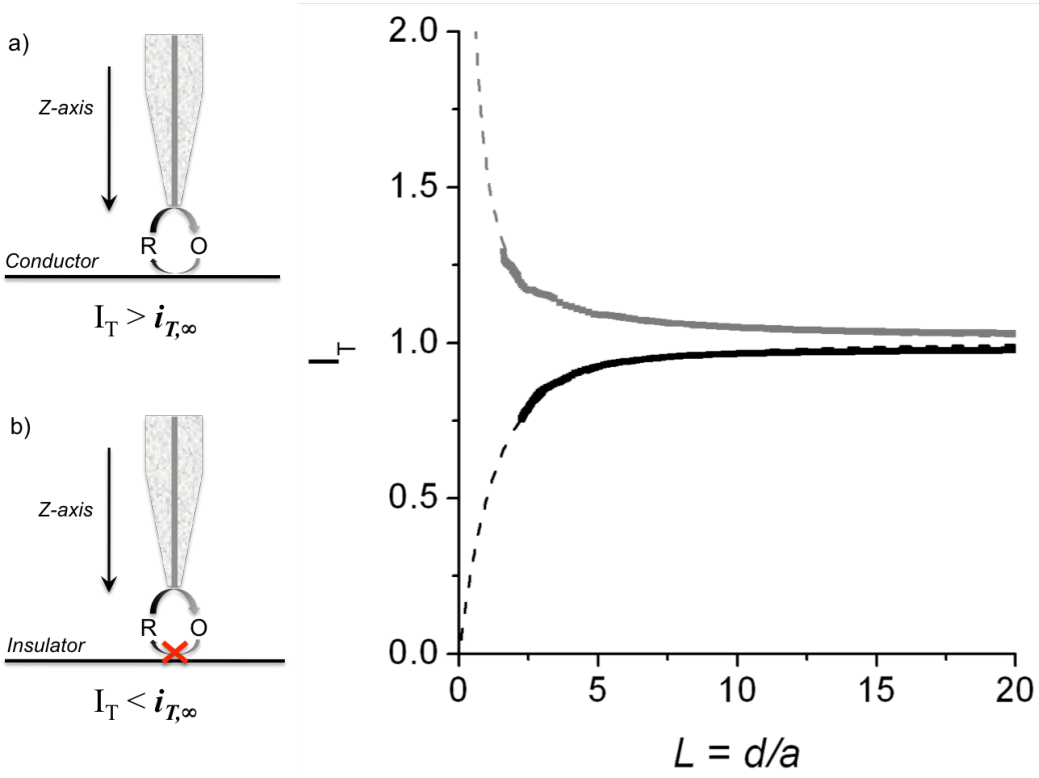

Figure 3. Schematic representation of the probe movement along z axis toward a conductor material (a) and an insulating material (b). Experimental (dots) and theoretical (dashed lines) approach curves for a pure positive (grey) and negative (black) feedback obtained using 10μm Pt UMEs with a RG = 10. The measurements were performed in PBS (pH 7.4) containing 1mM of FcMeOH. *E = + 0.3 V versus Ag/AgCl 3M KCl.*

4.1.5 Collection – Generation Mode

As we have already mentioned above, there are two possible modes for this typology. In the tip generation/substrate collection mode (TG/SC) the tip is held at a potential where an electroactive species is generated; the latter one diffuses across the tip/substrate gap to reach the substrate surface where the applied potential it is different, and the species will react and be collected in function of current generated. A TG/SC experiment includes measurements of both tip and substrate currents. In most cases the substrate is considerably larger than the tip, so that the collection efficiency ($i_{substrate}/i_T$) is essentially 1 (100%) for a stable

TG/SC mode

tip generated species. If the species reacts during its transit from tip to substrate $i_{substrate}/i_T$ becomes smaller, and its change with the separation d allows the determination of the rate constant of homogeneous reaction. These dynamic changes can be recorded as a function of time.

SG/TC mode The alternative mode is the substrate generation-tip collection (SG/TC) mode. In this case at the tip is measured the current due to a product of the reaction that occurs at the substrate. For example a scan in z direction can monitor the concentration profile in the diffusion layer generated by a macroscopic substrate, and ideally the tip should not perturb the diffusion layer at the substrate. While a scan along x or y can identify the parts of the sample in which the reaction takes place or occurs at higher rate. This mode is very useful for monitoring corrosion, enzymatic reactions and other heterogeneous processes that happen at the substrate surface. In this thesis this mode was used to detect at the probe living cell metabolism.

4.2 Applications of SECM

4.2.1 Overview of Some Examples This section illustrates a wide range of applications of SECM that have appeared during these last years. Below, we give an overview and some examples that might help to put the technique in perspective before the detailed treatments of few of them.

(*a) Imaging*: by scanning the tip in x-y plane and measuring current changes, one can obtain both the topographical of conductive and insulating substrates. Of particular interest is the use of SECM to perform "chemical imaging" observing differences in reaction rates at different locations on the surface. This mode is very useful in studying biological materials (e.g. enzymes sites), and other surfaces (see paragraph 4.2.2)[2a].

(*b) UME shape characterization*: by recording voltammogram and approach curves one can identify recessed tips or tips with shape different than a disk[2b].

(*c*) *Homogeneous and heterogeneous kinetics measurements*: by measuring an approach curve or voltammogram with the tip close to a substrate, one can investigate the electron transfer reactions rates at the electrode surface. Moreover, rate reaction constants of tip-generated species, as they diffuse

between tip and conducting substrate, can be determined from steady-state feedback current or TG/SC experiments or by transient measurements[2c].

(*d) Biological systems*: there have been a number of applications of SECM to biological systems. These include imaging of living cells or tissues, studies of enzymatic reactions and investigation of transports of species through skin[2d].

(*e) Reactions that occur on liquid/liquid interfaces, through membranes and thin films*: by employing locally several electrochemical methods one can study ion and electron transfer processes at the interface, the permeability of a membrane and the thickness of a film[2e].

(*f) Reactions that occur at insulating and semiconductor surfaces*: by following the current over time one can monitor rates of surface reactions, such as dissolution, adsorption and surface diffusion[2f].

(*g)* Due to its ability to position the tip with high spatial resolution in three dimensions, SECM can be also used to probe *electrochemistry in very small volumes of solution* (3 ÷ 20 μL), and in thin liquid layers[2g].

(*h) Fabrication*; it is proved that SECM can be used also to carry out metal deposition, metal and semiconductor etching, local polymerization and other surface modification procedures with high spatial resolution[2h].

4.2.2 SECM Imaging

A three-dimensional SECM image could be obtained in two ways: while the tip is scanned in the x-y plane, in the first method, called *constant height mode,* the UME is fixed along the z axis and the current changes are measured in function of the UME location (*x,y,i*). In the second case, called *constant current mode,* the current is fixed and the UME-substrate distance changes, necessary to keep the value constant, are measured in function of the probe location (*x,y,z*)[2a].

The resolution of such images is largely governed by the UME radius, *a*, and the distance between the probe and the sample, *d*. Smaller UME size and lower UME-sample operational distances increase the resolution of the image. The *constant current mode* is tricky to perform, because small electrodes are very delicate, and there might be irregularities in the sample surface, or a tilt of the substrate that can cause a "tip crash" during scanning[11]. While, in *constant height mode*, it is useful to keep the UME at a known distance from the sample in order to avoid any kind of damages.

Probe Approach Curve mode allows the electric probe to approach the surface

of the substrate, and it might be useful for studying surface processes as well. The step size is automatically adjusted to permit fast surface approach for larger distances (by using stepper motors), and for finer z-control movements over short distances a vertical piezo positioner is used. The current can be automatically stopped at a fixed percentage (we usually use ± 25%) of the steady-state current in order to avoid the probe touching the surface.

Probe Scan Curve mode controls the probe movement along x, y, and z direction, while the probe and substrate potentials are controlled and currents are measured. The rate of the UME movement has to be chosen in order to permit the reaction to take place at the electrode in steady state during scanning. By using this mode, we are able to measure flows through membranes and investigate local transport properties and kinetic parameters of intracellular enzymatic redox processes, such as for cellular respiration and metabolism.

SECM, such as STM and AFM, routinely offer μm resolution images of surface structures in bulk electrolyte solutions; however, SECM remains unique because, beside topography, it provides also images of local chemical and electrochemical reactivity of surface features. Since its response is also related to the rates of the heterogeneous reactions at the substrate. In particular, it is useful in identifying and understanding functional aspects of several substrate structures, such as membranes, polymers, leaves, films and biological systems.

4.3 Biological Systems

4.3.1 Introduction

The last two decades have seen the development of several SECM-based approaches in order to *i)* study the charge transfer reactions in biological systems, such as immobilized enzymes[12] and processes referred to whole cells[13,14], *ii)* map cellular redox activities[6,15,16] and cellular metabolism[17-19], and *iii)* image topography of biological specimens or biomolecules[20,21].

The two main advantages that make SECM suitable for investigating biological system are: (*1*) the measurements may be carried out in buffered solutions or also directly in cell culture medium, a preferred environment for most biological samples; (*2*) SECM is a SPM working in no contact mode, thus the interference with the sample is much lower in respect to other SPM techniques,

such as AFM or STM (Figure 4). The next paragraph presents just few biological SECM applications, selected from a broader range, mainly related on investigation of living cells.

4.3.2 *Experiments on Single Living Cells*

The use of SECM to study living cells offers several unique opportunities owing to the wide range of analytes that may be detected by the suitable choice of the UME. The technique is not invasive, sensitive, quantitative and capable of a good temporal and spatial resolution[2d]. The two main types of experiments conducted on living cells by SECM are generation/collection and amperometric feedback mode measurements[4]. Both of them involve the UME positioning in the proximity of the sample. By using approaches curves, the electrode is positioned at a known distance (*d*) from the plastic bottom Petri dish, on which living cells were cultured at low density to permit the imaging of single cells without interferences from neighbouring ones. The approach curve on plastic dish gives a negative feedback because the UME, which is used to oxidize (or to reduce) the redox species added in the electrolytic solution, is approaching an insulating material. Most of SECM profiles and images of living cells reported in literature[6,11-26], were obtained in *constant height mode,* where the probe is fixed on z and moved horizontally in the x-y plane above the substrate surface. Using SECM measurements, one can map *i)* the redox reactivity of a cell[6,15-16], *ii)* image the cell topography under either positive or negative feedback conditions[18-21], and *iii)* measure the fluxes of oxygen[18-21], ATP[22] and other metabolites (e.g. glucose and lactate)[17] across cell membrane.

A serious problem of using constant-height mode for cells imaging arises from the significant variations in height, size and shape among different cells. For example, among the scanned cells there can be some bigger than others, therefore it is challenging to get a high-resolution image of a heterogeneous field of cells without damaging any of them, and at the same time, if the distance UME-dish is too large, some flat cells may be not clearly imaged. One way to obviate this difficulty is to scan the dish at a distance with a small percentage of negative feedback, ensuring the imaging capability and a relative large UME-dish separation of scan. The second procedure is to scan a relative small area. The measurements in this work were carried out directly in the cell growth media without the serum, that it has been shown to disturb the electrical

signal (see *Chapter 6.1.8*) or in phosphate buffered saline (pH 7.4).

Monitoring Cellular Redox Balance

Imaging of cells in feedback mode could be used to measure the cell redox reactivity. SECM can monitor the release of redox species from living cells or the interaction of exogenously added redox species (i.e. redox mediators) with living cells providing information on cellular metabolism and/or topography. In case of a redox mediator that does not interact with the living cell, the recorded SECM current decreases while approaching the cell resulting in a purely negative feedback[15]. In this way cellular topography contribution can be mapped in every SECM measurement (see *Chapter 9*). Alternatively, an increase of current - with respect to the purely negative feedback - may be recorded when the redox mediator reacts with some cellular component capable to regenerate the redox mediator back to its pristine form (regeneration current)[23]. The electrochemical signal reflects the thermodynamic equilibrium involving the complex interacting with the redox systems present within the cell. The analysis of cellular redox balance is useful to quantify the changes of redox species associated for example to oncogene expression and malignant phenotypes[23]. Whereas, generation/collection mode usually refers to experiments that measure redox active or electroactive species, directly or indirectly, produced or consumed by the cell.

Monitoring Cellular Respiration

One of the main examples of SG/TC mode used in cell analysis is the study of the respiratory activity of a single cell[16], which probes the oxygen gradient concentration near the cell surface[18-19]. Also others redox species, capable of participating in the electron transport chain, might be monitored[17-22]. A lot of research groups reported investigation on oxygen consumption in a wide variety of living cells and living systems. By measuring the rate of oxygen consumption, some authors addressed a number of biomedical problems from the drug sensitivity of cancer cells[24] to viability of bovine embryos[25] and mitochondrial respiration in neuronal cells[26].

In our case the electrochemical detection of O_2 in normal and cancer cells has been investigated using a 10 μm Pt UME tip. When a potential of -0.7V is applied, the reduction of O_2 generating a current that is proportional to the amount of local O_2 concentration (see *Chapter 11*):

$$O_2 + 2\,H_2O + 2e^- \rightarrow H_2O_2 + 2\,OH^-$$

Low currents correspond to low oxygen levels, and such areas coincide with the locations of the living cells. Using this approach, some drugs, able to interact with the mitochondrial respiration chain, were employed to investigate the respiration capability of both cancer and normal cells.

Monitoring Cellular Metabolism

Another main application of the tip collection mode is the study of the cellular metabolism at single cell level, by probing gradient concentration of some metabolites, such as ATP[22], glucose and lactate[17], in the close proximity of cell surface. For real-time quantitative measurements of glucose and lactate on living cells, enzyme-based microelectrode biosensors were used (see *Chapters 5 and 6*). Such biosensors are very suitable for this type of investigation because enzymes achieve molecular recognition of substrates (i.e. analytes of interest) based on structural complementarity and they offer high selectivity toward a single analyte optimized by natural evolution[17]. The electrode efficiency depends on: *i)* the enzyme concentration entrapped into the polymer film attached to the probe, *ii)* the ability of the matrix to recycle the enzyme by reducing/oxidizing it and *iii)* shuttling the electrons to the electrode surface through the enzymatic layer.

Cliffel and co-worker[17] have manufactured enzyme UME biosensors for SECM use in detection of lactate and glucose. By employing such devices they obtained glucose uptake and lactate release profiles of single cancer cells as a proof of concept for the application of SECM toward the study of basic metabolic processes that are affected by disease in cancerous cells.

Inspired by Cliffel's work, in this work several methods of enzyme immobilization (e.g. cross-linking and electropolymerization) were investigated in order to achieve the best sensors in terms of sensitivity, response time, linear range and stability. By coupling these obtained sensitive and non-invasive enzyme-based UME biosensors with SECM, a further knowledge of metabolic alterations on cancer cells is provided. Indeed, glucose uptake and lactate release on both transformed and normal human breast cells were monitored, with high spatial and time resolutions, providing evidence about the glycolytic switching present in tumors. Follow out the metabolic differences between cancer and normal cells could be a powerful tool also in clinical application: for example for detecting cancer cells among neighbouring normal ones in patient biopsies.

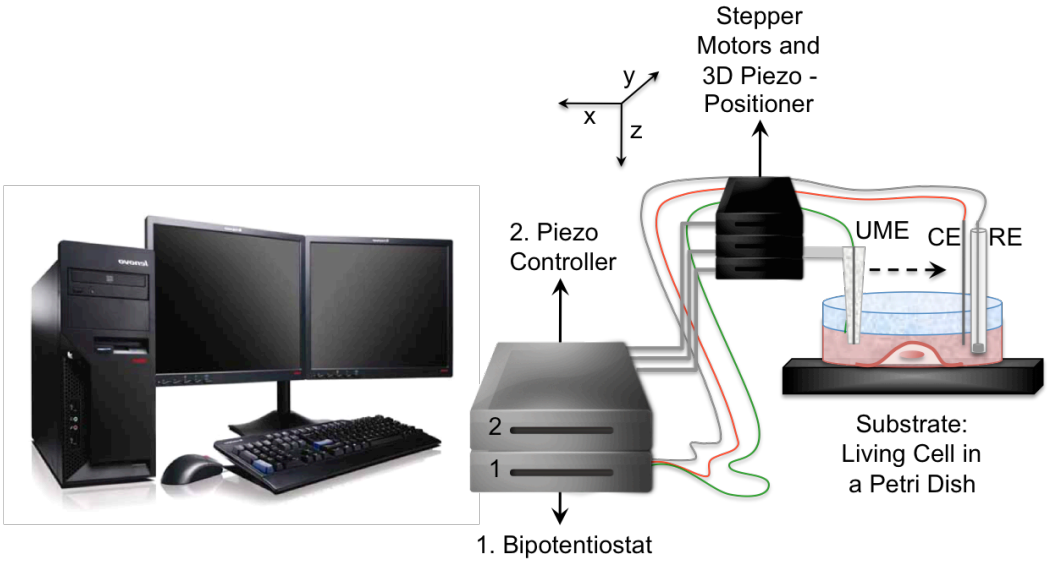

Figure 4. Block diagram of the BioSECM apparatus. Stepper motors and 3D piezo positioner control the movement of the probe: 10 μm Pt UME, which is the working electrode, CE (counter or auxiliary electrode) is a Pt wire, RE (reference electrode) is Ag/AgCl 3M KCl. The solution of analysis for metabolic measurements was chosen *ad hoc* to avoid perturbation of the cellular status (see *Chapter 6.1.8*). The UME can be modified by attaching enzymes, such as *glucose oxidase* and *lactate oxidase*, in order to monitor glucose and lactate level above a single living cell see (*Chapter 5* and *6*).

References

[1] (a) Bard AJ, Fan F-RF, Kwak J, Lev O, Scanning Electrochemical Microscopy. Introduction and principles. *Anal. Chem*. 61, pp. 132-138 (1989) (b) Kwak J, Bard AJ, Scanning Electrochemical Microscopy. Apparatus and two-dimensional scans of conductive and insulating substrates. *Anal. Chem*. 61, pp. 1794-1799 (1989)

[2] Bard AJ, Introduction and principles (Chapter 1). *Scanning Electrochemical Microscopy*. Bard AJ, Mirkin MV (Eds.), Marcel Dekker, New York (2001) (a) Fan F-RF, SECM Imaging (Chapter 4), (b) Mirkin MV, Theory (Chapter 5), (c) Borgwarth K, Heinze J, Heterogeneous electron transfer reactions (Chapter 6) – Unwin PR, Kinetics of homogeneous reactions coupled to heterogeneous electron tranfer (Chapter 7), (d) Horrocks BR, Wittstock G, Biological System (Chapter 11), (e) Mirkin MV, Tsionsky M, Charge-Transfer at the liquid/liquid interface (Chapter 8) – Bath BD, White BH, Scott ER, Imaging molecular transport across membranes (Chapter 9), (f) Macpherson JV, Unwin PR, Probing reactions at solid/liquid interfaces (Chapter 12), (h) Mandler D, Micro- and nanopetterning using the scanning electrochemical microscope (Chapter 13).

[3] Amemiya S, Bard AJ, Fan F-RF, Mirkin MV, Unwin PR, Scanning Electrochemical Microscopy. *Annu. Rev. Anal. Chem*. 1, pp. 95-131 (2008)

[4] (a) Sun P, Laforge FO, Mirkin MV, Scanning Electrochemical Microscopy in the 21st century. *Phys. Chem. Chem. Phys*. 9, pp. 802-823 (2007) (b) Mirkin MV, Nogala W, Velmurugan J, Wang Y, Scanning Electrochemical Microscopy in the 21st century. Update 1: five years after. *Phys. Chem. Chem. Phys*. 13, pp. 21196-21212 (2011)

[5] Tsionky M, Zhou J, Amemiya S, Fan F-RF, Bard JA, Dryfe R, Scanning Electrochemical Microscopy. Application of SECM to the study of charge transfer though bilayers lipid membranes. *Anal. Chem*. 71, pp. 4300-4305 (1999)

[6] Liu B, Rotenberg SA, Mirkin MV, Scanning Electrochemical Microscopy of living cells: different redox activities of nonmetastatic and metastatic human breast cells. *PNAS*. 97:18, pp. 9855-9860 (2000)

[7] http://www.wittstock.chemie.uni-oldenburg.de/gunther.wittstock/en/index.html

[8] (a) Wightman RM, Wipf DO, Electrochemistry at ultramicroelectrodes. *Electrochemical Chemistry*, Vol. 15, pp. 267-353 Bard AJ (Ed.) Marcel Dekker, New York (1898) (b) Montenegro MI, Queiròs MA, Daschbach JL (Eds.), *Microelectrodes: Theory and Applications*. Kluwer Academic Publisher, Dordrecht, Netherlands (1991) (c) Heinze J,

Ultramicroelectrodes in electrochemistry. *Angew. Chem. Int. Ed*. 32, pp. 1268-1288 (1993) (d) Forster RJ, Microelectrodes: new dimensions in electrochemistry. *Chem. Soc. Rev*. 23, pp. 289-297 (1994) (e) Zoski CG, Steady-state voltammetry (Chapter 6). *Modern Techniques in Electroanalysis*. Vanysek P (Ed.), Wiley-Interscience, New York (1996) (e) Zoski CG, Ultramicroelectrodes: design, characterization, fabrication. *Electroanalysis*. 14, pp. 1041-1051 (2002)

[9] Koichi A, Theory of Ultramicroelectrodes. *Electroanalysis*. 5, pp. 627-639 (1993)

[10] Mirkin MV, Fan F-RF, Bard AJ, Scanning Electrochemical Microscopy. 13 Evaluation of the tip shapes of nm-size microelectrodes. *J. Electroanal. Chem*. 328, pp.47-62 (1992)

[11] Takahashi Y, Shevchuck AI, Novak P, Babakinejad B, Macpherson J, Unwin PR, Shiku H, Gorelik J, Klenerman D, Korchev YE, Matsue T, Topographical and electrochemical nanoscale imaging of living cells using voltage-switching mode scanning electrochemical microscopy. *PNAS*. 109:29, pp. 11540-11545 (2012)

[12] Wittstock G, Schumann W, Formation and imaging of microscopic enzymatically active spots on an alkanethiolate-covered gold electrode by scanning electrochemical microscopy. *Anal. Chem*. 65, pp. 3605-3614 (1993)

[13] Kurulugama RT, Wipf DO, Takacs SA, Pongmayteegul S, Garris PA, Baur JE, Scanning electrochemical microscopy of model neurons: constant distance imaging. *Anal. Chem*. 77, pp. 1111-1117 (2005)

[14] (a) Liu B, Cheng W, Rotenberg A, Mirkin MV, Scanning electrochemical microscopy of living cells. Part 4. Mechanistic study of charge transfer reactions in human breast cells. *Anal. Chem*. 74, pp. 6340-6348 (2002) (b) Liu B, Cheng W, Rotenberg A, Mirkin MV, Scanning electrochemical microscopy of living cells. Part 5. Imaging of fields of normal and metastatic human breast cells. *Anal. Chem*. 75, pp. 4148-4154 (2003)

[15] Liu B, Cheng W, Rotenberg A, Mirkin MV, Scanning electrochemical microscopy of living cells. Part 2. Imaging redox and acid/basic reactivities. *J. Electroanal. Chem*. 500, pp. 590-597 (2001)

[16] (a) Yakusawa T, Kondo Y, Uchida I, Matsue T, Imaging of cellular activity of single cultured cells by scanning electrochemical microscopy. *Chem. Lett*. pp. 767-768 (1998) (b) Kaya T, Torisawa Y, Oyamatsu D, Nishizawa M, Matsue T, Monitoring the cellular activity of a cultured single cell by scanning electrochemical microscopy (SECM). A comparison with fluorescence viability monitoring. *Biosensors and Bioelectronics*. 18, pp. 1379-1383 (2003) (c) Yakusawa T, Kaya T, Matsue T, Imaging of photosynthetic and respiratory activity of a single algal protoplast by scanning electrochemical microscopy.

Chem. Lett. pp. 975-976 (1999)

[17] Ciobanu M, Taylor DE Jr, Wilburn JP, Cliffel DE, Glucose and lactate biosensors for scanning electrochemical microscopy imaging of single live cells. *Anal. Chem*. 80, pp. 2717-2727 (2008)

[18] Nebel M, Grützke S, Diab N, Schulte A, Schuhmann W, Microelectrochemical visualization of oxygen consumption of single living cells. *Faraday Discussion*. 164:19, pp. 19-32 (2013)

[19] Nebel M, Grützke S, Diab N, Schulte A, Schuhmann W, Visualization of oxygen consumption of single living cells by scanning electrochemical microscopy: the influence of the faraic tip reaction. *Angew. Chem*. 52, pp. 6335-6338 (2013).

[20] Yakusawa T, Kaya T, Matsue T, Dual imaging of topography and imaging of photosynthetic activity of a single protoplast by scanning electrochemical microscopy. *Anal. Chem*. 71, pp. 4637-4641 (1999)

[21] Schulte A, Nebel M, Schuhmann W, Single live cell topography and activity imaging with the shear-force-based constant-distance scanning electrochemical microscope (Chapter 12). *Methods in Enzymology*. Vol. 504, ©Elsevier Inc. (2012)

[22] Hecht E, Liedert A, Ignatius A, Mizaikoff B, Kranz C, Local detection of mechanically induced ATP release from bone cells with ATP microbiosensors. *Biosensors and Bioelectronics*. 44, pp. 27-33 (2013)

[23] Rapino S, Marcu R, Bigi A, Soldà A, Marcaccio M, Paolucci F, Pelicci PG, Giorgio M, Scanning electrochemical microscopy reveals cancer cell redox state. Paper revise and resubmit to *Electrochimica Acta*.

[24] Y-S Torisawa, Kaya T, Takii Y, Oyamatsu D, Nishizawa M, Matsue T, Scanning electrochemical microscopy – based drug sensitivity test for a cell culture integrated in silicon micro-structures. *Anal. Chem*. 75:9, pp. 2154-2158 (2003)

[25] Shiku H, Shiraishi T, Ohya H, Matsue T, Abe H, Hoshi H, Kobayashi M, Oxygen consumption of single bovine embryos probed with scanning electrochemical microscopy. *Anal. Chem*. 73, pp. 3751-3759 (2001)

[26] Takii Y, Takoh K, Nishizawa M, Matsue T, Characterization of local respiratory activity of PC12 neuronal cell by scanning electrochemical microscopy. *Electrochim. Acta*. 48, pp. 3381-3385 (2003)

Chapter 5

Enzyme-Based Ultramicroelectrode Biosensors

Abstract

Nowadays real time quantitative measurements of metabolites at single cell level, both *in vitro* in culture systems and *in vivo,* are feasible by the use of microsensors. In particular, enzyme-based micro-biosensors offer high selectivity toward a single analyte, optimized by natural evolution, and they give the opportunity to improve sensitivity, time scale and information content. Enzymes achieve molecular recognition of substrates (i.e. analytes of interest) based on structural complementarity, leaving little space for error. They catalyze with high specificity chemical reactions and for this reason they have been successfully widely employed in sensor designs. Moreover, enzyme-based amperometric biosensors are irreplaceable tools for the non-invasive study of metabolism at the cellular level.

Key words Enzyme electrode, Biosensor, Glucose Oxidase, Lactate Oxidase, Immobilization Techniques

5.1 Microelectrodes Designs for Enzyme-Based Biosensors

5.1.1 Introduction

An electrochemical biosensor is defined as a "*self-contained integrated device, which is capable of providing specific quantitative or semi-quantitative information using a biological recognition element retained in direct spatial contact with an electrochemical transduction element*"[1]. It is composed by a biological recognition element in contact with an electrochemical transduction element[2]. The sensitive biological element (e.g. tissues, cells, microorganisms, organelles, cell receptors, enzymes, antibodies and nucleic acids) is the component that interacts (binds or recognizes) with the analyte under detection, whereas the electrochemical transducer is designed to transform the signal, resulting from the interaction of the analyte

present into the surrounding medium with the biological element molecule, into an easily quantifiable electrical signal. In other setups the transducer can also be optical, acoustic, calorimetric, thermometric, piezoelectric and magnetic[2]. Translating the recognition of a molecule into an electrical signal can be performed in at least two different ways: *(1)* In many cases, the analyte can be bound to the biological receptor utilizing a very specific binding affinity (e.g. antibody/antigen interaction). This recognition results in a physiochemical change, that in combination with a tracer, such as fluorescent molecule, enzyme or radioisotope can generate a signal. There are some limitations in using this type of sensors because the binding capacity is strongly affected by environmental conditions, such as pH and temperature, and generally the interactions are irreversible[3]. *(2)* Most electrochemical biosensors, presently used in several fields, are based on the specific binding capabilities and catalytic activity of enzymes, which are directly immobilized on the surface of an electrode or microelectrode. Analyte detection is achieved in different ways: *i)* enzyme converts the analyte into a product that is electrochemically detectable, *ii)* enzyme is inhibited or activated by the specific analyte producing an electric signal, and *iii)* the changes of enzyme's properties due to the interaction with the analyte might be monitored. This type of biosensors has many advantages: first of all, they offer a high selectivity toward a single analyte, optimized by natural evolution. Enzymes achieve molecular recognition of substrates with high sensitivity (the analytes of interest) based on their structural complementarity, leaving little space for error. Thanks to the small electrode dimensions, they can enhance the time scale resolution and information content. Moreover, such biosensors catalyze with high specificity a broad range of chemical reactions and enzymes are not consumed during these reactions, thus the biosensor can be easily reused in continuous. For all of these reasons they have been widely and successfully employed in sensor designs. However, one of the main disadvantages of enzyme biosensors is their lifetime, which is limited by the enzyme stability.

Antibody – Antigen Interaction

Enzymatic Interaction

5.1.2 Biosensors in Medical Diagnostic

Leland C. Clark Jr. was an American biochemist and he is considered the "father of biosensors", inventing the first electrochemical device for measuring oxygen in blood, water and other liquids; today this polarographic

device is known as the *Clark electrode*. Some years later, Clark used this electrode for manufacturing the first biosensor that measured glucose concentration in blood, by monitoring the decrease of oxygen concentration due to the enzymatic activity of glucose oxidase[4].

Since then, a huge number of biosensors have appeared in literature and a great number with an application in medical diagnostics. Currently, 80% of the commercial devices based on biosensors are used in this domain[5], starting with the first commercial apparatus for monitoring glycaemia in diabetic patients produced by Yellow Spring Instruments (YSI Inc. 1975).

Apart from the impressive space occupied in the market and in literature by the glucose biosensors (Table 1) and other enzyme-based catalytic biosensors or immunosensors, recently DNA-based sensing has appeared for real applications in clinical diagnostic to detect the presence of pathogenic species responsible of infections, to identify polymorphism and to detect point mutations[6]. Despite the huge number of publications on biosensors in the diagnostics field, the commercialization of this technology is only minimally feasible, besides the blood glucose and lactate biosensors and few others. This is due to the fact that the validation of the procedures has to be conducted in real samples to prove the efficacy of the biosensors, in order to transfer these technologies from the laboratory to the diagnostics market[7].

Table 1. Market-leading biosensor companies and target/sector involved[2].

Company	***Target/sector***
Abbott (Molecular Diagnostics and Diabetes Care)	Glucose
Affymetrix	Pharmaceutical and general bioscience research
Applied and HTS Biosystems	Affinity chip
ARKRAY, Inc.	Glucose
Bayer Diagnostics/ Kyoto Daiichi/ Menarini	Glucose
Becton Dickinson	Glucose
Biacore	Affinity sensors for pharmaceutical
Biosite	Medical
Eppendorf	Glucose and Lactate
LifeScan	Glucose
Molecular Devices	Diagnostics
Nova Biomedical	Glucose, Urea, lactate and creatinine
Roche Diagnostics	Glucose
YSI	Glucose and lactate

Briefly, we could mention just the main fields of biosensor applications[1-2]:

1. Biosensors for metabolites analysis (glucose, lactate, O_2, etc.);
2. Biosensors for cancer biomarkers, such as prostate specific antigen (PSA), interleukin-6 (IL-6) and interleukin-8 (IL-8);
3. Biosensors for hormones detection (e.g. progesterone);
4. Biosensors for pathogens, such as virus, fungus and bacteria (i.e. *Salmonella* and *Listeria monocytogenes*) in food and water;
5. Determination of drug and drug metabolism in human body and in food;
6. Drug discovery and evaluation of biological activity of new compounds;
7. Routine analytical measurements of folic acid, biotin, vitamins, etc.;
8. Biosensors for cardiovascular diseases (e.g. *troponin I and troponin T*);
9. Nucleic acid biosensors to detect mutations of DNA/RNA;
10. Biosensors for toxic substances before and after bioremediation.

5.1.3 Crucial Features

Over the last decade the research activity in biosensors area strikingly increased in the clinical field. Nowadays, a lot of efforts are dedicated to the miniaturization of devices, without affecting sensitivity.

An optimal enzyme-based UME biosensor must have crucial features; high sensitivity (seen as current response correlated to analytes presence), low detection limits (in the order of μM to nM), fast response time (≈ sec), excellent spatial resolution (μm), good permeability, stability and reproducibility, reduced cost, easy-manufacturing and causing minimal perturbations to surroundings.

The main goal of this work is to develop a method to study non-invasively living cell metabolism with a high spatial and temporal resolution. The technique is based on functional imaging of cells using SECM coupled with enzyme-based UME biosensors for detecting metabolite gradients at single cell level. This system requires sensor specificity with appropriate spatial and temporal resolution within acceptable sensitivity and limits of detection (LOD) for each analyte. It is necessary to achieve optimum balance among all the figures of merit for our specific application. The major part of the thesis work was dedicated to the optimization of the enzyme immobilization onto UME probes and in the next sections some of the developed methods are discussed and described in details.

5.2 Oxidase-Based Biodetection

5.2.1 Introduction

One of the most spread class of enzyme-based biosensor are based on enzymes belonging to the class of oxidoreductases, which is directly immobilized on the electrode surface.

Cofactors

Oxidoreductases are enzymes that catalyze the transfer of electrons from a substrate to a *cofactor*, a molecule contained within the polypeptidic chain. There are a wide variety of cofactors like iron, copper ions, iron-containing hemes, but flavins (e.g. flavin adenine dinucleotide, $FAD/FADH_2$, or mononucleotide, FMN) and nicotidamines (e.g. NAD^+/NADH or $NADP^+$/NADPH) are the most frequently present[8].

Oxidases

Twenty-two different subtypes of oxidoreductases have been identified[9], but only *oxidases*, enzymes that use O_2 as electron acceptor, have been employed so far for biosensors in metabolites detection. For FAD-dependent oxidases, the oxidation of the substrate follows a two-step reaction:

$$Substrate + Enzyme\text{-}FAD \rightarrow Oxidized\ product + Enzyme\text{-}FADH_2$$

$$Enzyme\text{-}FADH_2 + O_2 \rightarrow Enzyme\text{-}FAD + H_2O_2$$

From an electrochemical point of view, these enzymes are well suited for the design of electrical biosensors, because they convert a molecule, which is not inherently electroactive (the substrate), into an active molecule such as hydrogen peroxide, which can be readily re-oxidised into molecular oxygen on the electrode surface, producing an electric signal:

$$H_2O_2 \rightarrow 2H^+ + O_2 + 2e^-$$

The current, which can be recorded by a potentiostat, is directly proportional to the substrate/analyte concentration.

Another advantage of using oxidases is that they employ oxygen as cosubstrate, which is available in non-limiting concentrations both in most biological media and *in vivo*. Only in particular conditions, such as hypoxia and ischemia (low pO_2), the enzymatic reaction can become O_2-limited, which might impact the performance of the electrode[10]. Additionally, it is worth to mention that oxidases activity is pH-dependent[11] and temperature-dependent[12];

typically, it increases with the temperature, until the enzyme is denatured, and its optimal pH range is from 5.0 to 7.5[11].

There are many oxidase enzymes available in nature, with a high number of potential uses. Since we are studying cell metabolism, we are looking for glucose uptake and lactate release at single cell level. Therefore, we mainly focused our attention on: *glucose oxidase* and *lactate oxidase*

5.2.2 GOx

Glucose oxidase enzyme (GOx) is a β-D-glucose:oxygen 1-oxidoreductase, which catalyzes the oxidation of β-D-glucose to β-D-glucono-δ-lactone, by utilizing oxygen as an electron acceptor with simultaneous production of hydrogen peroxide. GOx is a flavoprotein (FAD-dependent enzyme), thus the catalytic reaction can be divided into a reductive and an oxidative step[13]:

$$\beta\text{-}D\text{-}glucose + GOx - FAD \rightarrow \beta\text{-}D\text{-}glucono\text{-}\delta\text{-}lactone + GOx - FADH_2$$
$$GOx - FADH_2 + O_2 \rightarrow GOx - FAD + H_2O_2$$

GOx is a dimeric glycoprotein consisting of two identical polypeptide chain subunits that are covalently linked together via disulfide bond. Its molecular weight ranges from approximately 130 to 175 kDa[14]. It binds specifically to β-D-glucose and does not act on α-D-glucose (the other hemiacetal form of glucose); however, it is able to oxidise all of the glucose in solution (pH 7.0) because the equilibrium between α and β anomers is driven towards the β-side as it consumed in the reactions[13].

The most common microbial source for fermentative production of GOx is the *Aspergillus niger*[14]. There are several types of GOx commercially available, which differ for the number of enzymatic units per gram. We investigated three of them: *i)* GOx Type II (Sigma) 15÷50 U/mg solid, *ii)* GOx Type X-S (Sigma) 100÷250 U/mg solid and *iii)* GOx (Calbiochem®) ≥ 250 U/mg solid. By adopting cross-linking immobilization method (see *paragraph 5.3.3*), we compared the three enzymes in order to find the best one for our further studies on cellular metabolism. We observed that, once the enzyme is attached to the electrode surface, Calbiochem® GOx shows the best sensitivity but the highest response time, while GOx Type X-S displays the best compromise (Table 2). Therefore, we have decided to use the latter for the entire project (see *Chapter 6* for the procedure of characterization method).

Table 2. Comparison among several types of commercial GOx drop-cast on 10μm Pt UME

Enzyme	U/mg @ Lot	Sensitivity (pA/1mM of glucose)	Response Time (sec)
GOx Type II	17.3	78.6	2.3
GOx Type X-S	123.9	275.4	8.1
GOx Calbiochem®	312	343.1	19.5

5.2.3 LOx

Lactate oxidase (LOx) belongs to the α-hydroxy-acid oxidase flavoenzyme (FMN) family, which catalyzes the conversion of α-hydroxy acids to α-keto acids via a two-electron reduction of the FMN cofactor. Although the details of the mechanism are still under debate, the most widely accepted model is a ping-pong mechanism with sequential reductive and oxidative steps: the first step involves the production of α-keto molecule (pyruvate) from the α-hydroxy substrate (lactate), followed by the transfer of two electrons and two protons from the reduced cofactor to molecular oxygen to generate hydrogen peroxide, and ultimately to regenerate the oxidized cofactor, as follow[15]:

$$L\text{-}lactate + LOx - FMN \rightarrow pyruvate + LOx - FMNH_2$$

$$LOx - FAMNH_2 + O_2 \rightarrow LOx - FMN + H_2O_2$$

LOx is believed to be active as a tetramer (Figure 1). Each tetramer forms a biologically active unit and its molecular weight is approximately 50 kDa[16]. Most of the commercially produced LOx is isolated from *Pediococcus species* (Sigma) with an enzymatic activity ≥ 20U/mg solid.

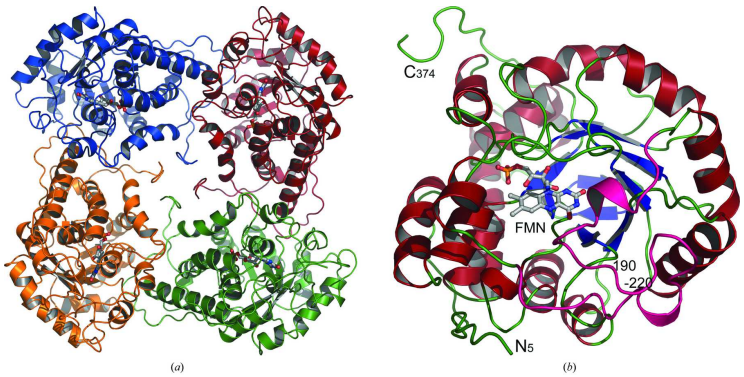

Figure 1. Overall structure of L-lactate oxidase. On the left the tetramer, describing half of the asymmetric unit. On the right the monomer structure viewed from the active sit where FMN cofactor is located [RCSB Protein Data Bank].

5.2.4 Electrode Materials for H_2O_2 Detection

The classical electrode material for the H_2O_2 detection is platinum. H_2O_2 oxidation has to be shown to be catalyzed by the presence of platinum oxides (Pt-$(OH)_2$) on the surface of the electrode[10].

$$H_2O_2 + Pt(OH)_2 \rightarrow Pt + 2H_2O + O_2$$

$$Pt + 2H_2O \rightarrow Pt(OH)_2 + 2H^+ + 2e^-$$

At platinum electrodes, H_2O_2 is oxidised at potentials above 0.4 V (anodic current) and is reduced lower than 0.1 V (cathodic current). Generally, in most microelectrode biosensors recording schemes, the current is recorded at a constant potential of 0.5 V ÷ 0.7 V vs. Ag/AgCl to achieve continuous and fast-response H_2O_2 detection.

A similar reaction can occur on other noble metals for examples palladium, ruthenium, or rhodium, but not on gold, which yields very low H_2O_2 oxidation current. Even with carbon the H_2O_2 detection is unfavourable; there is no detectable reduction and oxidation starts at much higher potential (≈ 0.75V). However, Pt is a rather soft metal, therefore, to avoid the material breach, for *in vivo* microelectrode applications or implantable devices, more rigid Pt/Ir (90:10) alloys are currently employed[10]. An elegant compromise for H_2O_2 detection consists on electrodepositing a thin layer of Pt (or another suitable metal) on carbon electrode; this procedure combines the valuable mechanical properties of carbon fibres with the optimal electrochemical properties of Pt.

5.3 Immobilization Methods & Protocols

5.3.1 Introduction

In order to transduce the signal, enzyme has to be confined on the electrode surface. Enzyme immobilization is a key step in biosensor preparation that impacts on the overall performance. Among the wide variety of techniques employable, we have investigated: ***i)*** covalent ***immobilization by cross-linking*** with glutaraldehyde, ***ii) enzyme entrapment in polymer matrices*** by means of various polymers (e.g. *o*-aminophenol, polypyrrole and derivates), and ***iii) adsorption through physical or electrostatic interactions*** (e.g. electrophoretic paints). For biological applications, cross-linking and electropolymerization are the most widely used methods, because of their reliability and stability.

In this section, the influence of the immobilization method developed for biosensor construction on its final operating parameters is explored. Moreover, the optimized experimental protocols for each method both applied to glucose oxidase (GOx) and lactate oxidase (LOx)-based biosensor are described in detail. All of them are compared in terms of sensitivity, LOD, linear range, response time, stability, reproducibility and spatial resolution. We also studied the permeability of the hydrogel matrix, the effects of the analysis solutions on the biosensor performance and the kinetics of the system (see *Chapter 6*).

5.3.2 Materials

The materials were purchased as follows: β-D-glucose BioXtra ≥ 99.5%, Sodium L-lactate ≥ 99%, glucose oxidase (GOx) Type X-S from *Aspergillus niger* (100-250U/mg), lactate oxidase (LOx) from *Pediococcus species* (37U/mg), glutaric dialdehyde (GDA) as 25% solution in water (GDA), *o*-aminophenol PESTANAL® (oAP), pyrrole ≥ 98% (Pyr), *o*-phenylenediamine (oPD), phenol (Phen), potassium phosphate monobasic and dibasic, acetic acid and sodium acetate, $[Ru(NH_3)_6]Cl_3$ hexaammineruthenium(III)chloride, ferrocenemethanol 97%, ferrocenecarboxylic acid 97%, sodium ferrocyanide, were purchased by Sigma Aldrich. Bovine serum albumin (BSA) from ID Bio, PBS (pH 7.4) and RPMI 1640 medium are from Lonza, DMEM medium (no glucose, no sodium pyruvate, no red phenol) from Gibco, Triton X-100 from VWR, and MQ water from Millipore. Pyrrole-derived monomer used in our studies was kindly supplied by Serge Cosnier's laboratory. The commercially available D-glucose is composed exclusively by α-anomer, due to the high solubility of β-anomer. For this reason the 50 mM glucose stock solutions were allowed to mutarotate at least 24h before using.

5.3.3 First Technique: Cross-linking

Cross-linking is a process based on the covalently binding of two or more molecules. Enzymes present a variety of functional groups that can be readily bound together by many cross-linking agents. This property has been extensively used for biosensor fabrications. The two main chemical functions in an enzyme are the amine ($-NH_2$) and carboxyl (-COOH) groups. Amino groups are present on N-terminal end and on every lysine residue. Similarly, carboxylic groups are present at C-terminal end and on every glutamic and aspartic acid residues. Because they are charged at physiological pH, amino

and carboxyl groups tend to be exposed on the outer surface of the protein, which make them primary candidates for reacting with a cross-linker agent[17]. An important parameter to tune is the distance between the reactive groups of the linker, which determine the flexibility of the protein matrix and the degree of freedom that the enzyme retain once immobilized. Immobilization by covalent linking using glutaraldehyde is one of the most used coupling method in enzyme technology[18-19]. It is a gentle procedure because the reaction proceeds in aqueous buffer solution under conditions close to physiological pH, ionic strength, and temperature[17-18].

GDA

Glutaraldehyde (GDA), a linear 5-carbon dialdehyde, is a small molecule (MW 100), a clear, colourless to pale straw-coloured, pungent oily liquid that is soluble in all proportions in water and alcohol, as well as in organic solvents[18]. GDA is commercial available, cheap and with a high reactivity. Bearing two aldehydes groups, it can rapidly react with amine groups of proteins and enzymes, at around neutral pH, and it is more efficient than other aldehydes in generating thermally and chemically stable ramified three-dimensional network (Figure 2)[19]. The reaction can be accomplished in a few minutes, and the method requires minimal equipment. For these reasons GDA is still used as a reference method on biosensor fabrication, even if it is a very toxic molecule and one should manipulate it with caution; hence, its possible clinical applications are limited[17]. The optimized procedure for immobilizing both GOx and LOx on UME biosensor using GDA is described below. The optimal conditions have been determined by trial and errors because the process is critically dependent on a delicate balance of factors, such as the nature of the enzyme (its lysine content may affect the reactivity with GDA), the pH, the ionic strength of the solution, the temperature, the reaction time, and the concentrations of both enzyme and reagents (GDA and the inert, lysine-rich protein carrier, added in the solution to avoid extensive modification of the enzyme within the matrix)[20-21]. The latter condition should be chosen carefully in order to favour intermolecular cross-linking between enzyme molecules instead of unwanted intra-molecular links. In fact, if low concentrations of enzyme and GDA are used, the system tends to induce intra-molecular cross-linking, by enhancing the probability that the functional groups of GDA will react with the same enzyme molecules[20]. If the

concentration of the cross-linker species is low, the enzyme may be not fixed properly and they would eventually escape from the matrix of the biosensor[20]. Meanwhile, at high GDA concentrations, the extent of cross-linking is high enough to form a tight structure by excluding water molecules to make the enzyme derivative insoluble. The enzymatic activity is found to be inversely proportional to the GDA concentration used, because extensive cross-linking may result in a distortion of the enzyme structure (i.e. the active site conformation)[21]. Because of this distortion, the accessibility and accommodation of the substrate may be reduced, thus affecting the retention of biological activity and the sensitivity of the biosensor[20].

The best biosensor performance was obtained using a final solution of 12:88 enzyme to bovine serum albumin (BSA) mass ratio, which serves as a matrix to protect the oxidase enzyme activity during immobilization[20]. The mixed solution is cross-linked with *1.4% (vol/vol) of GDA*[22-23].

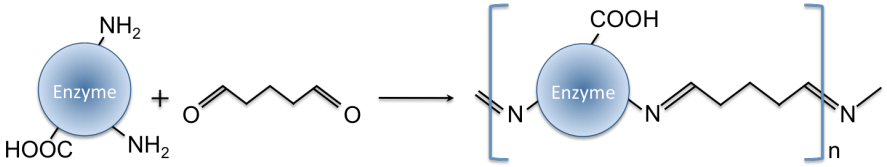

Figure 2. Reaction scheme for protein cross-linking by glutaraldehyde. Aldehyde groups react preferentially with amino groups present within the enzyme to produce covalent bonds.

GDA Protocol

The enzyme (8 mg/mL for GOx or 10 mg/mL for LOx) and BSA (62.5 mg/mL) are dissolved in PBS (pH 7.4) containing 0.02% v/v Triton X-100. After enzyme and BSA are thoroughly dissolved, 14 μL/mL buffer of 25% w/w GDA is added and quickly mixed. This solution, referred to the protein matrix, is set-aside for one minute until it turns slightly more yellow. It is mandatory to prepare a new solution for each biosensor because after a while the enzymatic solution tends to gelify and it is not possible to drop-cast it again. After 1 min, the enzymatic solution is hand-cast onto the surface of the UME by touching for 6-10 minutes the tip of the UME to a tiny droplet (5μL) of the solution deposited in a plastic dish. A thin layer adheres to the UME tip surface and it is let to air-dry for 2h, to prevent that the matrix dissolves or lifts off when used in solution. Optimal drying time vary depending on temperature, humidity and the type of enzyme. The biosensor can be stored at RT until use.

5.3.4 Second Technique: Polymeric Enzyme Entrapment

The basic principle of ***enzyme entrapment*** consists in creating a polymer layer on the electrode surface. The enzyme to be immobilized on the biosensor is added to the monomer solution, and during the polymerization process, enzyme molecules are mechanically, electrostatically entrapped or adsorbed in the matrix created by the polymer. Because there are no strong chemical bonds between enzyme and polymer, but the enzymes are mainly entrapped by physical constraints, it is presumed that such procedures result in better preservation of enzymatic activity[17]. Electropolymerization is a simple and attractive method for biosensor fabrication, and in literature are reported many different procedures to follow[24-36]. Monomers such as *o-aminophenol*, *pyrrole* and *pyrrole-derivatives* (Figure 3) are the most widely used, because they are conductive polymers, stable at RT and they can be easily used with different electrolytes, including aqueous solutions. We have investigated several methods for functionalizing the UME probe: in Table 3 and 4, the protocols are compared in terms of sensitivity and time of fabrication, by changing the type of monomer, the amount of enzyme used and the electrochemical technique. In general, during an electropolymerization process, the applied potential generates reactive radicals that react with neighbouring monomer molecules, thereby producing a polymer layer on the electrode surface. In this way it is easy to control the thickness of the layer, by adjusting the oxidation or reduction time, and the amount of enzyme entrapped into the polymer matrix, by calculating the enzyme remained in the monomer solution[24a]. Additionally, the relatively low potential required for electropolymerization provides sufficiently mild conditions to avoid enzyme denaturation[24a-b].

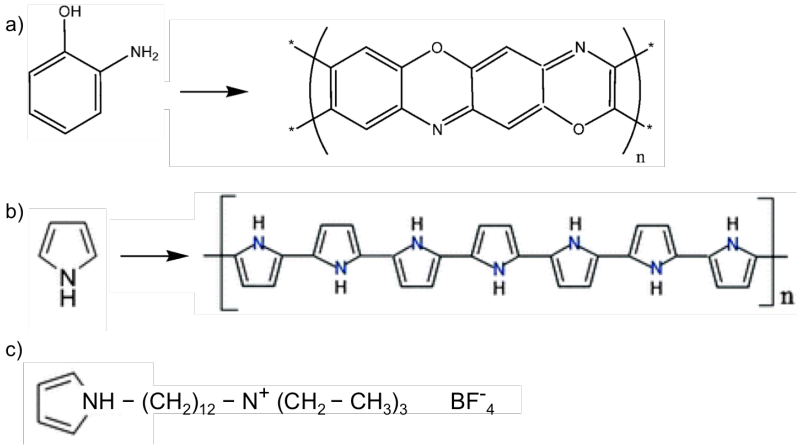

Figure 3. Molecular structures of the main monomers employed: (a) *o*-aminophenol, (b) pyrrole, and (c) the amphiphilic pyrrole derivative, kindly supplied by Cosnier's Lab.

Table 3. Comparison among some electropolymerization methods investigated for GOx 10μm Pt UME biosensor. All the potentials are given vs Ag/AgCl 3M KCl.

#	*Monomer*	*[GOx X-S] (mg/mL)*	*Electrochemical Method (Chap. 4)*	*Time of Fabrication*	*Sensitivity (pA/μM)*	*Ref.*
1	oAP	20	Cyclic voltammetry E = -0.24 ÷ -1.04 V	10 min	0.11	25
2	oAP	8	Cyclic voltammetry E = -0.04 ÷ -0.84 V	10 min	0.10	26
3	oAP	10	Amperometric i-t E = +0.65 V	2 h	0.20	22
4	oAP	0.8	Cyclic voltammetry E = 0.032 ÷ 0.832V	15 cycles at 50mV/s	0.14	27
5	Pyr	1	Double Pulse Amp E_1 = 0V; E_2 = 0.95V	10x t_1 : 5s; t_2 :0.1s	0.01	28
6	Pyr	4	Amperometric i-t E = +0.65 V	300 s	0.01	29
7	Pyr	8	Multi Step Pot. E_1 = 0V; E_2 = 0.95V	10x t_1 : 10s; t_2 :0.1s	0.06	30
8	Pyr	0.5	Amperometric i-t E = +0.62 V	260 s Q = $1.96 \cdot 10^{-7}$C	0.09	24b
9	Pyr	0.9	Chronoamperometry i = 0.05 mA	500 s Q = 25mC/cm^2	0.05	31
10	Pyr-derivate	3.75	Amperometric i-t E = +0.7 V	1000 s	0.015	32-33

Table 4. Comparison among some electropolymerization methods investigated for LOx 10μm Pt UME biosensor. All the potentials are given vs Ag/AgCl 3M KCl.

#	*Monomer*	*[LOx] (mg/mL)*	*Electrochemical Method (Chap. 4)*	*Time of Fabrication*	*Sensitivity (pA/μM)*	*Ref.*
1	oAP	2	Cyclic voltammetry E = 0.0 ÷ 0.8 V	15 cycles at 50mV/s	0.13	27
2	Pyr	2	Amperometric i-t E = +0.62 V	≈ 300 s Q = $1.96 \cdot 10^{-7}$C	0.16	24b
3	Pyr - Phen - oPD	2.8	Amp. E = +0.8 V Amp. E = +0.8 V Amp. E = +0.8 V	60 s 60 s 1800 s	0.11	34
4	Pyr - oPD	1.4	Amp. E = +0.7 V CV E = -0.3 ÷ 0.7V	170 s 20 sw 50mV/s	0.056	35
5	Pyr - oPD	1.4	Amp. E = +0.7 V Amp. E = +0.7 V	170 s 900 s	-	36

Herein the two main protocols based on electropolymerization for GOx biosensor are described in detail. They gave the best compromise for our biosensing setup, with comparable results in term of sensitivity, time of fabrication and enzyme consumption.

oAP Protocol

Protocol #4: *The enzyme (0.8 mg/mL for GOx type X-S) and the o-AP monomer (0.55 mg/mL) are dissolved in 0.2 M acetate buffer pH 5.0. The solution is degassed using Argon bubbling for at least 10 min and the electrochemical polymerization of enzyme film is carried out by cycling in the potential range from 0.032 to 0.832V vs Ag/AgCl 3M KCl at a scan rate of 50 mV/s. The film is grown for 15 cycles. The resulting enzyme electrodes were washed with MQ water and stored in 50 mM phosphate buffer pH 7.0 at RT until use.*

Pyr Protocol

Protocol #8: *enzyme (0.5 mg/mL for GOx type X-S) is dissolved in 0.1 M KCl pH 7.0 containing 0.05 M pyrrole. The solution is degassed using Ar for at least 10 min. Films are grown potentiostatically at 0.671 V vs Ag/AgCl 3M KCl for approximately 5 min. The amount of charge transferred during electropolymerization is measured by on-line integration of anodic current according to Euler's method. The thickness of the film is estimated by assuming that 45 mC/cm^2 of charge yields a film of 0.1 μm*[24-31]. *The resulting enzyme electrodes are washed with MQ water and stored in 50 mM phosphate buffer pH 7.0 at RT until use.*

Regarding LOx, we implemented the previous protocol by adding other two different polymer layers, in order to increase the biosensor sensitivity and to reduce the interferences due to the presence of other species.

Pyr + Phen + oPD Protocol

Protocol #3: *firstly polypyrrole layer is obtained by 1 min electrodeposition from 0.4 M monomer solution in PBS pH 7.4 at 0.8 V vs Ag/AgCl 3M KCl. Successively, a polyphenol layer is deposited, above the previous one, by 1 min electrodeposition from 5 mM monomer solution in PBS 7.4 at 0.8 V vs Ag/AgCl 3M KCl. Finally, a third enzyme layer is formed by 30 min electrodeposition from 5 mM o-phenylenediamine and 2.8 mg/mL of LOx dissolved in 0.2 M acetate buffer pH 5.0 at 0.8 V vs Ag/AgCl 3M KCl. The resulting enzyme electrodes are washed thoroughly with MQ water and stored in 50 mM phosphate buffer pH 7.0 at 4°C until further use.*

The use of an electrodeposited bilayers of polypyrrole and polyphenol between the Pt electrode and the enzyme layer provides satisfactory elimination of interferences due to electroactive species and allows the determination of lactate also in cell culture medium. The benefits of the co-immobilization of LOx during electrosynthesis of phenylenediamine include: excellent interference rejection characteristics, protection of the electrode surface from biofouling, an improved sensitivity and a great stability of the polymerized layer[17]. The electric process does not affect the enzymatic activity.

Limitations

However, the electrochemical formation of all these polymers proceeds via intermediate, highly reactive radical cations, which makes the exclusion of molecular oxygen indispensable, thus implying a complicate procedure that limits the reproducibility and the mass production capabilities. In addition, the enzyme concentration in the deposition solution has to be kept small due to the possible nucleophilic attack of protein side chains at the radical cations. For these reasons, electropolymerization has been proved to be a method more difficult to implement in respect to cross-linking one.

5.3.5 *Third Technique: pH shift-induced deposition*

Enzymes can be deposited by a mechanism involving their entrapment during the precipitation of organic layers, such as ***electrophoretic deposition paints*** (EDPs), triggered by a local pH change at the electrode surface[37].

The basic methodology has been widely used in automotive, tin and cans industries, as protection from corrosion, but it was recently adapted for biotechnological applications, using as substrates carbon-fiber or platinum micro-electrodes, and for modification in situ of scanning tunnelling microscopy tips. In fact, besides being attractive due to their electrical insulating properties, these materials are biocompatible and porous, so they can be used as encapsulating matrices for the entrapping of a wide variety of species, such as enzymes, proteins and other molecules[37].

EDPs

Currently, two different types of electrophoretic paints are commercially available: *i)* ***cathodic EDP*** based on positively charged polymers with amino groups containing side chains, and *ii*) ***anodic EDP*** based on negatively charged polymers with carboxylic group containing side chains. The water-

soluble forms of EDPs are mixture of micellar polyacrylates due to the presence of protonated amino groups, in the case of cathodic EDP, or of deprotonated carboxylic groups, in the case of anodic EDP.

Electrochemically induced pH-modulation of the solution in the diffusion zone of the electrode, caused by the oxidation or reduction of water, leads to pronounced changes in the polymer solubility and hence to precipitation on the electrode surface. Subsequent curing of the deposited polymer layer characterizes the hardness and the insulation properties of the film[37].

Cathodic and anodic electrophoretic deposition paints (Clearclad HRS) were kindly supplied by LVH Coating Ltd. (Coleshill, UK). On company suggestion, we have tried only the cathodic system, which is more immune to bioactive materials. On the contrary, anodic paint may provide a good environment, in terms of nutrient substrates, for growing bacteria and other microorganisms (personal communication); therefore, it is not suitable for biological analysis.

EDPs Protocol

The enzyme (2mg/mL of GOx type X-S) is dissolved in MQ water, successively, the cathodic Clearclad HRS EDP suspension (70 μL/mL, stock solution) were mixed and the enzyme/paint suspension is stored for 3h at 4°C. For enzyme/paint film formation, the cold preparation is filled into the electrochemical chamber. A potential-pulse profile (2.2V for 0.2s; 0.8V for 1s; 0V for 5s vs Ag/AgCl 3M KCl) is applied for 30 cycles, leading to the local generation of H^+ and concomitantly to the precipitation of the paint on the electrode surface simultaneously entrapping the enzyme. The modified electrode surface are rinsed with MQ water and stored before use at least 12h in PBS at 4°C [37].

5.3.6 $CuCl_2$ Nano-particles

Since we want to monitor the lactate release at single cell level, we expect to detect very low concentrations, in the order of nM to μM. For this reason, especially in lactate analysis, we need a really high sensitivity; however, we cannot increase too much the concentration of LOx onto the electrode surface, because otherwise there is no polymer nucleation process[20]. Therefore, for LOx, we decided to cover the electrode area with a layer of Cu-nanoparticles before polymer electropolymerization.

Copper is specifically selected in order to increase the electroactive area of the electrode and consequently to enhance the sensitivity of the UME biosensor. Moreover, the Cu nanoparticles can electrochemically oxidise lactate by themselves, it is relatively inexpensive, commercially available and the method for its deposition is well established. The diameter of Cu nanoparticles formed on the electrode surface should be around 200 nm[27].

$CuCl_2$-oAP Protocol

Cu is electrochemically deposited on Pt by applying a potential equal to 0.032V for 180 s (max Cu loading) in a 0.2 M acetate buffer solution (pH 4.0) containing 5.0 mM $CuCl_2$ (Sigma). Successively, Cu-modified UME is placed in 0.2 M deareated acetate buffer solution (pH 5.0) containing 1 mg/mL of LOx and 5.0 mM oAP monomer. The electrochemical polymerization of PoAP/LOx film is carried out by cycling the potential range from 0.0 to 0.8V vs Ag/AgCl 3M KCl, at a scan rate of 50 mV/s, at RT. The film is grown for 15 cycles. The resulting electrode is thoroughly washed with MQ and stored in PBS (pH 7.4) at 4°C [27].

References

[1] Thévenot DR, Toth K, Durst RA, Wilson GS. Electrochemical biosensor: recommended definitions and classification. *Biosensors and Bioelectronics*. 16, pp.121-131 (2001)

[2] Mascini M, Tombelli S, Biosensors for biomarkers in medical diagnostics. *Biomarkers*. 13:7-8, pp. 637-657 (2008)

[3] Kramer K, Hock B, Antibodies for Biosensors. *Ultrathin Electrochemical Chemo- and Biosensors*. Vol. 2. Springer Series on Chemical Sensors and Biosensors (2004)

[4] Clark LC, Monitor and control of blood and tissue oxygen tensions. *Transactions-American Society for Artificial Internal Organs*. 2, pp. 41-48 (1956)

[5] Dzyadevych SV, Arkhypova VN, Soldatkin AP, El'skaya AV, Martelet C, Jaffrezic-Reboualt N, Amperometric enzyme biosensors: past, present and future. *ITBM-RBM*. 29, pp. 171-180 (2008)

[6] Dell'Atti D, Tombelli S, Minnuni M, Mascini M, Detection of clinically relevant point mutations by a novel piezoelectric biosensor. *Biosens&Bioelec*. 21, pp. 1876-1879 (2006)

[7] Luong JHT, Male KB, Glennon JD, Biosensor technology: technology push versus market pull. *Biotechnol. Adv*. 26, pp.492-500 (2008)

[8] Walsh C, Flavin coenzymes: at the crossroads of biological redox chemistry. *Acc. Chem. Res*. 13, pp. 148-155 (1980)

[9] Moss GP, International union of biochemistry and molecular biology: recommendations on biochemical and organic nomenclature, symbols and terminology etc. (2010)

[10] Marinesco S, Frey O, Microelectrode designs for oxidase-based biosensors (Chapter 1). *Microelectrode Biosensors*. Marinesco S, Dale N. (Eds.), Humana Press c/o Springer Science (2013)

[11] Nakamura S, Fujiki S, Comparative studies on the glucose oxidases of *Aspergillus niger* and *Penicillium amagakiense*. *J. Biochem*. 63, pp.51-58 (1968)

[12] Pernot P, Mothet JP, Schuvailo O, Soldatkin A, Pollegioni L, Pilone M, Adeline MT, Cespuglio R, Marinesco S, Characterization of a yeast d-amino acid oxidase micro-biosensor for d-serine detection in the central nervous system. *Anal. Chem*. 80:9 (2008)

[13] Weibel MK, Bright HJ, The glucose oxidase mechanism. *The Journal of Biological Chemistry*. 246:9, pp. 2734-2744 (1971)

[14] Bankar SB, Bule MV, Singhal RS, Ananthanarayan L, Glucose Oxidase – An overview. *Biotechnology Advanced*. 27, pp. 489-501 (2009).

[15] Cespuglio R, Netchiporuuk L, Shram N, Glucose and lactate monitoring across the rat sleep-wake cycle (Chapter 11). *Microelectrode Biosensors*. Marinesco S, Dale N. (Eds.), Humana Press c/o Springer Science (2013)

[16] Leiros I, Wang E, Rasmussen T, Oksanen E, Repo H, Petersen SB, Heikinheimo P, Hough E, The 2.1Å structure of Aerococcus viridans L-lactate oxidase (LOx). *Acta Crystallogr Sect F Struct Biol Cryst Commun.* 62:12, pp. 1185-1190 (2006)

[17] Marinesco S, Vasylieva N, Enzyme Immobilization on Microelectrode Biosensors (Chapter 5). *Microelectrode Biosensors*. Marinesco S, Dale N. (Eds.), Humana Press c/o Springer Science (2013)

[18] Migneault I, Dartiguenave C, Bertrand MJ, Waldron KC, Glutaraldehyde: behaviour in aqueous solution, reaction with proteins, and applications to enzyme cross-linking. *Biotechniques*. 37:5, pp. 790-801 (2004)

[19] Broun GB, Chemically aggregated enzymes. *Methods in Enzymology.* Academic Press, New York (1976)

[20] Romero MR, Garay F, Baruzzi AM, Design and optimization of a lactate amperometric biosensor based on lactate oxidase cross-linked with polymeric matrixes. *Sensors and Actuators B*. 131, pp. 590-595 (2008)

[21] Chui WK, Wan LSC, Prolonged retention of cross-linked trypsin in calcium alginate microspheres. *J. Microencapsulation*. 14:1, pp. 51-61 (1997)

[22] Ciobanu M, Taylor DE Jr, Wilburn JP, Cliffel DE, Glucose and lactate biosensors for scanning electrochemical microscopy imaging of single live cells. *Anal. Chem*. 80, pp. 2717-2727 (2008)

[23] Eklund SE, Taylor DE Jr, Kozlov E, Prokop A, Cliffel DE, A microphysiometer for simultaneous measurement of changes in extracellular glucose, lactate, oxygen and acidification rate. *Anal. Chem*. 76, pp. 519-527 (2004)

[24] Shin MC, Kim HS, Electrochemical characterization of polypyrrole/glucose oxidase biosensor: (a) Part I. Influence of enzyme concetration on the growth an properties of the film. (b) Part II. Optimal preparation conditions for the biosensor. *Biosensors & Bioelectronics*, 11:1/2, pp. 161-169, 171-178 (1996)

[25] Zhang Z, Liu H, Deng J, A glucose biosensor based on immobilization of glucose oxidase in electropolymerized o-aminophenol film on platinised glassy carbon electrode. *Anal. Chem*. 68, pp. 1632-1638 (1996)

[26] Pan D, Chen J, Yao S, Tao W, Nie L, An amperometric glucose biosensor based on glucose oxidase immobilized in electropolymerized poly(*o*-aminophenol) and carbon

nanotubes composite film on a gold electrode. *Analytical Sciences*. 21, pp. 367-371 (2005)

[27] Pan D, Chen J, Yao S, Nie L, Xia J, Tao W, Amperometric glucose biosensor based on glucose oxidase in electropolymerized *o*-aminophenol film at copper-modified gold electrode. *Sensors and Actuators B*. 104, pp. 68-74 (2005)

[28] Habermüller K, Schuhmann W, A low-volume electrochemical cell for the deposition of conducting polymers and entrapment of enzymes. *Electroanal*. 10, pp. 1281-1284 (1998)

[29] Umaña M, Weller J, Protein-modified electrodes. The glucose oxidase/polypyrrole system. *Anal. Chem*. 58, pp. 2979-2983 (1986)

[30] Fortier G, Brassard E, Bélanger D. Optimization of a polypyrrole glucose oxidase biosensor. *Biosensors & Bioeletronics.* 5:6, pp. 473-490 (1990)

[31] Adeloju SB, Moline AN, Fabrication od ultra-thin polypyrrole-glucose oxidase film from supporting electrolyte-free monomer solution for potentiometric biosensing of glucose. *Biosensors & Bioeletronics*. 16, pp. 133-139 (2001)

[32] Cosnier S, Innocent C, A novel biosensor elaboration by electropolymerization of an adsorbed amphiphilic pyrrole-tyrosinase enzyme layer. *J. Electroanal. Chem*. 328, pp. 361-366 (1992)

[33] Coche-Guerente L, Cosnier S, Innocent S, Mailley P, Development of amperometric biosensors based on the immobilization of enzymes in polymer film electrogenerated from a series of amphiphilic pyrrole derivatives. *Analytica Chimica Acta*. 311, pp. 23-30 (1995)

[34] (a) Trojanowicz M, Geschke O, Krawczynski vel Krawczyk T, Cammann K, Biosensors based on oxidases immobilized in various conducting polymers. *Sensors and Actuators B*. 28, pp. 191-199 (1995) (b) Krawczynski vel Krawczyk T, Trojanowicz M, lactate solid-state biosensor with multilayer of electrodeposited polymers for flow-injection clinical analysis. *Biosensors & Bioeletronics*. 11:11, pp. 1155-1165 (1996)

[35] Palmisano F, Guerrieri A, Quinto M, Zambonin PG, Electrosynthesized bilayers polymeric membrane for effective elimination of electroactive interferents in amperometric biosensors. *Anal. Chem*. 67, pp. 1005-1009 (1995)

[36] Palmisano F, Centonze D, Quinto M, Zambonin PG, A microdialysis fibre based sampler for flow injection analysis: determination of L-lactate in biofluids by an electrochemically synthesised bilayers membrane based biosensor. *Biosensors & Bioeletronics*. 11:4, pp. 419-425 (1996)

[37] Kurzawa C, Hengstenberg A, Schuhmann W, Immobilization method for the preparation of biosensors based on pH shift-induced deposition of biomolecules containing polymer films. *Anal. Chem*. 74, pp. 355-361 (2002)

Chapter 6

Enzyme Ultramicroelectrode Biosensors Features

Abstract

Protein immobilization is a key step in biosensor preparation that impact on the overall performance. Among the wide variety of immobilization techniques currently available, only few of them have been proven to be reliably when applied in this thesis for SECM applications. In this chapter the full characterization of the features of GOx- and LOx-based UME biosensors, prepared within this thesis work, is reported. By using amperometric calibrations, the most important biosensor characteristics, which determine the analysis performance, such as sensitivity, detection limit, response time, reproducibility, spatial resolution, biosensor efficiency, permeability, selectivity and degradation are analyzed. A theoretical model is also introduced in order to describe the kinetics of the enzyme entrapped into the matrix.

Key words GOx and LOx UME biosensor, Sensitivity, LOD, Reproducibility, Spatial Resolution, Kinetics

6.1 Enzyme-Related Biosensors Parameters

6.1.1 UME Biosensors Calibration

Since each enzyme-based UME biosensor can perform differently according to the coating procedures, each electrode must be calibrated prior any SECM application. To investigate the influence of the immobilization method on the most important biosensor parameters, we determined their sensitivity, time resolution, reproducibility, stability, and kinetics by amperometric calibrations.

The calibration experiments are performed in PBS solution (pH 7.4) at room temperature (RT), where a known concentration of analyte, such as β-D-glucose or L-lactate, is added under slow stirring. The electric potential of the electrode is kept at E = +0.65 V vs Ag/AgCl 3M KCl, at which the oxidation of the H_2O_2 takes place; the system is allowed to equilibrate at least for 300 s. The current is

recorded during each analyte addition, and since H_2O_2 concentration is directly proportional to the concentration of the analyte, a typical amperometric calibration curve is obtained (Figure 1). Several range of analysis, from very low (0.01 - 0.5 mM) to relative high concentrations (1.0 - 10 mM) were explored, focusing the attention on the physiological ranges of glucose and lactate concentrations involved in the metabolic pathways of single living cells. A typical calibration plot for a drop-cast GOx (for the preparation and immobilization procedure see *Chapter 5.3.3*) 10 μm Pt UME biosensor exhibits fairly linear sensitivity to glucose for concentrations from 10 μM up to 4 mM (Figure 2a): this result shows that the physiological range of glucose concentration and its variation due to single-cell consumption are perfectly covered by the microsensor. After reaching the concentration of 4-5 mM any addition of glucose does not affect the current.

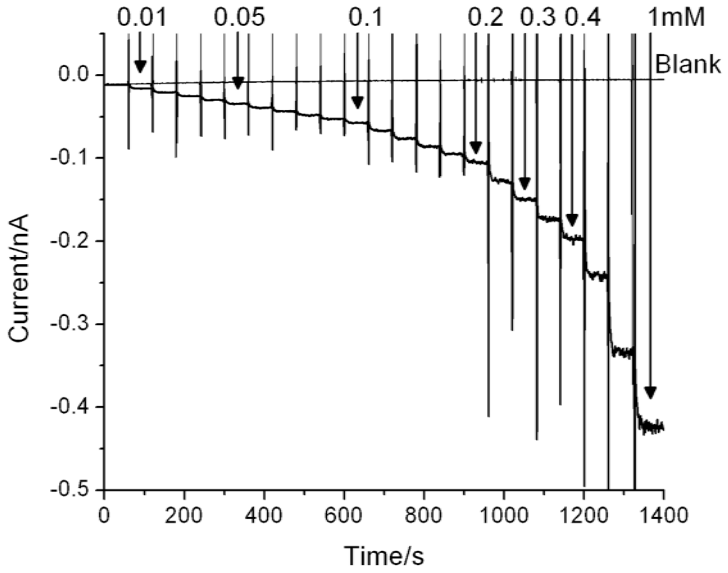

Figure 1. Typical example of amperometric calibration curve for a drop-cast GOx UME biosensor. The sensor is sensible even at small addictions of glucose and there is no response for blank ones. *E = +0.65 V vs Ag/AgCl 3M KCl.* Every current step corresponds to a glucose addition/concentration: 0.01, 0.02, 0.03, 0.04, 0.05, 0.06, 0.07, 0.08, 0.09, 0.1, 0.12, 0.14, 0.16, 0.18, 0.2, 0.25, 0.3, 0.35, 0.4, 0.5, 0.75, 1 mM.

The typical calibration plot for a drop-cast LOx UME biosensor (Figure 2b) displays two distinct linear ranges: from 0.1 to 0.5 mM lactate, that covers the physiological range for single-cell release, and from 0.5 to 2.0 mM lactate.

We studied the catalytic kinetics of GOx and LOx by performing some

experiments with the enzyme both free in solution and entrapped in the matrix and we verified that the decay in sensitivity at high concentration is due to a saturation of the enzyme and it is not caused by its constriction in the electrode matrix. Since the local concentration of lactate released from a single cell is very low (lower than 0.1 mM), the enzyme saturation does not hinder the detection for this purpose.

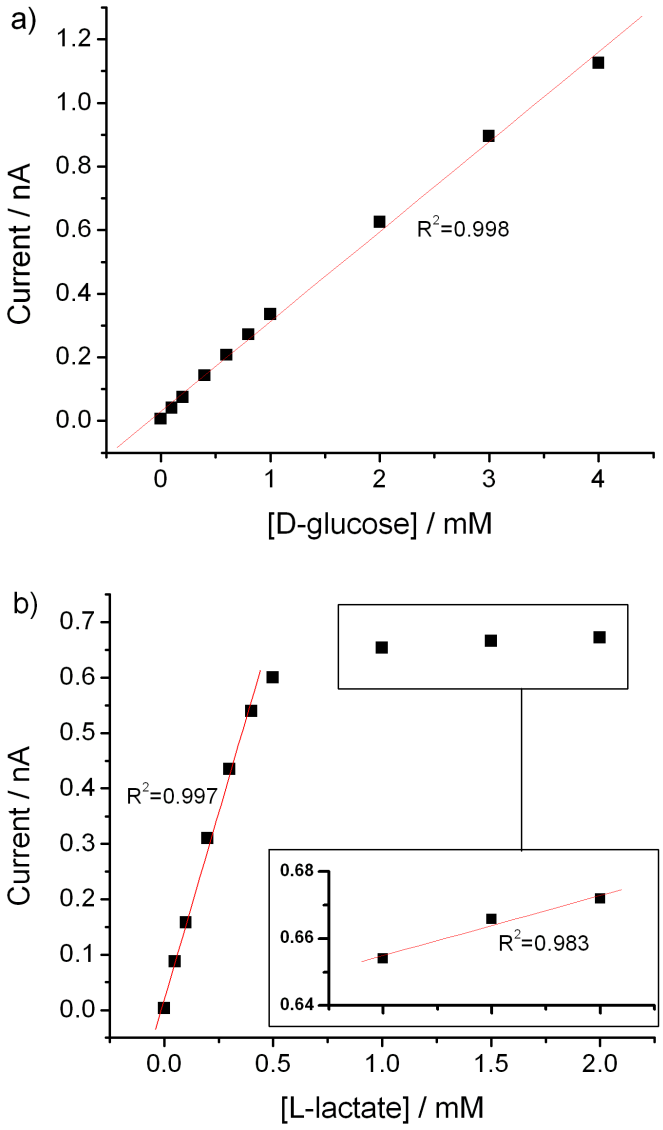

Figure 2. Calibration plots of drop-cast (a) GOx and (b) LOx-based 10 μm Pt UME biosensors. *E = +0.65 V VS Ag/AgCl (3M KCl)* in PBS buffer. (a) GOx-based biosensor displays a linear sensitivity to glucose for concentration up to 4 mM, while (b) LOx-based biosensor exhibits a linear sensitivity to lactate for concentration up to 0.4 mM.

6.1.2 Sensitivity

Electrochemical biosensors are mostly used in their linear range and the ***sensitivity*** of the sensor is defined as the initial slope of the current-

concentration curve and it is usually expressed in pA/μM of substrate or, more accurately, in μA/mM/cm^2 of electrode surface[1].

Our experiments show that UME sensitivity increases with thickness of the layer, due to the higher concentration of enzyme entrapped, up to a point that levels off, where there is the blockage of the analyte and H_2O_2 diffusion; however, response time becomes longer as a thicker diffusion barrier is applied to the UME.

Another critical parameter is the real amount of enzymatic units per grams of the purchased compound. We observed a huge difference on drop-cast LOx UME biosensor performance for LOx with the same code and from the same company but belonging to different stocks. LOx with 57 U/mg shows high sensitivity, up to 1.9 pA/μM, while with the stock containing 32 U/mg of LOx, the sensitivity drops off to 0.6 pA/μM. GOx compound is more homogeneous, because its extraction protocol is easier; therefore the sensitivity is not dependent on the used stock of the compound. Table 1 summarizes the values of sensitivity, detection limits and linear range for each protocol. The ***limit of detection*** (LOD) is determined using the widely applied criterion of three times the standard deviation of the noise[1]. The linear range is defined as the highest concentration for which a successful fit at $R^2 = 0.998$ is still possible[1]. Overall, the tests indicate that covalent immobilization methods using glutaraldehyde yield more sensitive biosensors than methods based on enzyme entrapment (electropolymerization and pH shift induced deposition).

LOD

Table 1. Calibration Data

Immobilization Method	***Enzyme***	***Sensitivity (pA/μM)***	***LOD (μM)***	***Linearity (mM)***
1. GDA	GOx LOx	0.91 1.94 ÷ 0.63	1 ÷ 10 1 ÷ 10	0 ÷ 4 0 ÷ 0.3
2. p-*o*-aminophenol	GOx LOx	0.14 0.13	50 50	0 ÷ 10 0 ÷ 0.3
3. Poly-pyrrole	GOx LOx	0.09 0.16	100 50	0 ÷ 10 0 ÷ 0.3
4. PPyr-Phen-oPD	LOx	0.11	100	0 ÷ 0.1
5. Cathodic EDP	GOx LOx	0.026 0.05	100 100	0 ÷ 5 0 ÷ 0.5
6. Cu Nanoparticles	LOx	0.018	100	0 ÷ 0.1

6.1.3 Response Time

UME biosensors designed for SECM applications should detect metabolites with a good temporal resolution. We observed that the response time becomes longer with the thickness of the matrix, containing the enzyme, as a ticker diffusion barrier is applied to the microelectrode. Additionally, enzymatic biosensor response times are limited by the kinetics of the enzymatic reaction and usually display response time of the order of seconds. We tested that the enzyme layer itself does not act as a diffusion barrier to H_2O_2 detection contributing to the signal response delay[1].

The UME ***response time*** is typically calculated as the time required for the current response to reach 90% of the maximum amplitude for the concentration step[1]. After testing the different types of biosensors, we found that the immobilization method significantly influenced the response time of the electrodes. For example the average 90% response times to 0.5 mM D-glucose for drop-cast GOx UME biosensors, built with the standard procedure, is around 2 ÷ 4 sec, for a double "deeping" matrix the time increases to 12 s. While for very thin coatings, such as for electropolymerization methods, the response time is faster, around 0.5 ÷ 1.5 sec. For the electrode with Cu nanoparticles the response time grows up to 35 s.

Several experiments were performed changing the thickness of the enzyme layer in order to obtain the best sensitivity with a suitable temporal resolution for our SECM measurements.

6.1.4 Stability

In order to work with living systems, the ***stability*** of the enzyme layer is also a very important parameter. Important aspects of biosensor stability are: *i)* its interaction with the solution of the analysis and *ii)* its susceptibly to fouling processes[1]. The typology of the material used for electrode construction and the method of enzyme immobilization can have significant impact on the lifetime of the biosensor. The stability of drop-cast and electropolymerized UME biosensors, both for GOx and LOx, was tested in simple PBS buffer. Regarding the first method (Figure 3a and 3c), we have the best sensitivity just after preparation (time 0h), while after 24h it is slightly decreased. Biosensors, prepared using GDA immobilization, are stable for up to 3 days. In contrast, with the second immobilization method (Figure 6b and 6d), at time 0h the sensors are less sensible than after 24h or 48h. We suppose that this effect is

due the slow reassembly of the enzymes into the polymer matrix. After 72h the sensitivity decreases until it reaches constant values and the sensors remain stable for several days.

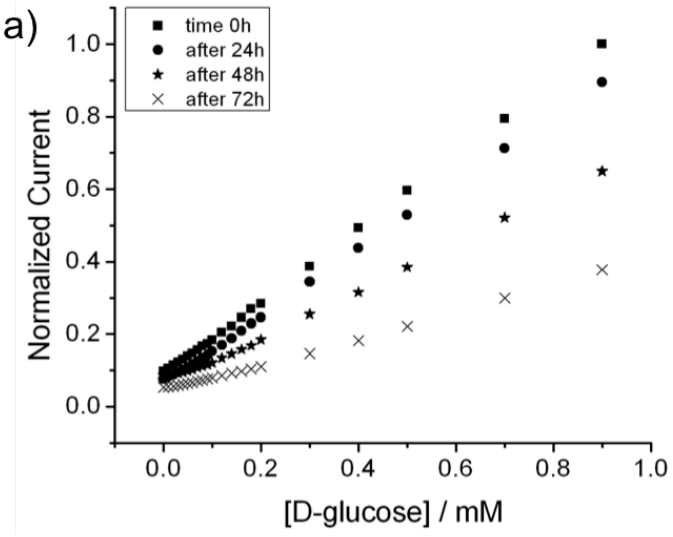

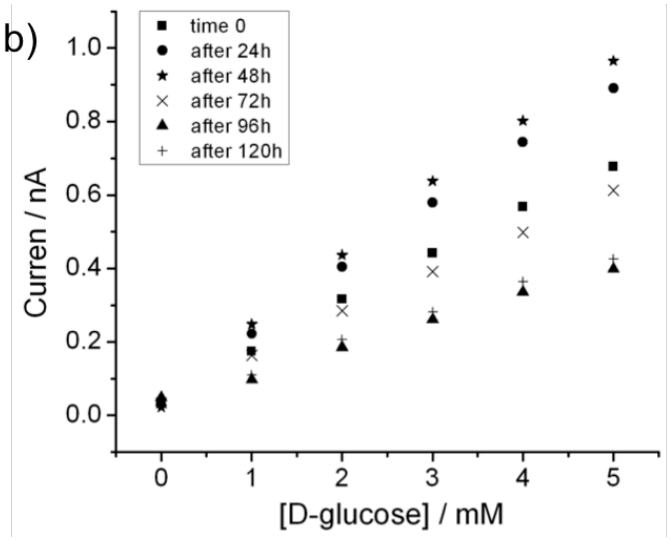

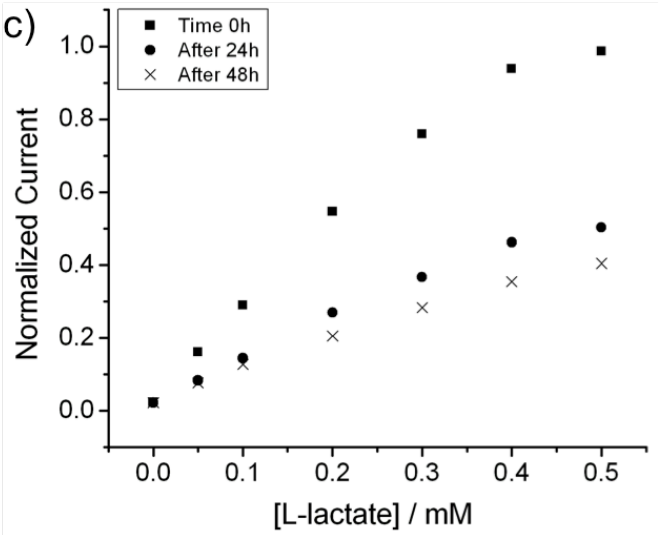

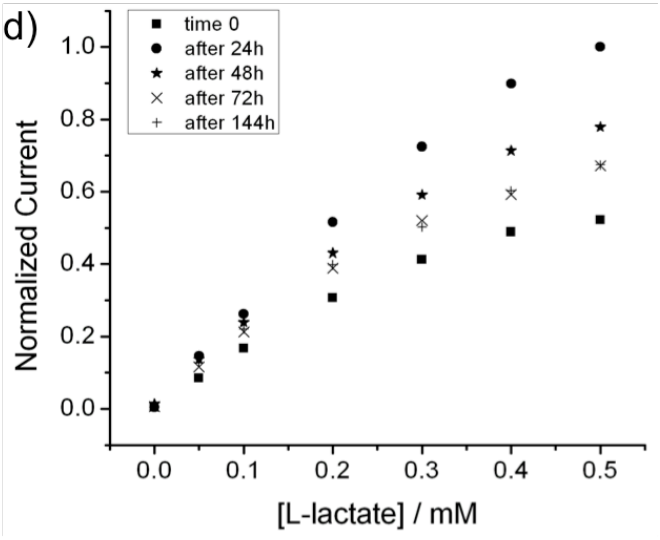

Figure 3. Representative measurements of biosensors stability in the linear range of analyte detection; serial amperometric calibrations in PBS: (a) drop-cast GOx-based, (b) electropolymerized GOx-based, (c) drop-cast LOx-based, and (d) electropolymerized LOx-based UME biosensors. The current of each point is normalized for the maximum response value obtained within the linear range.

6.1.5 Reproducibility

Reproducibility, defined as the ability to reproduce an entire experiment, is another biosensor feature to control. It was calculated for each method as the current variation for additions up to 1 mM of glucose or 0.1 mM of lactate for GOx-based and LOx-based UME biosensors, respectively. As reported in literature[2], electropolymerized methods have a good reproducibility (Figure 4), because there is an electrochemical control on deposition.

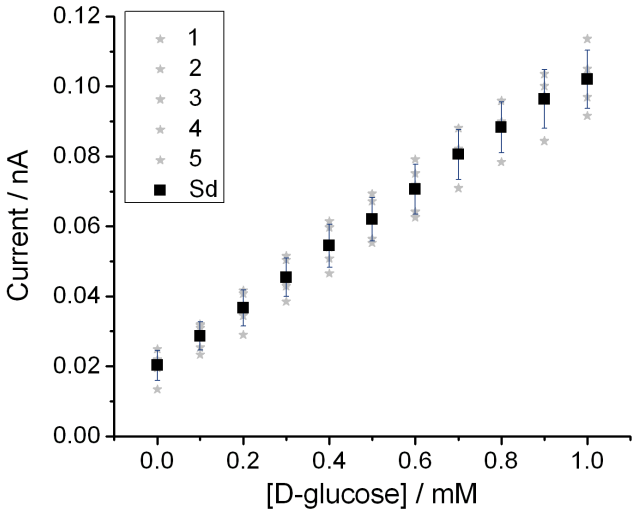

Figure 4. Reproducibility of electropolymerized GOx-based UME biosensors. Average value of current responses and standard deviation of five different experiments are reported. Calibrations were done in PBS buffer.

Considering five different experiments performed in different days and with different enzyme/polymer solutions in order to take into account the variability, we obtained a standard deviation in current response around 10% for GOx sensors and a value for LOx sensors of 18%. While for drop-cast methods the standard deviations are larger: the values are 22% for GOx UME biosensors and 26% for LOx ones.

6.1.6 Spatial Resolution

A key advantage of SECM is the ability to perform measurements with very high spatial resolution (micrometer range), such as experiments at single cell level. Therefore, the size of the electrode biosensor, the nature of the probe and the thickness of the enzymatic coating are of paramount importance to allow the monitoring of metabolite levels on single living cells. A large biosensor would increase the analyzed zone, decreasing the spatial resolution. The overall dimension of the UME biosensor and enzymatic matrix should be in the micron or sub-micron range, because the spatial resolution of SECM scales with the probe electrode dimension. Thinner is the enzymatic layer the higher will be the spatial resolution of the SECM experiments and microscopic information of cell metabolism can be obtained. For each method, the ***spatial resolution*** of the UME biosensor was calculated as the width of the current peak (w_{peak}) due to glucose concentration variation on the top of the scanned cell in respect to its real dimension (w_{cell}): the lower is the ratio higher is the spatial resolution.

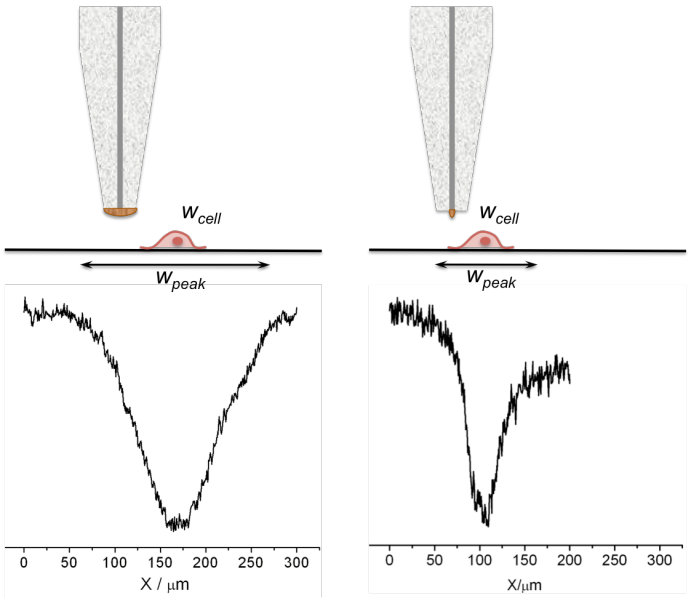

Scheme 1. Schematic representation of typical drop-cast (on the left) and electropolymerized (on the right) UME biosensors with their relative profiles.

Drop-casting method has the lower spatial resolution, because the drop of the solution containing the enzyme, when it dries, entraps the enzyme not only over the active part of the electrode (10 μm Pt) but also onto the glass support.

Hence, the biosensor converts the analyte in H_2O_2 for the entire dimension of the electrode and it is sensible to variations of analyte concentration in all the position of the active enzymatic layer. For more details see Table 2 and *Chapter 9* and *10*. However, the drop-cast method was extensively optimized and a spatial resolution comparable with the electropolymerized ones, in which the enzyme is locally deposited only onto the UME active part, was achieved.

Table 2. Calibration Data of one single set on analysis taken as representative.

Immobilization Method	***Enzyme***	***Deposition Time***	***Sensitivity (pA/μM)***	***Spatial Resolution*** (w_{peak} / w_{cell})
1. GDA	GOx[1]	10 min	0.34	6.2
[Classical approach]	LOx	10 min	1.94	5
1. GDA	GOx	6 min	0.91	2.8
[New approach]	LOx	6 min	0.95	1.8
2. p-*o*-aminophenol	GOx	-	0.14	2.1
3. Poly-pyrrole	GOx	-	0.09	1.4

6.1.7 AFM Analysis

The enzyme/polymer layer was characterized by Atomic Force Microscopy (AFM) in order to assess the full coverage of the electrode surface, the thickness and morphology of the electropolymerized enzyme-based biosensors (for technique principles and experimental details see *Appendix* #1).

AFM imaging of thin films requires the use of a solid and flat supporting surfaces, on which the film itself is deposited. Ideally, the substrate surface should be *atomically* flat and there should be not strong interactions between the film and the underlying surface. Relatively large roughness and strong interactions may cause image misinterpretation and wrong evaluations about surface ripple and deposited structures[3]. We chose Pt arrandee™ surface (platinum planar electrodes: 11mm x 11mm) as active surface to characterize our electropolymerized GOx biosensors and evaluate their homogeneity. Such Pt substrate surfaces have very smooth regions with large atomically flat

terraces (see Figure 5a and 5b) extending over more than 0.1 μm (sample 1). Following the protocol #4, already described in *Chapter 5.3.4,* we electropolymerized the *o*-aminophenol monomer in sample 2 and the solution composed by the monomer and the enzyme (in this specific case *glucose oxidase*) in sample 3. Figure 8 displays the Tapping Mode AFM images obtained for the three samples: 5(a)/5(b) are related to the bare Pt, 5(c)/5(d) represent the platinum covered only with the polymer layer and 5(e)/5(f) show the GOx enzyme entrapped into the polymer matrix onto the platinum surface.

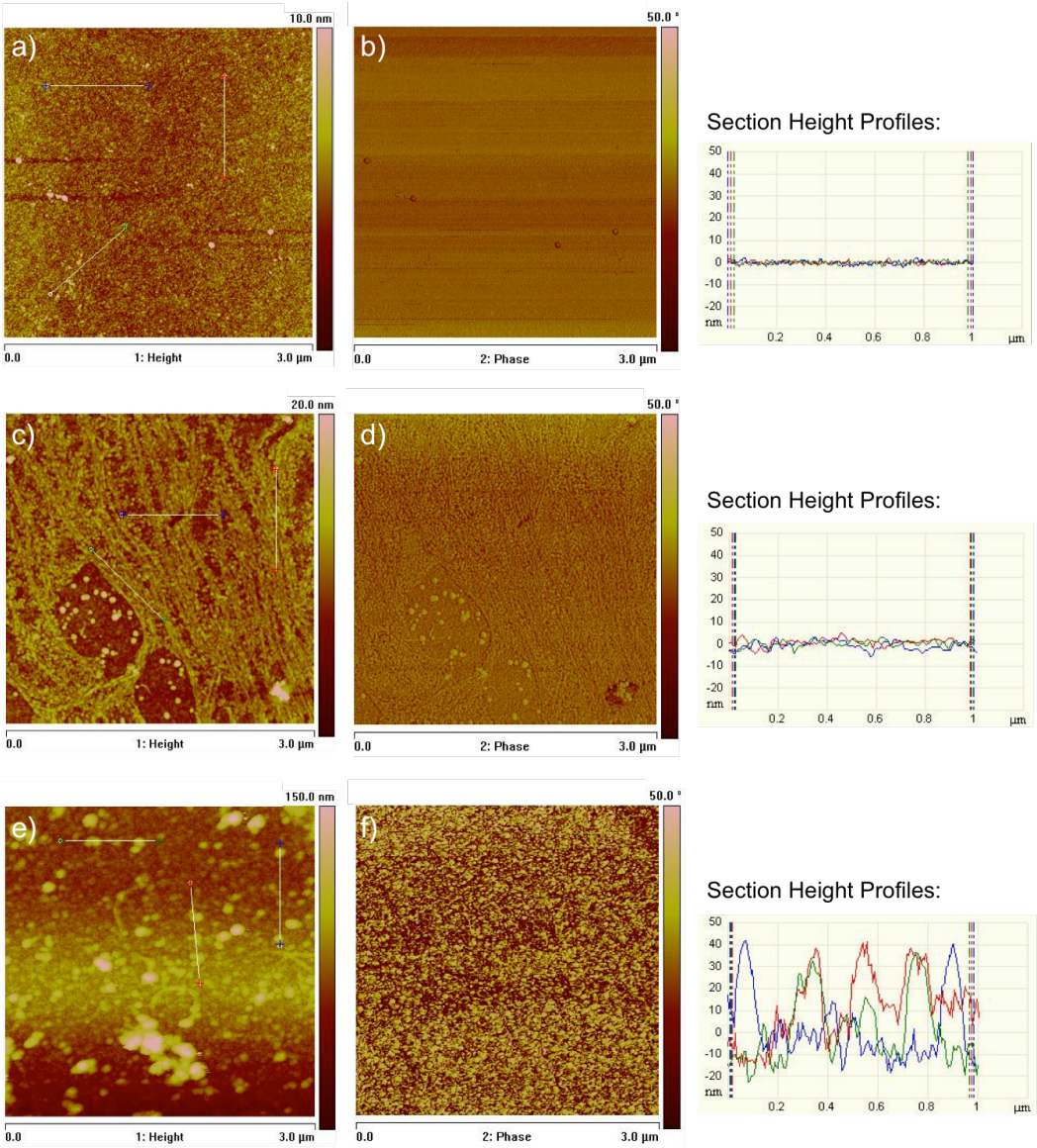

Figure 5. Tapping mode AFM images of: the bare platinum arrandee™, the poly-*o*-aminophenol layer on platinum, the enzyme (GOx) entrapped into the polymer matrix on platinum [(a), (c) and (e) correspond to height images and (b), (d) and (f) correspond to phase images]. On the right there are three 1μm-sections of the height profiles relative to each sample.

Table 3. Main surface parameters of the three analyzed samples expressed as mean values calculated on the previously presented height AFM images (surface area: 9 μm^2).

	***Pt arrandee*™**	***Pt – oAP***	***Pt – oAP/GOx***
Average Roughness (Ra)	0.74 nm	1.47 nm	15.3 nm
Average Height (Rz)	1.79 nm	3.87 nm	24.5 nm
Average Grain	26 nm	35 nm	66 nm

In tapping mode AFM the probe is excited into resonance oscillation with a piezoelectric driver and the oscillation amplitude is used as a feedback signal to measure topographic variations of the sample[4]. In this way high-resolution topographical (or height) images (Figure 5a, 5c and 5e) can be achieved without inducing destructive frictional forces on the "soft" and sticky samples under investigation. Moreover, thanks to the phase imaging system, incorporated in the used AFM setup, some material properties, such as homogeneity, adhesion and viscoelasticity can be monitored. Phase images (Figure 5b, 5d and 5f) can also act as a real-time contrast enhancement technique, as they highlight edges, such as grain edges, which can be obscured by rough topography, and they are not affected by large-scale height differences.

Table 3 summarizes the main physical parameters obtained by the analysis of the topographical AFM images of each sample (5a, 5c and 5d). The results show that both the average roughness and the average height drastically increase from sample 1 (bare Pt) to sample 3, where the polymer layer, encapsulating the enzymes, covers the platinum surface. This increase confirms that *i*) the *o*-aminophenol monomer efficiently polymerizes onto the active surface and *ii*) when the electropolymerization is carried out in presence of the GOx the enzyme is entrapped in, as it can be easily seen from the comparison of images 5c and 5e and even more evident considering the corresponding scan line sections in Figure 85.

Therefore, the proposed electropolymerization approach can be considered a valid method to form a very homogeneous layer, as can be noted also from the relative phase images (Figure 5b, 5d and 5f). Furthermore, the average grain sizes allow to evaluate the dimension and the space occupied by the enzyme entrapped into the polymer, which is in line with the literature[4-5], in which the GOx is assumed to be a dimeric globular protein having overall dimension of 7.0 x 5.5 x 8.0 nm^3.

6.1.8 *Effects of Analysis Solutions on Biosensors Performance*

Since the goal of the project is to study metabolic alterations on single living cells, it is mandatory to work in a physiological environment, which is also reach of metabolites to avoid stressing the cells and in order to evaluate their metabolism in standard conditions. At the same time the biosensor has to be enough sensitive and the components of the analysis solution should not affect the biosensor performance to locally monitor the little metabolites changes. In literature most of the *in vitro* experiments are usually performed in PBS buffer (pH 7.4), but we observed that the cells are negatively affected by this condition, because all the nutrients, vitamins, amino acids etc. are missing, and they start to block their metabolism within half an hour. For this reason, enzymatic layer responses to various analysis solutions were examined in order to find the best working condition. Several buffers were used and tested: 50 mM Phosphate Buffer (PB) pH 7.0, PBS pH 7.4, Hank's Balance Salt Solution (HBSS), PBS plus 2.5÷10% horse serum and 10 μM of insulin. The most common cell media were also analyzed, such as RPMI 1640, DMEM, DMEM/Ham's F-12, DMEM without red phenol, and the complete culture medium for the investigated cell lines (see *Chapter 7.1.3* for the composition). It is worth to mention that all the tested media are without glucose, because usually the latter one is present at very high concentration (around 11 mM), which hides the small variations during the analysis due to the cell consumption and exceeds the saturation limit of the developed GOx-based UME biosensors.

Considering the physiological range of the local glucose and lactate concentration variations (ranging from 0 to 0.1mM), the results (Figure 6) show that: *i)* the best sensitivity of drop-cast electrodes results in PBS, and PBS plus serum, because there are no other interfering species, such as some amino acids, and *ii)* it is not possible to use the complete cell culture medium with this UME probes because its mixture of compounds disturbs the sensor performance. While, in presence of RPMI or DMEM, both with and without glucose, composed by several inorganic salts, amino acids, vitamins and other components[7-8], the electrodes present a very reduced sensitivity. Consequently, at the beginning of the study, the SECM measurements coupled with the GOx-based biosensors for the investigation of glucose uptake of a single cell were performed in PBS containing 2.5% of horse serum and 10 μM of insulin. However, the measurements for LOx biosensors show that horse serum

interferes with the monitoring of lactate, due to its complex chemical composition, and also the sodium pyruvate contained in DMEM and Ham's media disturbs the detection of lactate (see next section). Therefore, considering all the tested solutions and in order to find the best compromise between biosensor sensitivity and cell growing conditions for both GOx- and LOx-based biosensors the measurements were performed in RPMI medium without glucose and serum. It is mandatory to find a common solution in order to simultaneously measure both glucose concentration variations and lactate release on the same cell for further combined studies on cellular metabolism.

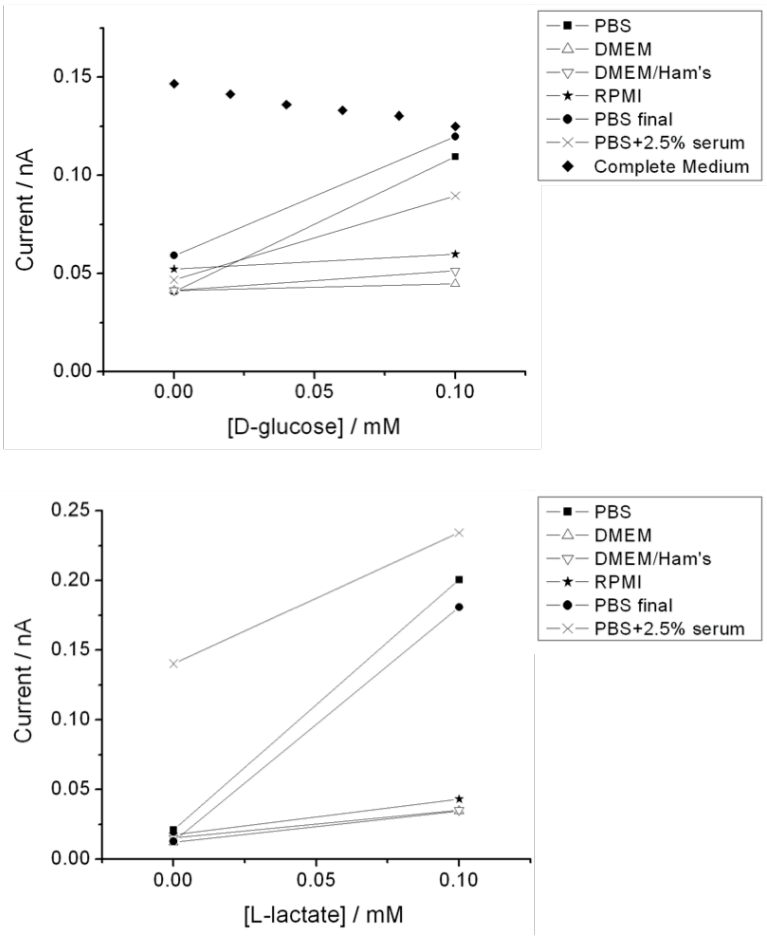

Figure 6. Calibration plots of GOx- and LOx-based biosensors in different analysis solutions: only the glucose and lactate physiological ranges were considered.

6.1.9 *Other Sensoristic Parameters*

The main analytical parameters of the enzyme-based biosensor performance are related to: *i)* the sensitivity of the sensor to the target analyte (e.g. glucose and lactate) and to the enzyme-transducer molecule H_2O_2, and *ii)* its ability to block electroactive interference species. In this section a brief discussion of evidences of the used enzyme biosensors is given in order to elucidate their behaviour.

Biosensor Efficiency

The ***biosensor efficiency*** (BE%) is a very useful parameter, which normalizes the biosensor response with respect to H_2O_2 sensitivity[9].

$$BE\% = \frac{slope(Substrate)}{slope(H_2O_2)} \times 100\%$$

Where *slope (Substrate)* is the related to the enzyme-based biosensor sensitivity and corresponds to the linear range for substrate calibration and *slope (H_2O_2)* is the calibration slope for H_2O_2, measured at the same electrode biosensor[9].

In theory, the maximum value of BE% is 100% if the following hypothesis are satisfied: *i)* presence of enough active enzyme on the surface to generate sufficient H_2O_2 to mimic its flux during calibration, *ii)* all the hydrogen peroxide molecules, produced by the enzyme, have to be oxidized at the electrode surface, and *iii)* the diffusion coefficient of substrate (D_S) should be equal to the diffusion coefficient of H_2O_2 ($D_{H2O2} = 1.0x10^{-5}$ cm^2 s^{-1}).

Since these hypotheses are not completely satisfied in real conditions because: D_S is usually less than D_{H2O2} and some hydrogen peroxide is lost into the bulk solution, then $(BE\%)_{max} < 100\%$. In literature an empirical maximum value for BE% is given close to 60%[10]. For our manufactured drop-cast GOx UME biosensors, considering the linear range of concentrations for both glucose and hydrogen peroxide (ranging from 0 to 1 mM), the mean BE% calculated is around 45%, which is not too far from the theoretical value.

Permeability

Another important parameter of enzyme-based biosensor is the ***permeability*** of the enzymatic matrix, seen as its capability to allow the transport of the analyte (or another molecule) from the bulk solution up to the electroactive part of the electrode[9]. Aspects involved in membrane transport include: *i)* the permeant's partition coefficients, which reflect the interaction between the chemical species and the enzymatic matrix, *ii)* the species diffusion coefficients and *iii)* the matrix thickness[11-12].

Because the first two values are not known accurately, the 'true' permeability cannot be determined in a straightforward manner[11]. Instead, the *apparent permeability* has been defined as the ratio of the analyte (or the enzyme-transducer molecule H_2O_2) currents recorded with the same electrode, before and after deposition of the enzymatic matrix[9].

$$P(H_2O_2)\% = \frac{slope(H_2O_2) - Pt(GOx/GDA)}{slope(H_2O_2) - Pt} \times 100\%$$

The *apparent permeability* is therefore a relative, normalized measurement of the analyte/substrate flux to the metal surface when the coating is present. This parameter has been proved useful for comparing permoselective matrix properties for biosensors applications. The ideal value should be close to 100 ± 10%, but for polyphenol layer the value has been estimated lower than 10%[13]. We have estimated the *apparent permeability* value of our manufactured drop-cast GOx UME biosensors in respect to hydrogen peroxide equal to 30% considering a linear sensitivity to H_2O_2 concentration ranging from 0 to 1 mM.

Another way to have an immediate qualitative idea about the permeability of the coating is to perform a cyclic voltammetry using the Pt UME probe, with and without the matrix, in a solution containing a redox mediator, such as $[Ru(NH_3)_6]^{3+}$, which is well-known to be a reversible redox couple:

$$[Ru(NH_3)_6]^{3+} + e^- \rightarrow [Ru(NH_3)_6]^{2+} \quad [E_{red} = -0.11V \text{ vs } Ag/AgCl\ 3M\ KCl]$$

Despite the presence of the coating, which causes a slightly increase of capacitive current, the electrode is perfectly able to reduce the redox mediator, as shown in Figure 7. The oxidative signal around 0.1 V could be due to a not identified species present in RPMI medium.

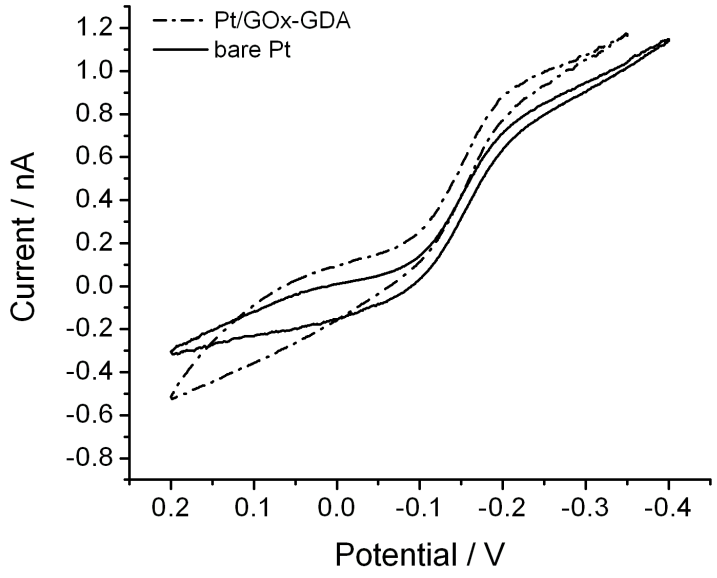

Figure 7. Cyclic voltammetry of 500 μM $[Ru(NH_3)_6]^{3+}$, in RPMI medium. With the enzymatic coating the capacitive current slightly increases due to the organic layer itself. Speed: 20mV/s.

Selectivity

A very important quality criterion of a biosensor is its capability to detect signals free from interferences. The ability to discriminate between the analyte and the interfering components in a complex mixture is expressed in terms of ***selectivity*** of the sensor; specificity is just the ultimate of selectivity[14]. A high selectivity is crucial for biosensor applications.

The effect of some species that are commonly present in cell culture medium for cell growth were tested; interferences due to penicillin/streptomycin, insulin, glutamine, epidermal growth factor, and cholera toxin, were investigated on our drop-cast LOx-based UME biosensors. Figure 8 shows that there is no response in current due to the addiction of these species, while the current increases adding lactate in presence of the other medium additives.

As already mentioned, other components, such as horse serum and sodium pyruvate, have effects on our LOx-based UME biosensors. The exact composition of the serum is unknown and it may contain lactate or lactate oxidase itself that may influence the analysis, while pyruvate can intercalate into the matrix, producing H_2O_2 itself, hence in both cases the final measurement of lactate could be misrepresented. However, the sensitivity to these interfering species is much lower in respect to lactate, therefore we can overlook this issue.

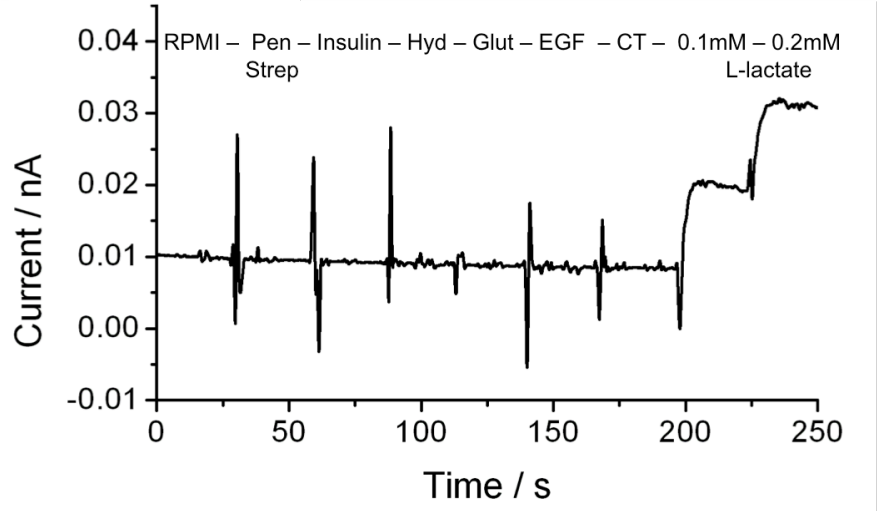

Figure 8. Typical amperometric calibration of a LOx-based UME biosensor in RPMI medium. After 300 s of equilibration time the current is recorded at E = 0.65 V vs Ag/AgCl 3M KCl. Each spike corresponds to a single addiction, in sequence: 10 mg/mL of penicillin/ streptomycin, 10 mg/mL of insulin, 500 ng/mL of hydrocortisone, 10 mg/mL of glutamine, 20 ng/mL of growth factor, 50 ng/mL of cholera toxin and finally 0.1 mM of lactate (twice).

Biofouling

Upon electric potential application, enzyme-based biosensors undergo an equilibration phase that might cause a loss in sensitivity due to a slow partial oxidation of the Pt electrode surface and/or a modification of the enzymatic matrix; the outcome of this equilibration time is a progressive and continuous reduction of the oxidation current registered at the electrode[15].

Sensors are composed by: a sensitive bioreceptor and an electrochemical transducer, and both of them can be affected by the applied potential. For example, concerning the bioreceptor, namely the enzymatic coating, there are several phenomena that can occur, such as the saturation and the depletion of the enzyme, the denaturation or degradation of the matrix, etc. While regarding the transducer part, we have to consider that the enzymatic reaction produces hydrogen peroxide that is detected at the electrode surface, therefore the platinum, even if is an inert metal, can be modified by this reaction and the effective active area might decrease. We have noticed that the sensitivity both to H_2O_2 and to glucose or lactate, after 20s of equilibration time, is much bigger that after 300s, but after 300s each addition has the same current response, so that the system is completely equilibrated. Moreover, working with living systems, in complex media, could damage the enzymatic matrix; hence, biosensor decreases its sensitivity to the analyte, but at the same time this degradation increases its permeability to hydrogen peroxide or other redox mediators that could reach more easily the electrode surface.

The sum of these processes, that gives a loss in sensitivity, is called electrode ***biofouling***, and for this reason it is mandatory to perform amperometric calibrations before and after any SECM measurements, in order to find the correction factors indispensable for the elaboration data.

In literature there are reported some non-conductive polymers[16] and patented protection layers[17], that are employed to prevent electrode fouling, a common problem in the biosensors field.

6.2 Kinetics of Enzyme-Based UME Biosensors

6.2.1 Introduction

Generally, enzymatic biosensors convert a specific substrate to its product while producing electrochemically detectable peroxide. The activity of the most

enzymes can be described by the Michaelis-Menten (MM) equation[1]:

$$V = \frac{d[P]}{dt} = \frac{V_{\max} \times [S]}{K_M + [S]}$$

where V is the reaction rate to the substrate, [S] is the concentration of the substrate, V_{max} represents the maximum rate of conversion, and K_M is the Michaelis constant (see definition below), which correspond to the substrate concentration when the reaction rate is half of V_{max}. When the diffusive effects may be neglected, as in the present case, and a quasi steady-state (QSS) has been established for enzymatic reaction, the rate of the process is given by the following equation[3-6]:

$$V = \frac{I}{2FA}$$

therefore, the current-concentration relationship that characterized a biosensor can be approximated by the modified equation:

$$V = \frac{I}{2FA} = \frac{I_{\max} \times [S]}{K_M^{App}}$$

where I is the current and I_{max} is the maximum current recorded by the biosensor, F is the Faraday constant (96485 s·A·mol^{-1}), A is the geometric area of the electrode (for ∅ 10 μm Pt, A = 7.85x10^{-7} cm^2), and K_M^{App} is the apparent MM constant for the biosensor. K_M^{App} is related not only to the K_M of the enzyme immobilized on the electrode, but also depends on other parameters such as the diffusion rates of the substrate (glucose and lactate), O_2, and hydrogen peroxide within the enzymatic layer. Because of these reasons, the K_M^{App} of a biosensor could be very different from the K_M of its free enzyme[1].

To experimentally determine the relationship between the current detected by the biosensor and the substrate concentration, we measured the current steps produced by the addition of increasing amounts of enzyme substrate to the recording medium. Plotting the value of the oxidation current against the substrate concentration gives a curve that can be fitted to the modified MM equation to yield the approximate value of K_M^{App}.

A graphical representation widely employed for enzymatic reactions, when the

QSS has been establish, is the Lineweaver-Burk plot, where the reciprocal values of the oxidation current are plotted against the reciprocal values of substrate concentration. From the linear fit of the straight line the approximate value of K_M^{App} (Figure 9) can be calculated: the values found for glucose biosensors are very variable, ranging from 1.5 ± 0.5 mM with glutaraldehyde fixation to around 4.3 ± 0.7 mM and 4.1 ± 1.5 mM for *o*-aminophenol and polypyrrole, respectively. As we expected, K_M^{App} is substantially lower than the K_M of the free enzyme, which is normally between 26 mM and 30 mM[1]. The K_M^{App} of lactate biosensors is slightly variable, ranging from 0.16 ± 0.05 mM with glutaraldehyde fixation to 0.06 ± 0.05 mM for polymer entrapment. The first value is close to the K_M of the free enzyme, which was measured for our LOx sample, equal to 0.35 mM.

The theoretical calculations of MM model predict that the linear range of biosensor sensitivity should extend up to concentrations around $K_M^{App}/10$, our biosensors do not follow this rule[1], therefore this suggest that our micro-biosensor may not follow the theoretical kinetics of Michaelis-Menten model.

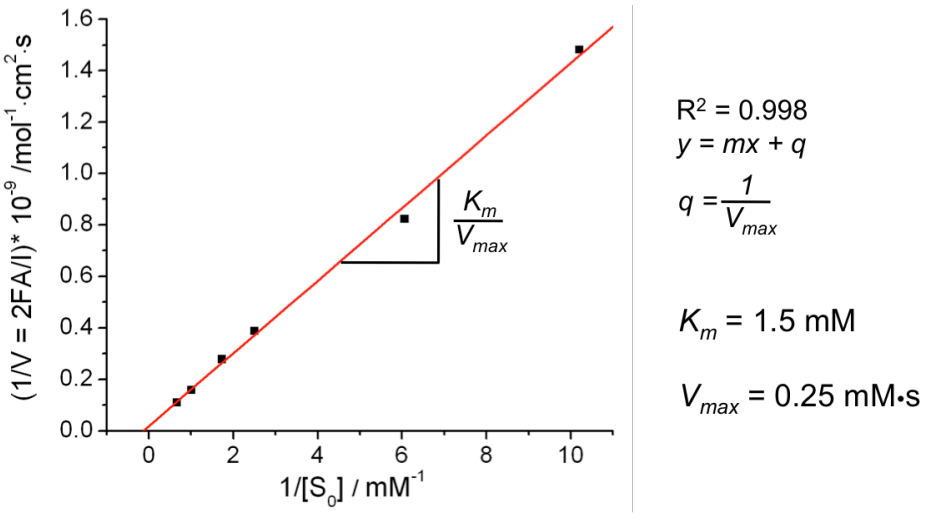

Figure 9. Typical linear Lineweaver-Burk Plot of a drop-cast GOx UME biosensor; glucose addiction from 0.1 mM to 2 mM. [E] << S_0. From the linear fitting we can calculate V_{max} from the intercept, and consequently K_m from the angular coefficient.

We further investigated the kinetics of drop-cast GOx UME biosensors in presence of very small amounts of substrate (from 1 μM to 100 μM): a very interesting situation because the typical concentration of substrate in respect to

the enzyme in living cells is [E] ≈ [S_0][18]. Analyzing the enzymatic kinetics at small substrate concentrations, we found that there is no linear dependency between the reciprocal values of oxidation current and substrate concentrations (Figure 10). These results suggest, once again, that the enzyme entrapped in those biosensors, at such low concentrations, might not follow the Michaelis-Menten theoretical kinetics.

Nevertheless, the enzymatic reaction rates are fast enough compared to the speed movements of the electrode during SECM measurements; therefore the enzyme-based biosensors can monitor metabolite changes without being affected by enzymatic kinetics restriction.

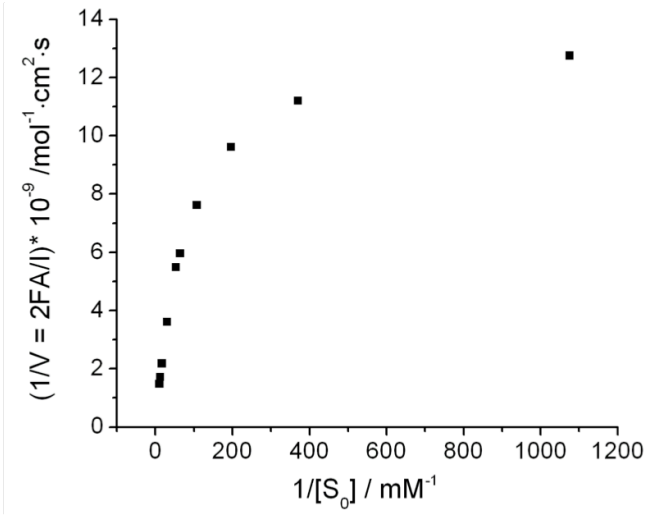

Figure 10. Lineweaver-Burk Plot of a drop-cast GOx UME biosensor; glucose addiction from 1 μM to 100 μM. [E] ≈ [S_0].

In literature there are several sophisticated mathematical models that describe the behaviour of enzymes in membranes[19]; these complex analyses are often needed to understand and optimize the behaviour of thick conducting layers. We used a recently introduced theoretical model[20] that can accurately predict formation of product even if the initial enzyme and substrate concentrations are comparable, such as in our developed drop-cast UME biosensors.

6.2.2 New Stochastic Model

Most of enzymatic reactions can be reduced to a two-steps process and are described by the following diagrammatic equation:

$$E + S \underset{k_{-1}}{\overset{k_1}{\rightleftharpoons}} C \xrightarrow{k_2} E + P$$

where *E*, *S*, *C* and *P* denote the time dependent concentration of the enzyme, the substrate, the intermediate complex, and the product, while k_1 ($M^{-1}s^{-1}$), k_{-1} (s^{-1}) express the forward and the reverse constants for enzyme/substrate complex formation respectively and k_2 (s^{-1}) express the catalytic rate constant.

The mathematical formalism of this equation depends on the environment in which the reaction occurs. In homogeneous environment, all the *k* are constant, and it should be noticed that k_{-1} and k_2 are frequencies of reaction competitive with each other and their comparison is essential to find analytical solutions[4]. In a general system, the common condition $[E] << S_0$ ensures the applicability of MM model kinetics. However, as observed, when the concentrations of the substrate are very small, the kinetics becomes oscillatory. As a consequence, in order to understand and quantify the real enzymatic activity, the formation product over time has to be considered to estimate the rate constants.

In order to assess this new model[20], several amperometric calibration measurements have been done by using our drop-cast GOx UME biosensors and by adding in solution glucose concentrations ranging from 1 μM to 60 μM (values lower or equal to the hypothetical enzyme concentration entrapped into the matrix that is estimated to be around 40 μM). The K_M^{App} calculated by mean of the classical MM approach is equal to 15.86 μM.

The experimental data were also fitted with the model -*ad hoc*- developed in order to estimate the real reaction rates (*k*), that are not constant at each experiment, but they are dependent on substrate concentration. Figure 1q shows just two examples of a set of experimental measurements of current vs time, upon addition of 2.5 μM of glucose ($[E_0] > [S]$) and 60 μM of glucose ($[E_0] \approx [S]$), fitted with the new theoretical equation.

Table 4 summarizes the main kinetics values obtained for the best fitting of the experimental data. It is worth to mention that for each group of experiments, each data set follows a different behaviour: this demonstrates the possibility of the existence of extra mechanisms that play important role. The results in the table reveal that: *i)* as the initial concentration of the substrate increases the forward rate constant decreases and the backward and catalytic rates increase, but in any case the backward rate constant is lower than the catalytic rate constant, *ii)* the theoretical concentrations of E_0 are different from the hypothetical values due to expectable reasons, such as the enzyme freezing

owing to the matrix entrapment, and as a consequence, *iii)* the ratio between the initial enzyme and substrate concentration is always greater than 0.1. In this case the analytical solution can give reasonable results only if $k_{-1} < k_2$.

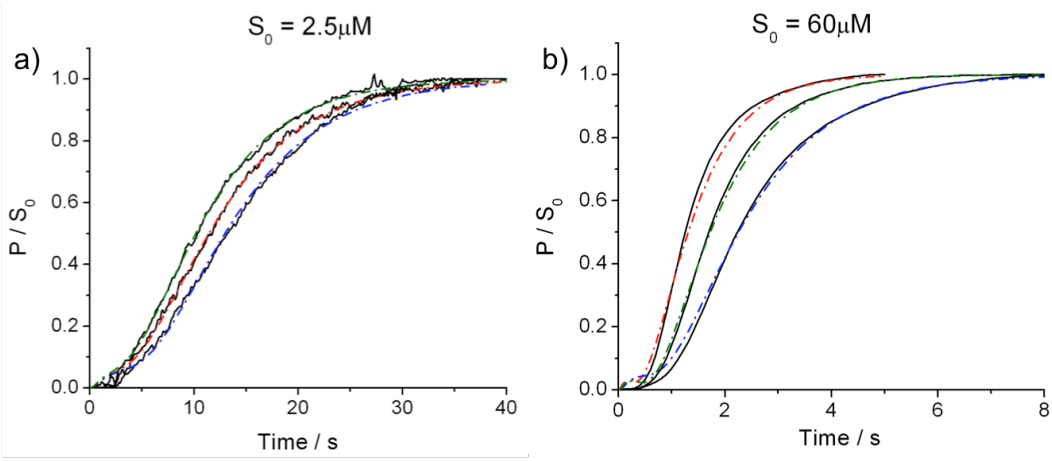

Figure 11. Representative graphs of amperometric calibrations; the current is firstly converted in product concentration and then the latter is normalized for the final substrate concentration. Each black line corresponds to an experimental data, while the colour lines correspond to the fitting obtained using the developed model.

Table 4. Mean reaction rates obtained for drop-cast GOx UME biosensor. In the first set of experiment we added (1) 2.5 μM, (2) 5 μM, (3) 20 μM and (4) 60 μM of glucose.

#	***So (μM)***	***Eo (μM)***	***k_1x10^5 ($M^{-1}s^{-1}$)***	***k_{-1} (s^{-1})***	***k_2 (s^{-1})***	***K_M (μM)***	***So/Eo***
1	2.5	0.48	7.61	0.173	0.285	**0.602**	4.81
2	5	0.6	5.61	0.317	0.815	**2.018**	8.03
3	20	3.33	5.211	1.06	3.851	**9.42**	6.04
4	60	6.23	4.25	3.315	7.083	**24.5**	8.72

Figure 12 shows the dependency of k_1 (M^{-1} s^{-1}), k_{-1} (s^{-1}), k_2 (s^{-1}) and K_M over different substrate concentrations. As the initial concentration of substrate increases the MM constant, K_M, the backward (k_{-1}) and the catalytic rate (k_2) linearly increase. Instead, the forward rate (k_1) constant decreases and its reduction does not follow a linear trend. The mean average value over the four different fits is K_M = 9.13 μM, smaller than the corresponding value estimated by the classical methods. In the classical Michaelis-Menten regime, under homogeneous conditions, the rates are constant (independent of substrate concentration) because the substrate molecules are in excess and they have a high and equal probability to be captured by active sites of the enzyme.

Therefore, the rate constants are not affected by the concentration of substrate. Whereas, the enzymatic mechanisms at microscopic point of view are linked to a perfect balance among the involved species: if this balance breaks down, a strong dependence of reaction rates on substrate concentration is generated[21].

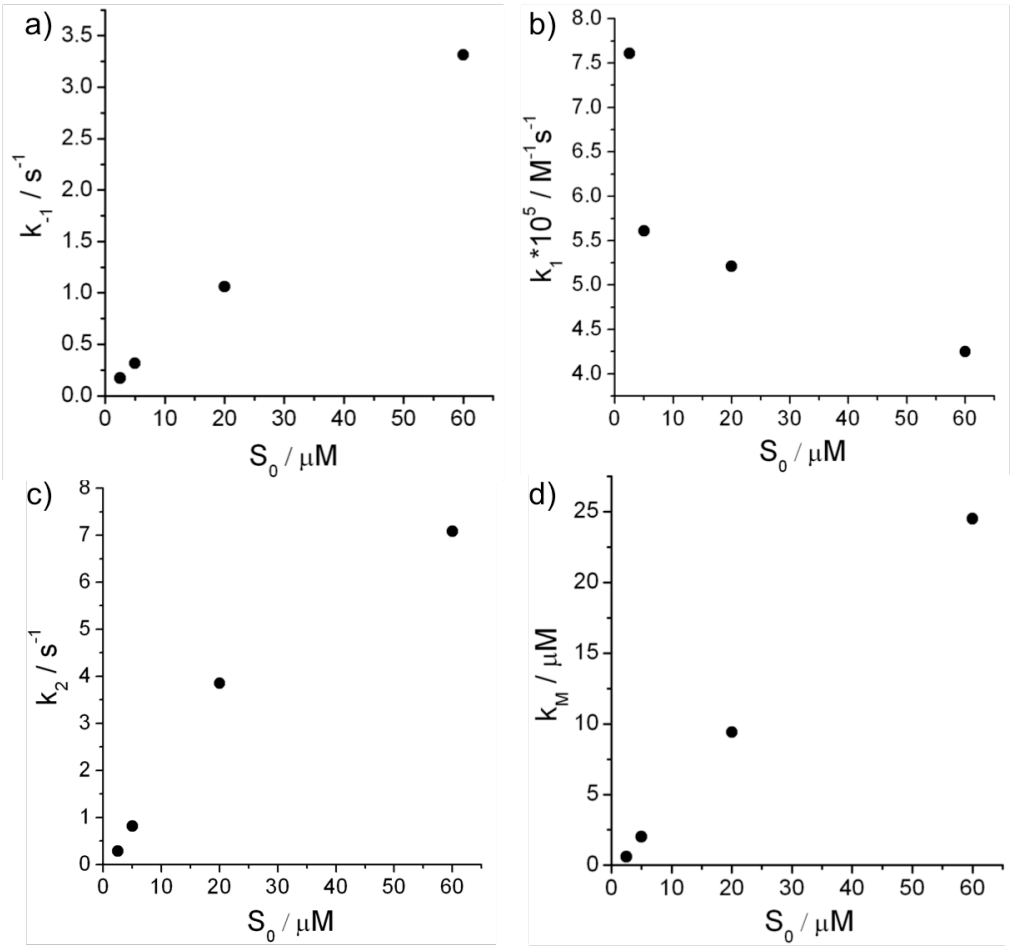

Figure 12. Graphical representations of the dependency between the enzymatic reaction rates and the substrate concentrations. k_{-1}, k_2, and k_M are increasing, while k_1 is decreasing with $[S_0]$.

6.3 Conclusion and Remarks

In investigating the most used immobilization procedures available in the field of biosensors for UME application, the goal of this thesis was to identify the most efficient methods and to select them for the coupling with SECM in order to study metabolism in living cells.

Considering that the local variations of glucose concentration and the absolute concentration of lactate around a single cell are very low, the sensitivity is the

most critical parameter to take care. After assessing and comparing the different modification routes, we concluded that the most sensitive electrodes are the ones obtained by drop-casting, which have also the highest enzyme concentration entrapped in the hydrogel matrix used to modify the probe. Other advantages of this deposition route are the easy manufacturing procedure and the low realization costs. Additionally, in these years a procedure to fine control the thickness of the drop cast matrix layer was developed, achieving a good reproducibility of the electrodes and a good spatial resolution; reproducibility and cost effective procedures are essential characteristics of "disposable" sensors.

Therefore, for the application of SECM toward the study of the basic metabolic processes, very sensitive and non-invasive drop-cast GOx and LOx UME biosensors were mainly employed in order to obtain glucose uptake and lactate release profiles of single living cells.

However, considering the operational parameters of all the tested and manufactured biosensors, it is not possible to identify a single specific immobilization procedure, which optimizes all the biosensor parameters. For example, cross-linking with GDA gives the highest sensitivity, but it is mitigated by its slightly lower resolutions both temporal and spatial. Moreover, GDA lacks the electrochemical control on membrane growth, which is available with electropolymerized methods. A lot of efforts are needed to build up a consensual protocol for enzyme immobilization that would satisfy all the criteria such as low toxicity, simplicity, stability, sensitivity, fast kinetics and fine control of deposition.

References

[1] Marinesco S, Vasylieva N, Enzyme Immobilization on Microelectrode Biosensors (Chapter 5). *Microelectrode Biosensors*. Marinesco S, Dale N. (Eds.), Humana Press c/o Springer Science (2013)

[2] Ciobanu M, Taylor DE Jr, Wilburn JP, Cliffel DE, Glucose and lactate biosensors for scanning electrochemical microscopy imaging of single live cells. *Anal. Chem*. 80, pp. 2717-2727 (2008)

[3] Otsuka I, Yaoita M, Nagashima S, Higano M, Molecular dimensions of dried glucose oxidase on a Au(111) surface studied by dynamic mode scanning force microscopy. *Electrochimica Acta*. 50, pp. 4861-4867 (2005).

[4] Parra A, Casero E, Lorenzo E, Periente F, Vazquez, Nanomechanical properties of globular proteins: lactate oxidase. *Langmuir*. 23, pp. 2747-2754 (2007)

[5] Stark RW, Drobek T, Heckl WM, Tapping-mode atomic force microscopy and phase-imaging in higher eigenmodes. Applied Physisc Letters. 74:22, pp. 3296-3298 (1999)

[6] Cecchet F, Marcaccio M, Margotti M, Paolucci F, Rapino S, Rudolf S, Redox mediation at 11-mercaptoundecanoic acid self-assembled monolayers on gold, *J. Phys. Chem*. 110, pp. 2241-2248 (2006)

[7] http://www.lifetechnologies.com/it/en/home/technical-resources/mediaformulation.116.html

[8] http://www.lifetechnologies.com/it/en/home/technical-resources/media-formulation.49.html

[9] O'Neil RD, Characterization of polymer-enzyme composite biosensors for brain monitoring in vivo (Chapter 6). *Microelectrode Biosensors*. Marinesco S, Dale N. (Eds.), Humana Press c/o Springer Science (2013)

[10] McMahon CP, Rocchitta G, Serra PA, Kirwan SM, Lowry JP, O'Neil RD, The efficiency of immobilised glutamate oxidase decreases with surface enzyme loading: an electrostatic effect, and reversal by a polycation significantly enhances biosensor sensitivity. *Analyst*. 131, pp. 68-72 (2006)

[11] Pyati R, Murray RW, Permeation and portioning of ferrocene ethylene oxide and propylene oxide oligomers into electropolymerized films from acetonitrile and polyether solutions. *J Phys Chem*. 98, pp. 111129-11135 (1994)

[12] Centoze D, Malitesta C, Palmisano F, Zambonin PG, Permeation of solutes through an electropolymerized ultrathin poly-o-phenylendiamine film used as an enzyme-entrapping membrane. *Electroanalysis*. 6, pp. 423-429 (1994)

[13] Craig JD, O'Neil RD, Electrosynthesis and permselective characterization of phenol-based polymers for biosensor application. *Anal. Chem. Acta*. 495, pp. 33-43 (2003)

[14] Vessman J, Stefan RI, Van Staden JF, Danzer K, Lindner W, Burns DT, Fajgelj A, Müller H, Selectivity in analytical chemistry (IUPAC Recommendations 2001) *Pure Appl. Chem*. 73:8, pp. 1381-1386 (2001)

[15] Marcu R, Rapino S, Trinei M, Valenti G, Marcaccio M, Pelicci PG, Paolucci F, Giorgio M, Electrochemical study of hydrogen peroxide formation in isolated mitochondria, *Bioelectrochemistry*. 85, pp.21-28 (2012)

[16] Wilson GS, Gifford R, Biosensors for real-time in vivo measurements. *Biosensors and Bioelectronics*. 20, pp. 2388-2403 (2005)

[17] (a) Dale N, Hatz S, Tian F, Laludet E, Listening to the brain: microelectrode biosensors for neurochemicals. *Trends in Biotechonology*. 23, pp. 420-428 (2005) (b) Dale NE, Llaudet E, Droniou M, Coating WO2004048603 A2.

[18] Albe KR, Butler MH, Wright BE, Cellular concentrations of enzyme and their substrates. *J. Theor. Biol*. 143, pp. 163-195 (1990)

[19] Sivasankari M, Rajendran L, Analytical expressions of steady-state concentrations of species in potentiometric and amperometric biosensor, *Natural Science*. 4:12, pp. 1029-1041 (2012)

[20] Bakalis E, Kosmas M, Soldà A, Rapino S, Zerbetto F. Paper in preparation

[21] Yang J, Pearson JE, Origins of concentration dependence of waiting times for single-molecule fluorescence binding, J. Chem. Phys. 136:24, pp. 244506- 244517 (2012)

PART II

CASE STUDIES

Chapter 7

In Vitro Cell Culture Models

Abstract

Understanding the mechanism behind the metabolic alterations, which characterize cancer cells and collocate them among neighbouring healthy ones, represents a promising approach for diagnosis and treatment. *Ras* encoding gene is frequently mutated in human tumors; therefore, activation of Ras pathway, in *in vitro* cell cultures, offers a good experimental system to study the molecular mechanisms of transformation. pBabe-puro-based retroviral constructs were used to express an oncogenic form of *ras* (H-RasGlycine12Valine, RasV12) in human mammary epithelial cell line: MCF10A. Moreover, in order to assess the efficacy of some metabolism interacting anticancer drugs, other human cancer cell lines were investigated, such as A549 (lung carcinoma), HeLa (cervical carcinoma) and HepG2 (liver carcinoma).

Key words MCF10A RasV12, MCF10A pBabe, A549, HeLa, HepG2, Cell Cycle, Cell Counting, Western Blot

7.1 Human Mammary Epithelial Cells (MCF10A)

7.1.1 Introduction

Breast cancer is one of the most common malignancies affecting women in Western countries[1]. Despite extensive research efforts worldwide for understanding and eradicating this type of cancer, the cellular processes leading to carcinogenesis have yet to be definitively elucidated. Mutations in the cellular genome, affecting the expression or function of protein controlling cell growth, differentiation and survival, are considered to be the main cause of cancer. Metabolic alterations have been reported as one of the main effect of carcinogenesis[1]. Identify the altered genes involved in the various tumor types and understand the role and the effects of these genetic mutations on cell metabolism would be very useful also to elucidate therapeutic target.

Ras Oncogene in Human Cancer

A family of genes that is frequently found to lead alterations, causing cancer, is the one of the *ras* genes[2]. Point mutations occurring in Ras codons at the critical positions 12 (*H-ras*), 13 (*K-ras*), and 61 (*N-ras*), leading to an altered protein amino acid sequence, convert these genes into active oncogenes[2]. *Ras* genes can be found mutated in a variety of tumor types, although the incidence of *ras* activating mutations varies greatly. The highest incidences are found in adenocarcinoma of the pancreas, colon, lung, thyroid tumors and myeloid leukemia[2]. Despite extensive research, the signals that induce activation of Ras and the proteins affected by Ras in the signal transduction cascade are still not fully undertood. However a relationship between the presence of *ras* mutations and clinical and histopathological features of the tumor may exist.

7.1.2 *In vitro Cancer Model: RasV12 & pBabe MCF10A*

The *in vitro* model employed for this study is an immortalized, non-tumorigenic epithelial cell line derived from human fibrocystic mammary tissue (MCF10A). These cells are defined as "normal" breast epithelial cells as they have a near diploid karyotype and are dependent on hexogeneous growth factors for proliferation[3]. MCF10A cells were infected using a puromycin-resistant retroviral construct containing an oncogenic form of *ras*, H-RasVal12, (pBabe-RasV12) or an empty vector (pBabe) used as a control[4]. Forty-eight hours post infection cells were selected using 2 μM puromycin for 4 days (for details see *paragraph. 7.1.4*).

Human breast epithelial MCF10A cells were obtained from ATCC: crl-10317 (American Type Culture Collection, Manassas (VA), USA).

RasV12-transformed MCF10A cells display a slightly altered morphology (Figure 1a and 1b), an increased aerobic glycolysis, glucose consumption, lactate production and reduced respiration rate with respect to the control cells expressing the empty vector pBabe. Indeed, as preliminary results, we measured lactate release in cell culture medium, expressed in nM/cell/hour, with the EnzyChrome Lactate Assay kit (Bioassay Systems, see Appendix 1). As shown in Figure 1c, Ras cells display an amount of lactate release significantly higher than control cells. Moreover, O_2 consumption rate was measured, previously in our lab, with an oxygraph under basal conditions using the same number of cells ($3x10^6$ cells/mL) in order to monitor how the expression of oncogenic *ras* results in reduced respiratory activity of these cells (Figure 1d)[5].

7.1.3 MCF10A Growth Media

Cells were cultured in Dulbecco's Modified Eagle's Medium (DMEM)/Nutrient Mixture F-12 Ham (1:1) (Gibco-Life Technologies Corporation) supplemented with 5% horse serum, 2 mM L-glutamine, 50 U/mL penicillin/streptomycin, 0.01 mg/mL insulin, 500 ng/mL hydrocortisone, 50 ng/mL cholera toxin and 20 ng/mL epidermal growth factor (EGF)[6]. Cells were kept in incubator at 37°C, 10% CO_2, 21% O_2 and split upon trypsin digestion every three or four days using a splitting ratio of 1:6 or 1:12 avoiding cells to reach full confluence.

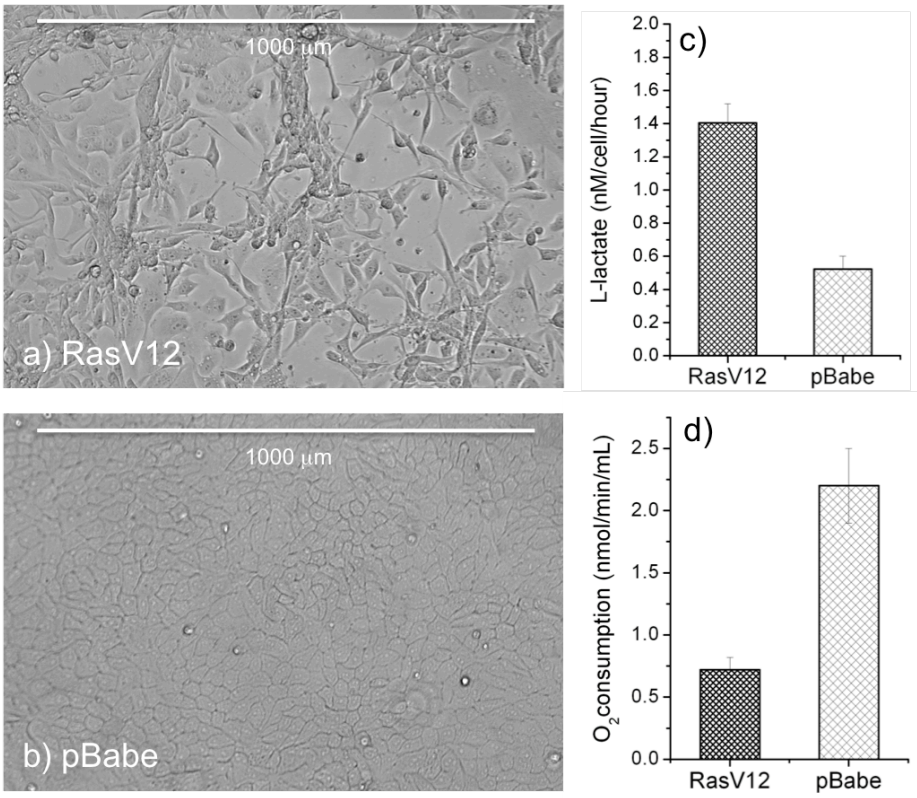

Figure 1. Transmission optical microscopy images of confluence dishes of RasV12 (a) and pBabe (b) MCF10A cells. Phenotypically, Ras-V12 expression resulted in altered morphology, including blown up and less spread shape, filopodia-like structure and loss of contact inhibition. (c) Lactate production and (d) basal respiration of Ras-V12 and pBabe cells. The values represent the means of three independent experiments ± standard error.

7.1.4 RasV12 Retroviral Infection

For MCF10A cells infection, the supernatant produced by the amphotropic packaging cell line Phoenix were used. 24h prior transfection Phoenix cells were plated at 2.000.000-3.500.000 cells per 10 cm plate in DMEM, 10% bovine calf serum, 2 mM L-glutamine, 50 U/ml penicillin/streptomycin. Phoenix cells were transfected using calcium phosphate co-precipitation method. 5min prior transfection, to each plate of Phoenix was added 25 μM

chloroquine that inhibits lysosomal DNases. 15-20 μg DNA was diluted in 0.2 M of $CaCl_2$ solution and 0.5 mL 2xHBS was added quickly while bubbling vigorously with the pipettor. The mix was incubated at RT for 10 min and then was distributed evenly on top of the Phoenix cells. After 8h the medium of Phoenix cells was changed with a fresh one. 24h post transfection the target cells were plated in normal growth medium, 300000 cells per 10 cm plate. 48h post transfection the medium of target cells was replaced with the viral supernatant produced by Phoenix cells filtered through a 0.45μm filter and supplemented with 1μg/ml polybrene. 48h post infection MCF10A cells were selected with 2 μg/ml puromycin [4].

7.1.5 Ras Expression by Western Blot Analysis

RasV12 protein expression and Ras-induced activation of the Raf/MEK/ERK signaling pathway were revealed by western blot analysis of cellular protein extract using antibodies against *ras* and the phosphorylated form of ERK kinase, a *ras* downstream effector (Figure 2). Briefly, cells were washed with ice-cold PBS and lysed in RIPA buffer, 1 mM PMSF, and both protease and phosphatase inhibitors. After lysis on ice for 30 min, cells were centrifuged at 18000 g for 15 min, and supernatants analysed for protein content. Protein concentration of lysates was determined by the Bradford assay (Bio-Rad). Equal amounts of protein were separated on Sodium Dodecyl Sulphate - PolyAcrylamide Gel Electrophoresis (SDS-PAGE) and transferred onto a PVDF Immobilon-P membrane (Millipore). SDS-PAGE and Western blotting were carried out by standard procedures. Membranes were blocked with 5% of BSA in Tris-buffered saline (TBS), 0.1% Tween20 (TBS-T) for 30 min at RT and probed with anti-H-Ras (C-20) (Santa Cruz Biotechnology), anti-p44/42 MAP Kinase (Erk1/2) (Cell Signaling Technology), and anti-Phospho-p44/42 MAPK (Thr202/Tyr204) (E10) (p-Erk1/2) (Cell Signaling Technology) antibody in blocking solution overnight at 4°C. After three washes in TBS-T, membranes were incubated 1h at RT with the appropriated horseradish peroxidase-conjugated secondary antibodies diluted in blocking solution. After three washes in TBS-T, detection was performed using enhanced chemiluminescence Western Blotting System (GE Healthcare). Vinculin was used as internal control in order to normalise for gel loading and transfer efficiency.

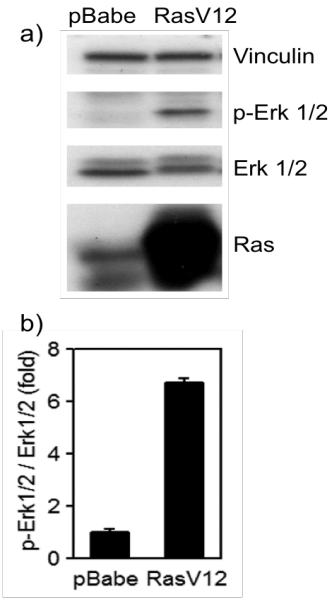

Figure 2. RasV12 expression transforms MCF10A cells. (a) Representative Western blot analysis of total protein lysate of MCF10A cells infected with empty retroviral vector (pBabe) or retroviral vector expressing RasV12 probed with anti-total Erk1/2, anti-phosphorylated form of Erk1/2 (p-Erk1/2), anti-Ras and anti-vinculin antibodies. Cropped images were obtained from the same gel/blot probed sequentially with the different antibodies. (b) In the graph is reported the ratio of p-Erk1/2 / total Erk1/2 as resulted from densitometric analysis of the blot. Protein levels were quantified by densitometric analysis of immunoblots using ImageJ software from NIH Image.

7.1.6 Ras Expression by Immuno-fluorescence Analysis

Protein expression and the subcellular localization of Ras protein in pBabe and RasV12 MCF10A cells was revealed by immunofluorescence (Figure 3). MCF10A cells were plated on glass coverslips and subjected to immunostaining protocol. Briefly, cells were fixed with 4% PFA in PBS, permeabilized using 0.1% Triton X-100, 0.2% BSA, in PBS and blocked with 2% BSA for 30 min. *Ras* staining was subsequently performed using anti-Ras primary antibody properly diluted in blocking solution. After incubation, cells were washed in PBS and stained with the appropriate anti IgG Alexa Fluor® antibody. Nuclei were stained with DAPI diluted in PBS, prior to final mounting using Mowiol (Calbiochem) or an anti-fade glycereol-based mounting medium. Slides were examined with a widefield fluorescence microscope and images were processed with ImageJ (NIH).

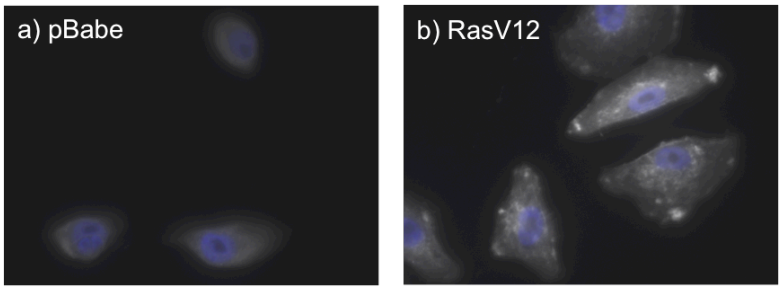

Figure 3. Fluorescence images of pBabe and RasV12 MCF10A cells after immunofluorescence staining with anti-Ras antibody (white) and *dapi* nuclear dye (blue). Ras proteins are expressed in all cell lineages. When *ras* genes are "switched on" by an incoming signal, those mutated genes become oncogenes, that lead to activated the production of permanently activated Ras proteins (panel b; more fluorescent signal –white color- means more Ras proteins).

7.2 Other Models of Human Carcinoma Cell Lines

7.2.1 A549

A549 cells are adenocarcinomic human alveolar basal epithelial cells, developed in 1972 through the removal and culturing of cancerous lung tissue in the explanted tumor of a 58-year-old male. *In vitro* this type of cells grows as a monolayer of cells, adherent or attaching to the bottom of the culture dish.
A549 cell line is known to have a fast metabolism, causing ***high levels of lactate released***[7]; for this reason it is widely used as an *in vitro* model for type II pulmonary cancer for assessing the efficacy of some new metabolic drugs, which should inhibit the lactate release during anaerobic glycolysis.

Growth Media

Cells were cultured in Dulbecco's Modified Eagle's Medium (DMEM) (Gibco-Life Technologies Corporation) supplemented with 10% fetal bovine serum (FBS) South-America, 2mM L-glutamine and 50U/mL penicillin/streptomycin[8]. Cells were kept in incubator at 37°C, 10% CO_2, 21% O_2 and were passed upon trypsin digestion every three or four days using a splitting ratio of 1:4 avoiding cells to reach full confluence.

7.2.2 HeLa

HeLa cells are human cervical carcinoma epithelial cells, which were taken from a patient who died of cancer in 1951, Henrietta Lacks. The cell line was found to be remarkably durable and prolific, because these cells do not die after *in vitro* cell division. Before this "immortal" model, cells cultured from other cells would survive in culture only for few days. This has represented an enormous bond to medical and biological research. HeLa cells are known to have a slow metabolism comparing to other cancer cells, but still higher than normal cells[7]; the model was employed to monitor the level of lactate release during proliferation.

Growth Media

Cells were cultured in Dulbecco's Modified Eagle's Medium (DMEM) (Gibco-Life Technologies Corporation) supplemented with 10% fetal bovine serum (FBS) South-America, 2mM L-glutamine and 50U/mL penicillin/streptomycin[9]. Cells were kept in incubator at 37°C, 10% CO_2, 21% O_2 and were passed upon trypsin digestion every three or four days using a splitting ratio of 1:3 avoiding cells to reach full confluence.

7.2.3 HepG2

HepG2 cells are human liver carcinoma epithelial cells, derived from the liver tissue of a 15-year-old male with a well-differentiated hepatocellular carcinoma. *In vitro* they grow in adherence to the bottom of the culture dish, forming small and circumscribed groups of cells (Figure 4).

Because of their high degree of morphological and functional differentiation *in vitro*, HepG2 cell line is a suitable model for studying intracellular trafficking and protein dynamics through the cellular membranes, for exploring the liver metabolism and for enhancing the drug targeting studies. It is worth to underline that these cells have a particular metabolism, since they recycle the lactate produced from anaerobic glycolysis in order to support their high proliferation (personal communication).

Growth Media

Cells were cultured in RPMI 1640 Medium (Gibco-Life Technologies Corporation) supplemented with 10% fetal bovine serum (FBS) South-America, 2 mM L-glutamine and 50 U/mL penicillin/streptomycin[10]. Cells were kept in incubator at 37°C, 10% CO_2, 21% O_2 and were passed upon trypsin digestion every three or four days using a splitting ratio of 1:3 avoiding cells to reach full confluence.

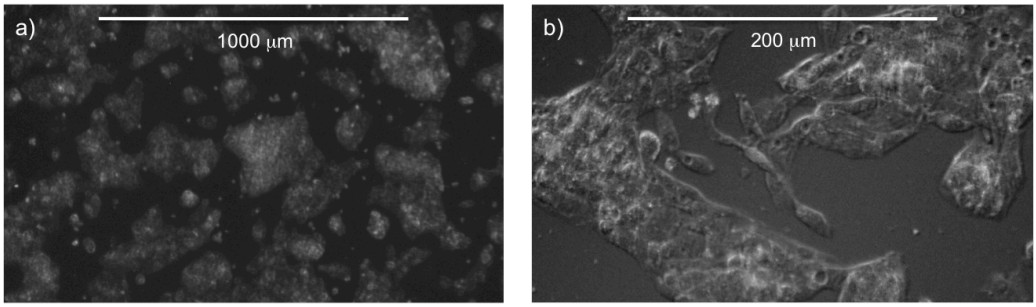

Figure 4. Transmission optical microscopy images of HepG2 cells. Low (a) and high (b) magnification.

References

[1] Stewart B, Wild CP, Word Cancer Report (2014)

[2] Bos JL, *Ras* oncogenes in human cancer: a review. *Cancer Research*. 49, pp. 4682-4689 (1989)

[3] Debnath J, Muthuswamy SK, Brugge JS, Morphogenesis and oncogenesis of MFC10A mammary epithelial acini growth in three-dimentional basement membrane cultures. *Methods*. 30, pp. 256-268 (2003)

[4] Grignani F, Kinsella T, Mencarelli A, Valtieri M, Riganelli D, Lanfrancone L, Peschle C, Nolan GP, Pelicci PG, High-efficiency gene transfer and selection of human hematopoietic progenitor cells with a hybrid EBV/retroviral vector expressing the green fluorescence protein. *Cancer Research*. 58, pp. 14-19 (1998)

[5] Marcu R, Rapino S, Trinei M, Valenti G, Marcaccio M, Pelicci PG, Paolucci F, Giorgio M, Electrochemical study of hydrogen peroxide formation in isolated mitochondria. *Bioelectrochemistry*. 85, pp. 21-28 (2012).

[6] Soule HD, Maloney TM, Wolman SR, Peterson WD Jr, Brenz R, McGrath CM, Russo J, Pauley RJ, Jones RF, Brooks SC. Isolation and characterization of a spontaneously immortalized human breast epithelial cell line, MCF-10. *Cancer Research*. 50:18, pp. 6075-6086 (1990)

[7] Giard DJ, Aaronson SA, Todaro GJ, Arnstein P, Kersey JH, Dosik H, Parks WP, In vitro cultivation of human tumors: establishment of cell lines derived from a series of solid tumors. *Journal of the National Cancer Institute.* 51:5, pp. 1417-1423 (1973)

[8] Abcam.com "A549 (human lung adenocarcinoma epithelial cell line) whole cell lysate" (ab7910)

[9] Abcam.com "HeLa (human epithelial carcinoma cell line) whole cell lysate" (ab29545)

[10] Abcam.com "HepG2 (human hepatocellular liver carcinoma cell line) whole cell lysate" (ab7900)

Chapter 8

Investigation of D-Glucose Uptake on Breast Cancer and Normal Human Cells

Abstract

We contributed to develop a sensitive, cheap and not invasive glucose biosensoring technique able to provide detailed and spatially resolved information on metabolism of cancer cells by monitoring their glucose uptake. The method is based on electrochemical measurements using *ad hoc* manufactured GOx-based UMEs used as a probe of Scanning Electrochemical Microscopy (SECM). This system allows the investigation the cell metabolism with high spatial and time resolutions, since it can resolve the electrochemical activity across the surface of a single cell and it can dynamically record metabolic changes in time. By SECM approach curves the UME biosensor is positioned at a known distance above cells, then the tip is laterally scanned at constant height to get the glucose uptake profiles of the cells and bi-dimensional images. With this set up, we were able to monitor the glucose consumption of both transformed and normal human breast epithelial (MCF10A) cells, confirming the Warburg's observations[1].

Key words GOx, glucose biosensors, ACs, SECM (profiles and images), *Warburg Effect*, RasV12 and pBabe.

8.1 Drop-cast 10 µm Pt GOx-based UME Biosensors

8.1.1 Approach Curves

As already described in previous chapter, we optimized the drop-casting method for the realization of GOx-based UME biosensors, achieving a very precise procedure in order to control the thickness of the drop-cast matrix, which is necessary for having a good spatial resolution, maintaining at the same time high sensitivity and reproducibility. In order to use SECM for the study of metabolic processes of cancerous cells, we employed these drop-cast GOx sensors as probes of our BioSECM apparatus (Chapter 4).

We have measured glucose uptake profiles on normal and transformed human breast epithelial MCF10A cells. As a reminder, MCF10A cells were infected either by a pBabe empty retroviral vector, used as control, and by a vector expressing the oncogene RasV12. RasV12 transformed cells have already been shown to be a good cancer *in vitro* model[2].

By using approaches curves (ACs) the electrode tip is positioned at a known distance from the plastic bottom Petri dish on which cells are cultured at low density to permit the imaging of single cells without interference from neighbouring ones. The tip-substrate separation distance is very accurately controlled by piezo and stepper motors, and the tip movement along the axes is monitored through the current response (ACs) and by the optical inverted microscope to minimize the risks of damaging the enzymatic film of the biosensor during the experiment. The optical microscope is also useful to check the morphology of scanned cells. During ACs we can monitor either the analyte (such as glucose) or a redox mediator added in the solution, which may have a faster feedback response at the electrode surface. The approach curves were performed on the dishes recording a negative feedback. Figure 1 shows a typical approach in which the current decreases with decreasing of the UME/dish distance because of the hindering of redox mediator; in this specific case we used $[Ru(NH_3)_6]^{3+}$ (E_{red} = -0.3V vs Ag/AgCl, 3M KCl).

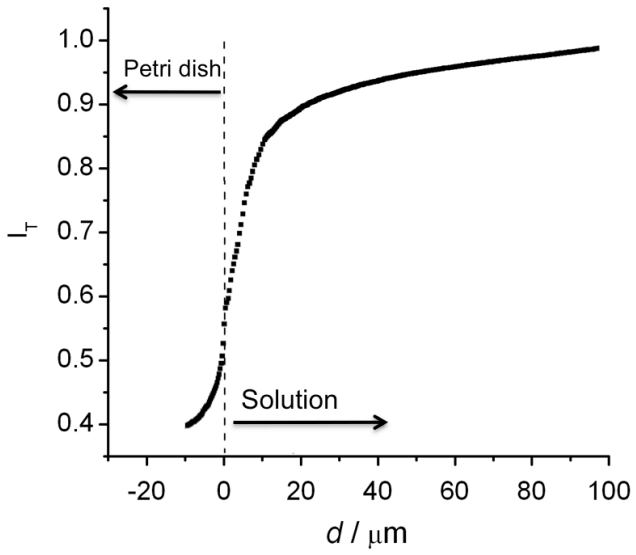

Figure 1. Typical approach of a drop-cast GOx 10 μm Pt UME biosensor to the Petri dish. E = -0.3 V vs Ag/AgCl, 3M KCl, in PBS buffer containing 500μM of $[Ru(NH_3)_6]^{3+}$. The current has been normalized in respect to the steady-state bulk current value. The vertical dashed line represents the point where the UME touches the Petri dish coming from the solution side.

The vertical dashed line represents the point where the UME biosensor touches the Petri dish. The distance of UME-dish contact is defined the zero distance. The final current does not reach the zero value probably due to the presence of the enzymatic matrix. It is worth to underline that we cannot use the classical ACs representation, with I_T vs $L = d/a$, because with the enzymatic coating it is difficult to exactly define the active part of the electrode (a).

For approach curves performed using the glucose signal during the approach, which is indirectly measured by the oxidation of H_2O_2, secondary product of the catalytic reaction of the enzyme entrapped into the matrix attached at the electrode tip, the shape of ACs for enzyme-coated UMEs do not obey to the classical SECM feedback theory (Figure 2). In fact, the current decreases slowly and the attempts of fitting them to simple kinetically limited (or mass transfer limited) feedback modes for SECM did not succeed. The reason of this behaviour is the very complex processes occurring at the tip.

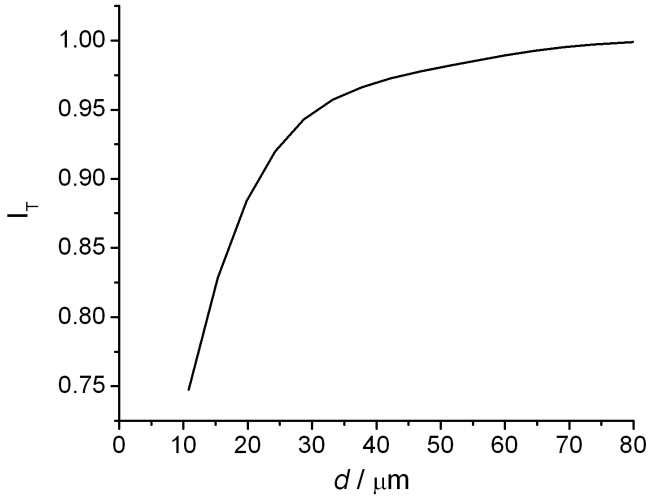

Figure 2. Typical approach curve of a drop-cast GOx 10 μm Pt UME biosensor to the Petri dish. E = +0.65 V vs Ag/AgCl, 3M KCl, in PBS buffer containing 10 μM of insulin, 0.1 mM of glucose and 2.5% of horse serum. The current has been normalized respect to the steady-state bulk current value. During ACs experiments the current is blocked at 75% of the total steady-state current value, in order to avoid sensor damaging.

After the approach curve, the tip is retracted at the desired distance from the dish using the z-axis motor controller of the SECM, and it is scanned horizontally in a plane parallel to the bottom Petri dish above the living cells to get their metabolic profiles of glucose uptake (Scheme 1). The images are carried out in constant

height mode. It is possible that the hydrogel matrix slightly adheres to the surface of the dish or the geometry of the enzymatic film can be disturbed during scans. For this reason, beyond the control of matrix degradation, it is necessary to perform calibration experiments prior and after any SECM applications, which clearly indicate if the UME biosensor is altered or not upon recording ACs or SECM scans.

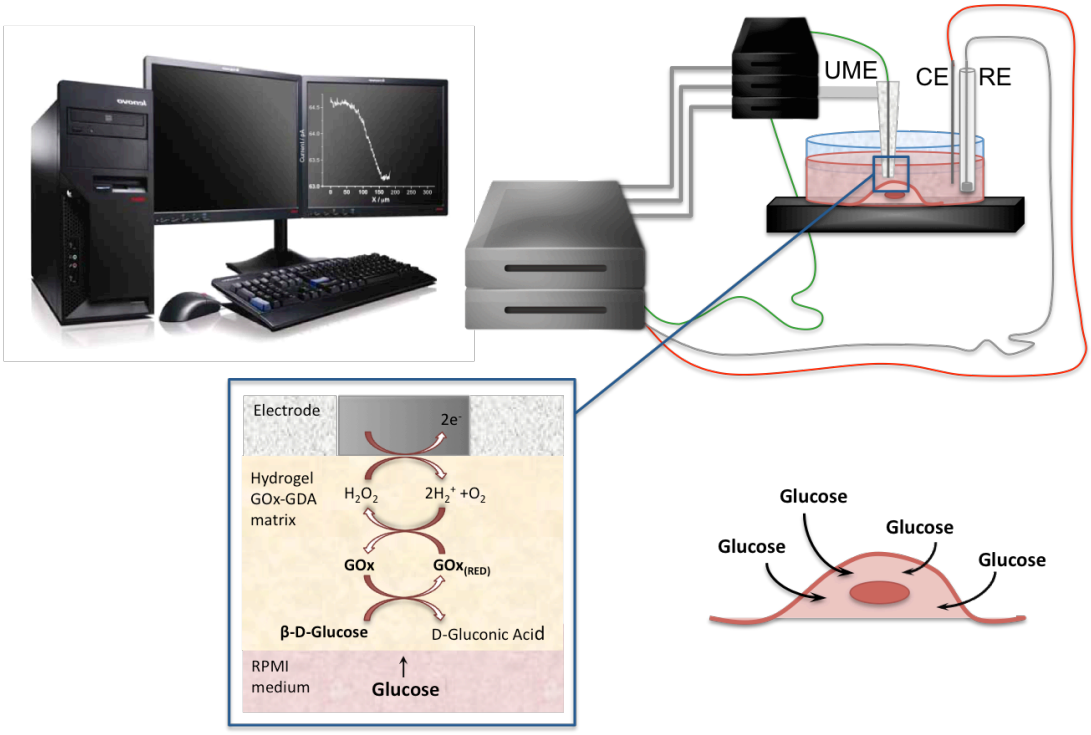

Scheme 1. Schematic representation of SECM glucose uptake profile above a single cell by mean drop-cast GOx-based UME biosensor.

8.1.2 Glucose Uptake Profiles

The amperometric current recorded at the UME tip is directly correlated with the local concentration of the metabolites and with the distance due to the negative feedback. For glucose investigation the current above single cell is lower because the cell is consuming glucose and its concentration locally decreases with respect to the bulk solution that contains 0.1 mM of glucose (Figure 3).

The first experiments were conducted in simple PBS buffer containing 0.1mM of glucose, 10 μM of insulin and 2.5% of horse serum in order to have a good sensitivity of GOx UME biosensors, but administrating to the cells essential growth factors. By using cell counting and cell cycle analysis by Flow Cytometry (FACs), we controlled that these conditions do not affect the cellular metabolism of the analyzed cell line in the time required to perform the SECM measurements. For more details see next sections: *8.3.1 and 8.3.2.*

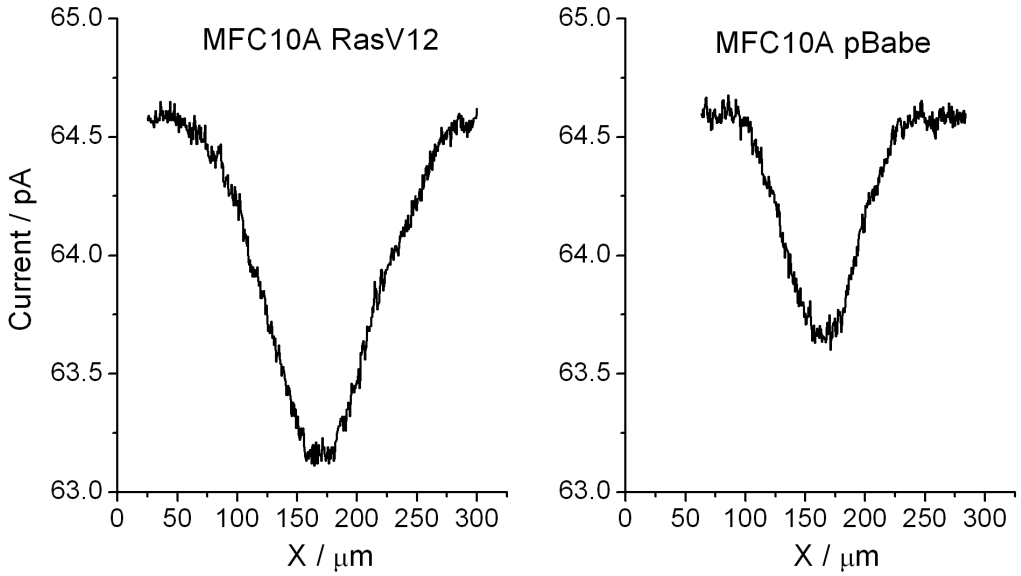

Figure 3. Representative SECM measurements of glucose uptake profiles of single RasV12 (oncogene) and pBabe (control) MCF10A cells, obtained by using a single drop-cast GOx-based UME biosensors in PBS buffer containing 10 μM of insulin, 0.1 mM of glucose and 2.5% of horse serum. E = +0.65 V vs Ag/AgCl 3M KCl. Scan speed 3 μm/s.

In order to obtain the value of concentration depletion of glucose, due to the uptake of single cell, the current of each scan is normalized by the current obtained from the calibration post SECM analysis, in which a known amount of analyte is added. Usually, we add 0.5 mM of glucose, in order to remain in the linear range of electrode sensitivity; the sensitivity in general slightly decreases comparing with calibrations done before SECM experiments (Figure 4).

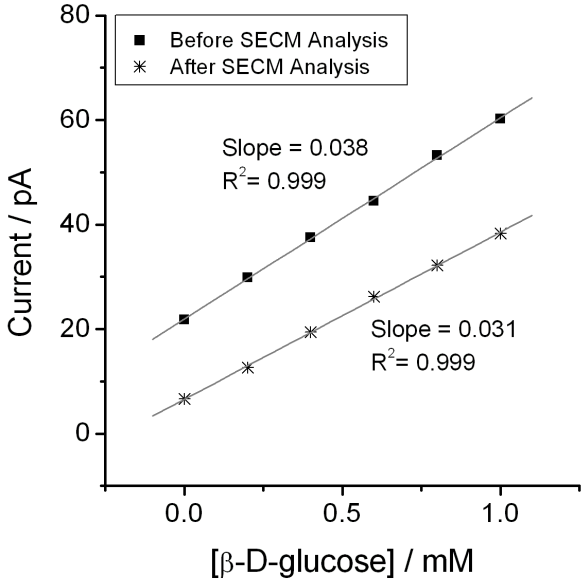

Figure 4. Drop-cast GOx UME biosensor sensitivity to glucose prior and after approach curves and SECM experiments.

Upon performing several experiments on pBabe and RasV12 MCF10A cells, belonging to different culturing dishes, the results show for the first time at this high spatial resolution, that glucose uptake is statistically higher for transformed cells than in normal ones, proving exactly what Warburg noticed almost 90 years ago (Figure 5). A value of 27.61 ± 14.33μM for RasV12 and of 14.93 ± 0.38μM for pBabe were obtained. For statistics, we employed different drop-cast UMEs, prepared with the same experimental protocol but changing enzymatic solutions. The standard deviation of transformed cells is larger likely due to the heterogeneity of Ras vector infection entity. This effect can only be noticed with a single cell experimental setup.

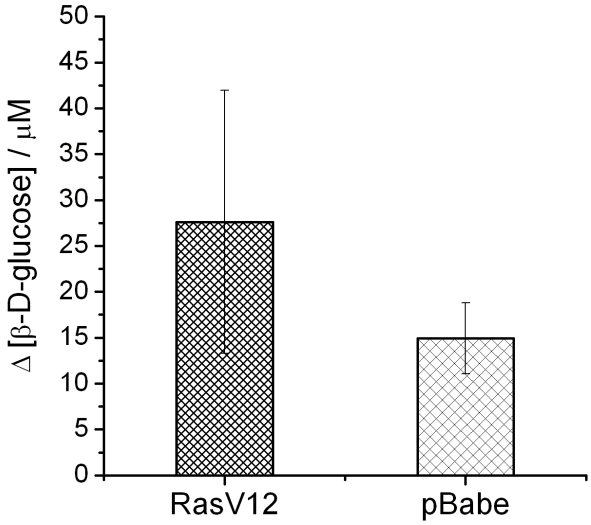

Figure 5. Local variation of glucose concentrations due to the cell consumption at single cell level. The decrease of glucose concentration for transformed (RasV12) MCF10A cells is 27.61 ± 14.33 μM upon 9 exp, while for normal (pBabe) MCF10A cells is 14.93 ± 0.38 μM upon 11 exp.

Considering that the cell topography is not flat, the electrode-sample separation distance changes during scanning and the current above the cells decreases for two main reasons: one is the real cell's consumption of glucose and the other one is due to the cell topographical contribution, which hinders the diffusion of glucose to the sensor. To discriminate the topographical contribution to the current decrease, we adopted a strategy to record at the same time *i)* the molecular fluxes and *ii)* the topography of living cells using the same enzymatic probe. We will discuss this issue in depth in *Chapter 9*. However, even if those values have still to be corrected for the topography, the results are in line with the hypothesis of aerobic metabolism; in fact, the hemispherical topography of pBabe and

RasV12 cells are quite similar (see previous studies in *Chapter 11*), thus we expect to approximately subtract the same current values from both.

8.2 Electropolymerized 10 μm Pt GOx-based UME Biosensors

8.2.1 Approach Curves

Although the drop-cast electrodes are more sensitive and easier to manufacture, they have less spatial resolution and reproducibility with respect to the electropolymerized ones, as discussed in *Chapter 6*. Therefore we employed electropolymerized with *o*-aminophenol GOx-based UME biosensors to obtain SECM profiles and images of local variations of glucose concentration at high spatial resolution. Before imaging, approach curves are performed in order to position the electrode tips above the single living cells without touching them (Figure 6). The images are carried out in constant height mode.

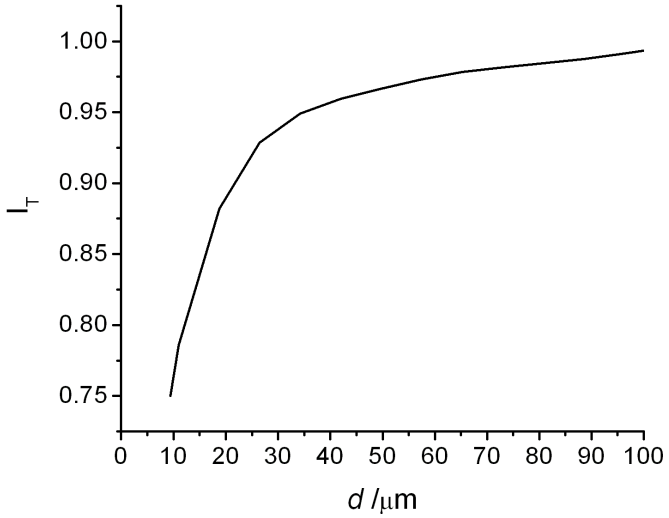

Figure 6. Typical approach curve of an electropolymerized (*o*-aminophenol) GOx 10μm Pt UME biosensor to the Petri dish. E = +0.65 V vs Ag/AgCl, 3M KCl, in PBS buffer containing 10 μM of insulin, 0.1 mM of glucose and 2.5% of horse serum. The current has been normalized respect to the steady-state bulk current value and it is blocked at 75% of the total steady-state current.

8.2.2 Glucose Uptake Profiles

The amperometric current recorded at the UME is lower for RasV12 than pBabe MCF10A cells (Figure 7); as a consequence, the glucose uptake for transformed cells results, once again, higher than normal ones (Figure 8). The values of glucose concentration depletion, obtained with these probes, slightly increase compared to drop-cast biosensors. This increase is due to the fact that with a

thinner enzymatic layer the probe-cell working distances are smaller; therefore, the UME biosensor above the cell is more sensitive to little variations in glucose concentration due to the cell consumption.

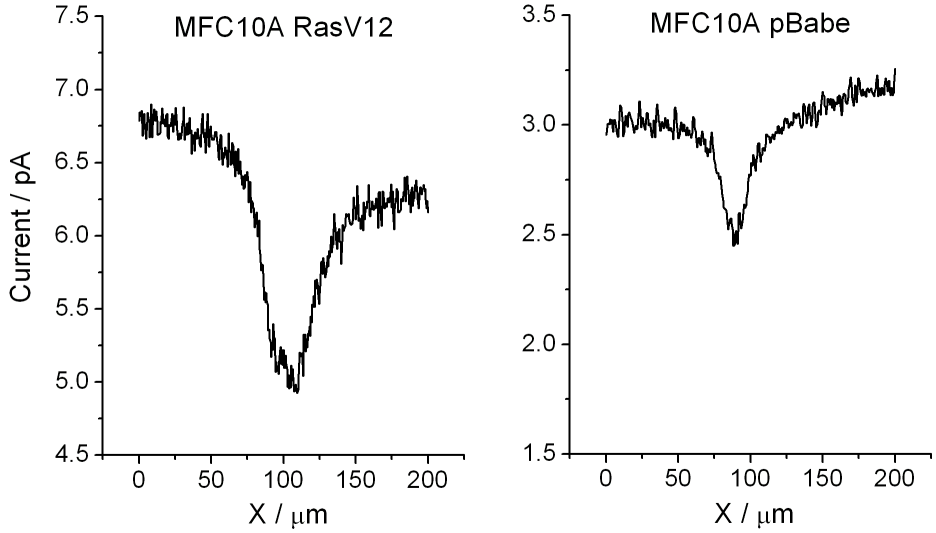

Figure 7. Representative SECM measurements of glucose uptake profiles for single cancer (RasV12) and normal (pBabe) MCF10A cells, obtained by using electropolymerized GOx-based UME biosensors in PBS buffer containing 10 μM of insulin, 0.1 mM of glucose and 2.5% of horse serum. E = +0.65 V vs Ag/AgCl 3M KCl. Scan speed 3 μm/s.

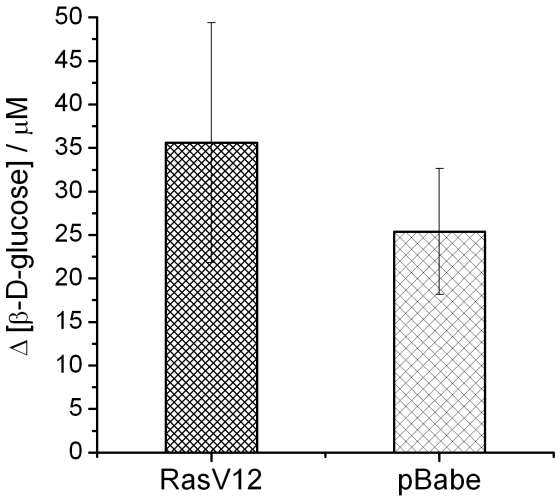

Figure 8. Local variation of glucose concentrations due to the cell consumption at single cell level. The decrease of glucose concentration for cancer (RasV12) MCF10A cells is 35.61 ± 13.79 μM upon 5 exp, while for normal (pBabe) MCF10A cells is 25.4 ± 7.23 μM upon 5 exp.

8.2.3 SECM Imaging

As aforementioned, with the electropolymerized method the spatial resolution of measurements considerably increases. Considering for example a RasV12 MCF10A cell, with a diameter of 20 ÷ 40 μm; the width range of the current peak

of glucose uptake, using a drop-cast GOx UME biosensor, is around 150 ÷ 230 μm, while, using an electropolymerized one the width range is 70 ÷ 125 μm, which is closer to the expected gradient around a cell of such dimension. Thanks to this feature, electropolymerized GOx UME biosensors are suitable to obtain SECM images of single and multiple cells, as shown in Figure 9. Comparing Figure 9c and Figure 9d a good correlation between the optical and the electrochemical images, achieved measuring the local variations of glucose concentration is observed.

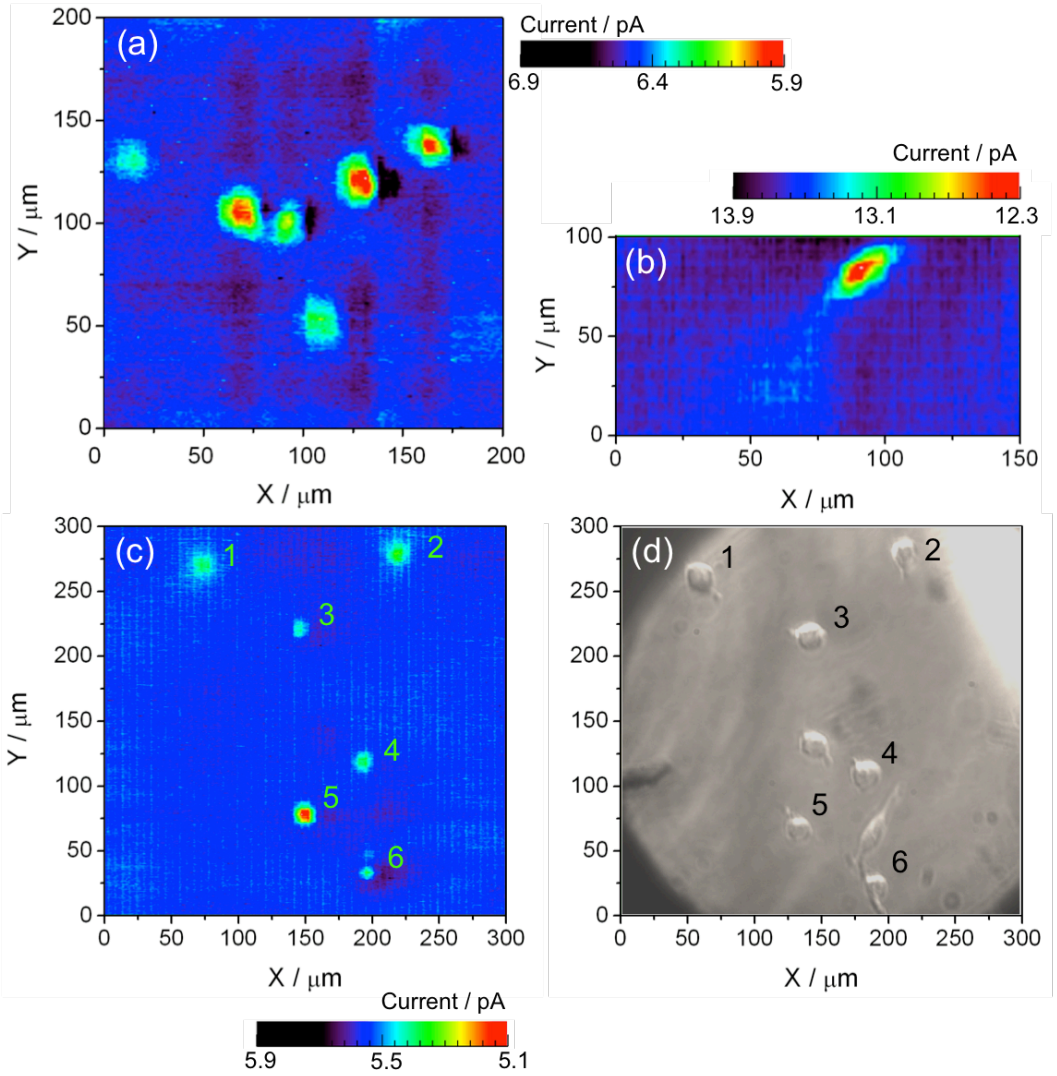

Figure 9. Representative SECM images at constant height of multiple (a) and single (b) RasV12 MCF10A cells. (c) and (d) show the comparison between the electrochemical and the optical images of the same culturing dish area. SECM experiments are performed with electropolymerized 10 μm Pt GOx-UME biosensors in PBS buffer containing 10 μM of insulin, 0.1 mM of glucose and 2.5% of horse serum. Scan speed 15 μm/s. E = +0.65 V vs Ag/AgCl 3M KCl.

From Figure 9c, one can observe that two cells are missing compared to the optical image; probably they were either removed during the SECM analysis or these cells have a much lower metabolism and they cannot be visualized.
However, from SECM images of glucose uptake we can conclude that the current is lowest on the top of the cell and the uptake profile is uniform around the single cells. Furthermore, it is possible that glucose uptake observed here is a combination of both diffusion and distribution profile of glucose and other nutrients around the single cell[3]. Consequently, for the study of cell metabolism one should acquire glucose uptake images in conjunction with measuring the cellular production of an analyte, such as lactate[3].

Electropolymerization method has many advantages, such as great spatial resolution and reproducibility, but *i)* it lacks in sensitivity, *ii)* the matrixes are more breakable, and *iii)* the protocol of polymer layer formation is more complex in respect to drop-cast. In fact, as already explained, the electrochemical formation of all these polymers strictly requires the exclusion of molecular oxygen from the electropolymerization solution, thus implying complicated procedures that limits their applications. For these reasons the drop-cast method is preferred to implement the further metabolic studies, which has a more facile manufacturing protocol. With this purpose, in these years we developed a procedure to finely control the thickness of the drop-cast matrix, achieving a very good reproducibility of the electrodes and a satisfactory spatial resolution, with a peak width in the order of 100 μm (see *Chapter 9* for more details; in which we discuss on the cell topography contribution).

8.3 Effects of Solutions Analysis on Cellular Metabolism

8.3.1 Cell Counting

Since we are working at single cell level, the local variations of metabolite concentrations are very small, in the order of micro or even submicro-molar. For this reason it is mandatory to use a sensor with high sensitivity, but at the same time the working environment should not adversely affect cell metabolism. We have deeply addressed this fundamental issue, by studying cell viability and cell cycle of our cell line model in different solutions analysis and at the same time

assessing the UME biosensor sensitivity in the same solution (*Chapter 6*).

The most common way to assess cell viability is to count viable cells is using Trypan Blue exclusion method (for the experimental protocol see Appendix #2). Briefly, Trypan Blue is a vital dye, whose reactivity is based on the fact that the chromophore is negatively charged and does not interact with cell unless the membrane is damaged. Hence, all the cells that exclude the dye are viable.

Figure 10 represents the cellular-growth curves of RasV12 and pBabe MCF10A cells in different environments: in complete MCF10A medium (with 5% of serum), used as control, in medium with 1% of serum or without it and in RPMI with 1% of serum or without (as we observed that 5% of serum interferes too much with our biosensors performance).

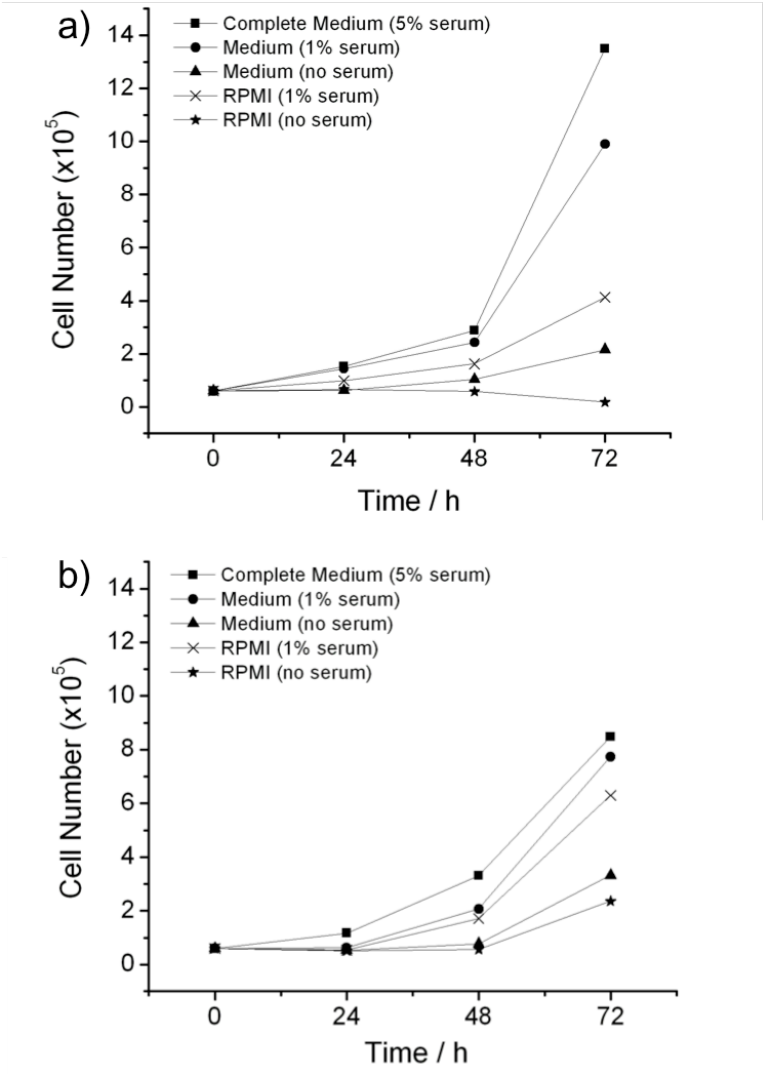

Figure 10. Representative cellular-growth curves of RasV12 (upper part) and pBabe (lower part) MCF10A cells in different solutions: (■) complete MCF10A Medium (5% of horse serum), (●) Medium (1% serum), (▲) Medium (no serum), (×) RPMI (1% serum), (★) RPMI (no serum).

From the cellular-growth curves, we can assert that: *a*) in normal conditions (complete medium, full of all the nutrients), cancer (Rasv12) cells are more proliferative than normal ones, as expected, *b*) both types are affected by the decrease of serum concentration, but *c*) cancer cells suffer more this condition, because, while normal cells simply slow down their growth, cancer cells die, and *d*) both types are alive in RPMI within 24h from the treatment.

For the PBS buffer + 2.5% serum, a large mortality is already observed after 6h of treatment, expecially for RasV12 cells. However, the complete SECM experiments take less than 3 hours, and we decided to check the cell cycle by Flow Cytometry Analysis (FACS, see next section) in order to check that durign the experiments cells did not arrest theri cell cycling.

8.3.2 Cell Cycle by FACs

The cell cycle is a series of events that lead to cell division and replication, consisting of four phases: G_1, S, G_2 and M. The activation of each phase depends on the proper completion of the previous one. The cell cycle starts with the G_1 phase, during which the cell increases its size, increasing their supply of nutrients and proteins. During the S phase the cell synthesizes DNA, and in the G_2 phase it synthesizes proteins to prepare for cell division. Finally during the M phase (mitosis) the cell divides and the two daughter cells enter the G_1 phase. Cells that have temporarily stopped dividing can enter a resting phase called G_0[4-5].

In cell biology *Cell Cycle Analysis* by Flow Cytometry (FACs, for the experimental protocol see Appendix #3) is a method to distinguish cells into the different phases. A fluorescent dye is used, such as propidium iodide (PI), which intercalates into DNA, and as a consequence, the fluorescent intensity of the stained cells is correlated with the amount of DNA they contain. As the DNA content of cells duplicates during S phase of the cell cycle, the relative amount of cells in G_0/G_1, *S* or G_2/M phases can be determined, as the fluorescence of cells in G_2/M phase will be twice as high as that of cells in G_0/G_1[4-5].

Cell cycle anomalies can be symptoms of various kinds of cell damage (e.g. DNA damage) or lack of nutrients, such as serum deprivation, which cause the cell cycle interruption at certain points. Therefore, monitoring the cell cycle gives information about the cell status and the cellular balance[5].

We have analyzed the cell cycle by flow cytometry of RasV12 and pBabe MCF10A cells after 3h of incubation in complete medium, used as control

(Figure 12), in RPMI medium and in PBS + 2.5% of serum.

These are the two main analysis solutions, which we have identified as the best compromises among all, in which the sensors are still sensitive and the cell viability is active.

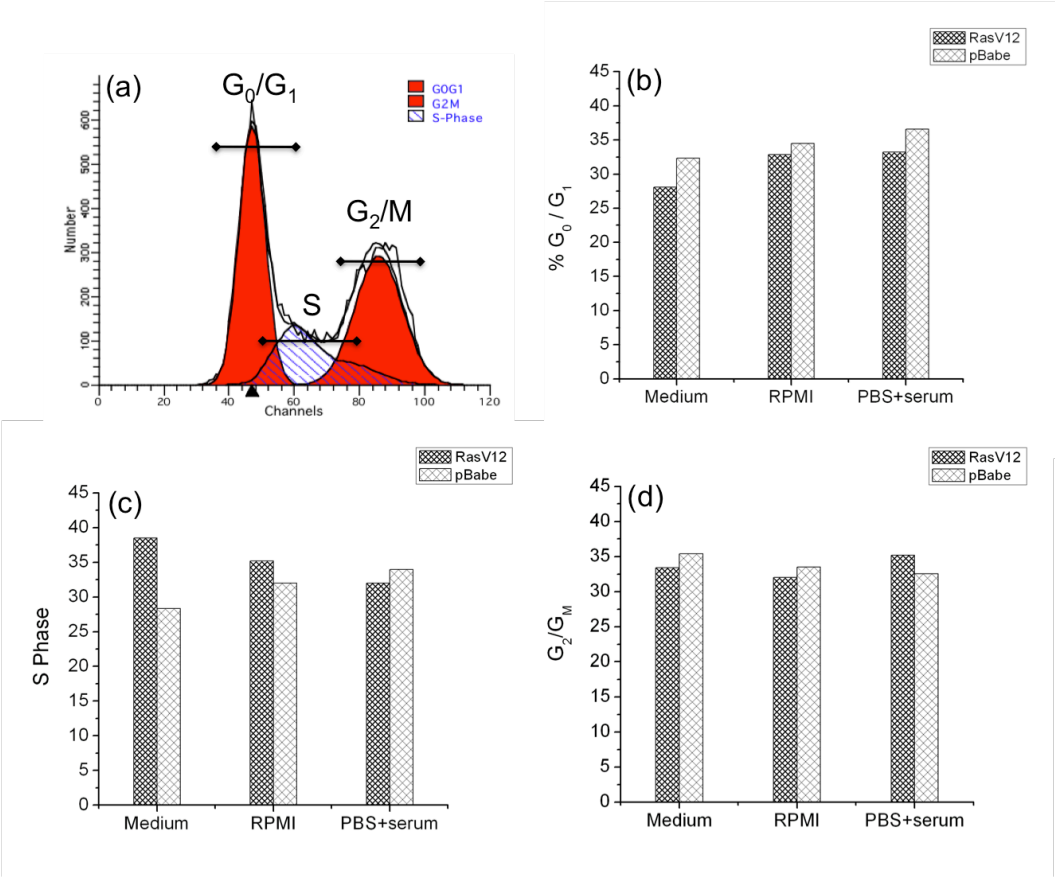

Figure 12. (a) Typical flow cytometric analysis for cells cycle distribution. Diagrams about the percentage of RasV12 and pBabe MCF10A cells in the correspondent phases: (b) G_0/G_1 phase, (c) S phase and (d) G_2/M phase in the different media.

After 3h we did not observe a visible variations in cell cycles due to the changing environment; in fact, as it is shown in diagrams of Figure 12, among all systems, the amount of cells in G0/G1 phase, S phase and G2/M phase are close to each others. It means that the metabolism is not altered during our experiments.

However, as we have noticed extensive cell death after few hours in PBS, particularly in RasV12 expressing cells; therefore, we have used RPMI medium (without glucose) as the most suitable analysis solution.

References

[1] Warburg O, On the origin of cancer cells. *Science*. 123:3191, pp. 309-314 (1956)

[2] Bos JL, *Ras* oncogenes in human cancer: a review. *Cancer Research*. 49, pp. 4682-4689 (1989)

[3] Ciobanu M, Taylor DE Jr, Wilburn JP, Cliffel DE, Glucose and lactate biosensors for scanning electrochemical microscopy imaging of single live cells. *Anal. Chem*. 80, pp. 2717-2727 (2008)

[4] Lodish H, Berk A, Zipursky L, Matsudaira P, Baltimore D, Darnell J, Molecular Cell Biology Ed. 4th, New York: W.H. Freeman (2000)

[5] Pozarowsji P, Darzynkiewicz Z, Analysis of cell cycle by flow cytometry. Methods Mol Biol. 281, pp. 301-11 (2004)

Chapter 9

Study of Cell Topographic Contribution

Abstract

The cell topography is not flat on the Petri dish and, as a consequence, the electrode-sample distance changes during scanning, complicating SECM measurements and their analysis. In this chapter, our strategy for measuring the cellular topographical contribution upon metabolism studies is described. We have adopted a voltage-switching mode scanning electrochemical microscopy in which our drop-cast enzyme based UME biosensors are used as probes to acquire, simultaneously, high-quality topographical and electrochemical images of living cells. This is possible by changing the applied potential so as to change the faradaic current from a hindered diffusion feedback signal, attributed to a redox mediator that does not interact with cells and suitable for distance control and topographical imaging, to the electrochemical flux measurement of the analyte of interest, such as glucose or lactate.

Key words Topographic contribution, RasV12 and pBabe MCF10A cells, glucose, metabolism, $[Ru(NH_3)_6]Cl_3$

9.1 Voltage-Switching Mode on SECM

9.1.1 Introduction

The cell topography is not flat on the Petri dish, as a consequence, the electrode-sample distance changes during scanning, complicating the SECM measurements and their analysis. Various approaches for studying cellular topographic contribution have been developed and investigated in these years, such as AFM[1-3], shear-force[4-7], impedance[8-11], faradaic current[12-13], ion current[14-16] and electrochemical[17-19] feedback distance-control. However, most of the approaches require additional probe modifications for distance control or they lack in terms of resolution. We adopted a voltage-switching mode[20-21] developed to perform measurements of cellular topographic contribution and electrochemical fluxes using the same enzymatic probe.

9.1.2 *Operational Strategy on Glucose Uptake Analysis*

In glucose analysis, current decreases above the cells for two reasons: one is the real consumption of glucose and the other one is due to the cell topographic contribution, which hinders the diffusion of glucose to the sensor.

To discriminate between the topographic contribution and the functional response, we adopted a voltage-switching protocol to record at the same time *i)* the molecular fluxes and *ii)* the topography of living cells, using the same enzymatic probe. We added in the analysis solution a hydrophilic redox mediator, that cannot cross the cell membrane, and whose redox potential cannot interfere with the oxidation of hydrogen peroxide, E_{ox} = +0.65V vs Ag/AgCl 3M KCl. After testing a variety of electrochemical mediators to control their toxicity on our cell line model, we selected hexaammineruthenium chloride, $[Ru(NH_3)_6]Cl_3$, 500 μM as the most suitable redox mediator with a E_{red} = -0.3V vs Ag/AgCl 3M KCl (Figure 1 displays a schematic representation of the analytical protocol).

We performed approach curves with our optimized drop-cast GOx UME biosensor by monitoring the activity of the redox mediator, which exhibits a pure negative feedback due to its hindered diffusion. The desired distance of probe from the cell surface corresponded to current diminished by 75% compared to bulk solution. Then the approach of probe was stopped and tip was scanned horizontally parallel to the bottom Petri dish passing over the cell surface. The current at the tip is lower above the cell than elsewhere because of hindered diffusion of the redox mediator, and this provide the necessary feedback to obtain the topographical profiles. Subsequently, a second scan was carried out along the same line, for the detection of metabolic fluxes, after switching the UME potential to +0.65V, corresponding to H_2O_2 oxidation (Figure 2). As a matter of fact, both the cell metabolic activity and topography contribute to determine the level of the latter signal whereas the former contains only the topographic contribution.

Subtracting the topographic signal from the current measured at +0.65 V, (Figure 2) and normalizing those values using calibration curves recorded after SECM analyses, the absolute value of glucose concentration changers associated to cellular uptake was finally estimated.

Adopting this protocol, cells with arrested metabolism could be discriminated from healthy ones (Figure 3).

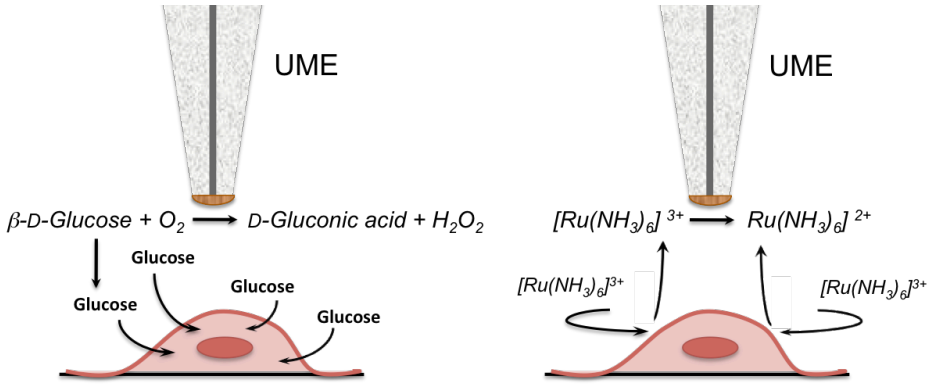

Figure 1. Schematic representation of the two mechanisms that occur at the drop-cast GOx UME biosensor during SECM glucose uptake analysis. On the left there is the reaction involved in glucose uptake monitoring, while on the right there is the cellular topographic contribution measurement, performed by adding in RPMI 500 μM of $[Ru(NH_3)_6]Cl_3$, as redox mediator.

Voltage Switching Mode

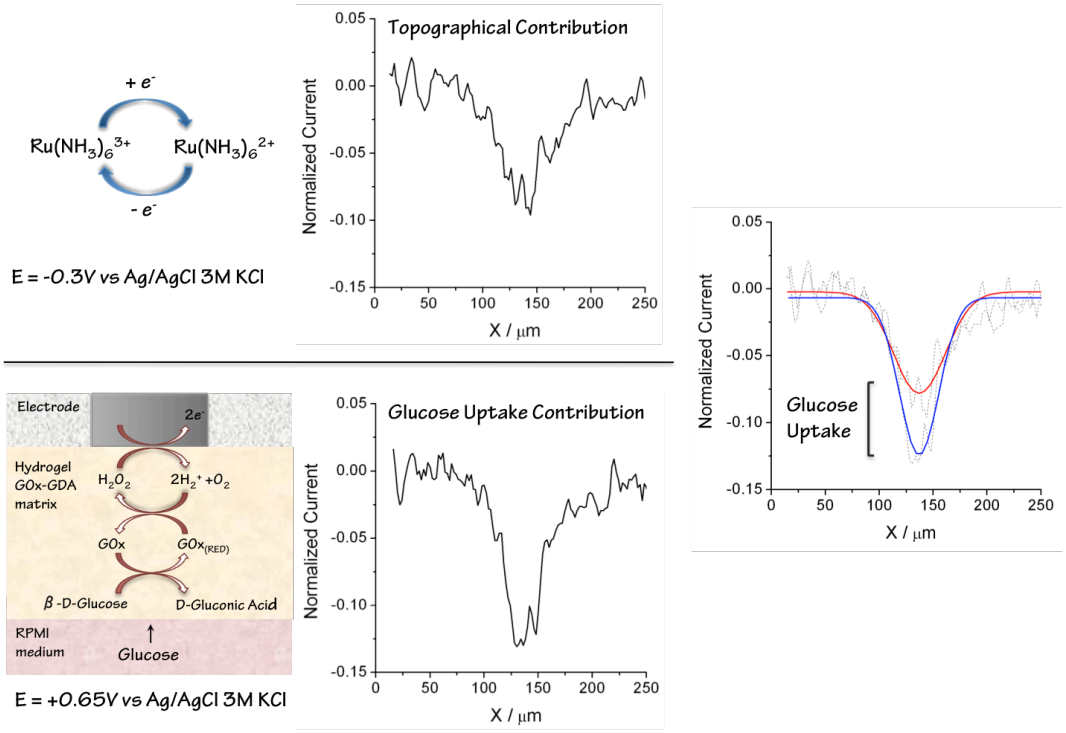

Figure 2. Schematic representation of a typical voltage-switching mode/SECM analysis in monitoring glucose uptake at single cell level. The upper part shows the mechanism and the real SECM measurement of cellular topographic contribution of a RasV12 MCF10A cell using $[Ru(NH_3)_6]^{3+}$ as redox mediator. *E* = -0.3 V vs Ag/AgCl, 3M KCl. The current is directly correlated to the distance between the electrode surface and the cell membrane. The lower part shows the glucose uptake contribution of the same cell. *E* = +0.65 V vs Ag/AgCl, 3M KCl. The measurements were performed with the same drop-cast 10 μm Pt GOx UME biosensor in RPMI medium containing 1 mM of glucose, 10 μM of insulin and 500 μM of $[Ru(NH_3)_6]^{3+}$. On the right we compare the two profiles, the currents were normalized by the respective steady-state bulk current values. The subtraction of the two lines gives the real of glucose concentration variations due to uptake of a single cancer cell that is 13 μM (Δ β-D-glucose).

Healthy & Metabolically Stopped Cells

Living cells exhibhit two different current profiles, as described above: a higher one corresponding to the hydrogen peroxide oxidation current and the lower one due to the feedaback response of the redox mediator. The first one is linked to both the cellular glucose uptake and topographical contribution, while the second one is due only to cell topography. By contrast, in case of metabollically or death cell the two profiles are perfectly superimposable, as the glucose metabolism of dead cells is stopped and the recorded signal is due only to the cellular topographical contribution, as shown in Figure 3.

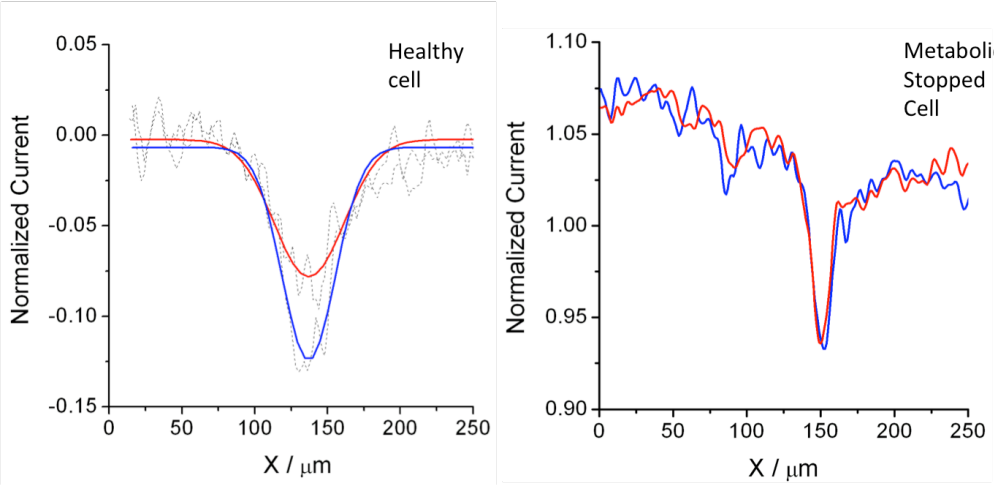

Figure 3. Difference in feedback between healthy cell and metabolic stopped cancer cells. Blue lines refer to the H_2O_2 detection, while red lines refer to cell topography. The measurements were done in 500 μM of $Ru(NH_3)_6]Cl_3$,/RPMI, 1 mM of glucose and 100 μM of insulin. For metabolically stopped cell the profiles are identical, meaning that cell is not consuming glucose.

The number of the voltage-switching mode experiments has to be increased for improving the statistical analysis, but the preliminary results on RasV12 and pBabe MCF10A cells, obtained on different culturing dishes, confirmed that the cellular topographic contribution for pBabe and RasV12 MCF10A cells are quite similar. In this specific case, the topographical contribution calculated for transformed cells (RasV12) is around 45% of the total current response, while for pBabe it is around 69%. This issue confirms the altered morphology that we usually observe on cancer cells, which are commonly smaller and more spherical and rigid than normal cells. Therefore, after subtracting this contribution, the glucose uptake for cancer cells remains statistically higher than in normal ones, as a proof of the *Warburg Effect* (Figure 4). The standard deviation of transformed cells is larger due to the heterogeneity of Ras vector.

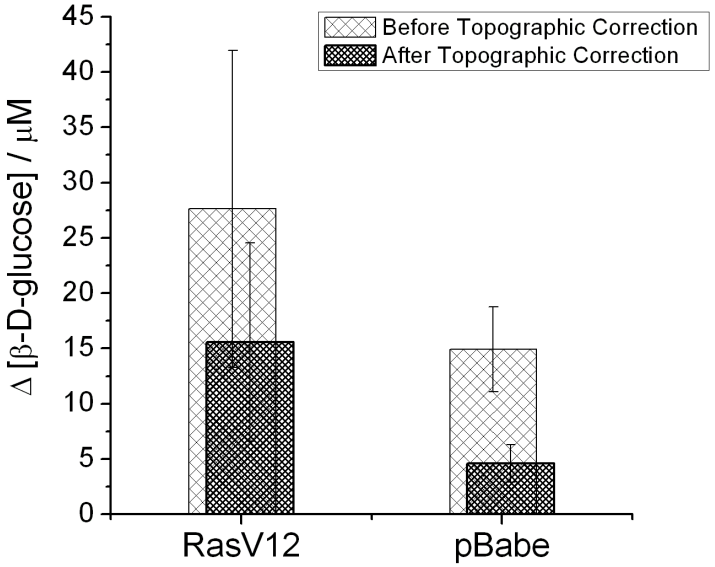

Figure 4. Statistical diagram that compares glucose concentrations locally consumed at single cell level before and after topographic correction. The absolute amount of glucose uptake for RasV12 MCF10A cells is around 15.57 ± 8.9 μM upon 4 experiments, while for pBabe MCF10A cells is around 4.6 ± 1.7 μM upon 2 experiments.

9.1.3 Biofouling Correction

Another important aspect to take care during the analysis of the electrochemical response is the biofouling of the hydrogel matrix.

As already discussed, the outcome of equilibration times is a progressive and continuous reduction of the oxidation current registered at the electrode. Additionally, when we consider an enzymatic biosensor, several events detrimental to its functioning may occur, such as saturation of the enzyme, the depletion and/or the degradation of the hydrogel matrix, etc. Therefore, the sensitivity of the GOx UME biosensor to glucose may in some cases decrease while, at the same time, its sensitivity to the redox mediator, $[Ru(NH_3)_6]^{3+}$ whose access to the active part of the electrode may be easier through the membrane defects, would increase or stay constant. A way to control and monitor this phenomenon is to perform amperometric calibrations after any SECM investigation using known amounts of glucose and $[Ru(NH_3)_6]^{3+}$, in order to find correction factors for the data elaboration. Figure 5 shows an example of this treatment of experimental data, after a measurement where the hydrogel matrix was very damaged. The peaks due to the cell topography are much higher than those correlated with the glucose uptake. However, in the post measurement calibrations, the GOx UME biosensor current response to $[Ru(NH_3)_6]^{3+}$ (Figure 5d) exhibits a sensitivity almost seven times higher than

that to glucose (Figure 5c) (3.42 nA per 1 mM $[Ru(NH_3)_6]^{3+}$ *versus* 0.495 nA per 1 mM of β-D-glucose addiction). The ratio between glucose and $[Ru(NH_3)_6]^{3+}$ sensitivity can be calculated, and by normalizing by this value both scans (Figure 5a), recorded in voltage-switching mode, the real cellular topographical contribution is obtained and subtracted from the metabolic current. This is an extreme example; usually, the degradation does not affect to such an extent the measurements because of the high matrix stability. Nevertheless, for each measurement calibration curves have to be performed to exactly determine the sensitivity of the biosensors.

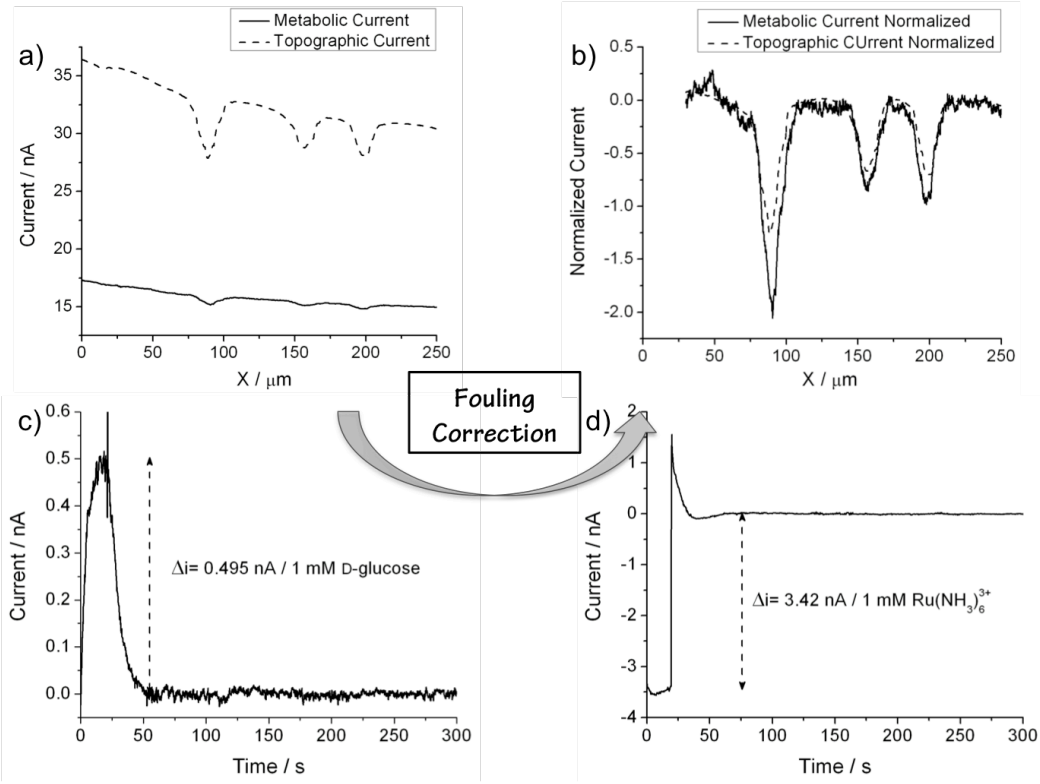

Figure 5. Example of biofouling and fouling correction, in case of high damaged matrix. (a) Linescans correlated to hydrogen peroxide (lower scan) and to $[Ru(NH_3)_6]^{3+}$ (upper scan) above 3 RasV12 MCF10A cells. (b) Correct profiles for biofouling factor. Drop-cast GOx UME sensitivity to (c) 1 mM of glucose and (d) 1 mM $[Ru(NH_3)_6]^{3+}$.

9.2 Redox Mediators

9.2.1 Redox Mediator Selection

Aim of this paragraph is to describe the investigation performed to assess the suitable redox mediators for topographical control during SECM glucose and lactate measurements. Redox mediators used for feedback imaging must meet

several criteria: *1)* the mediator must be nontoxic for cells, or at least over the time course of the experiments, *2)* the mediator should not cross the cell membrane, *3)* the redox potential of the mediator should be distinct from the redox potential of the analyzed species, and *4)* the release of metabolites from the cell must not be adversely affected by the presence of the mediator.

An extensive list of redox mediators is present in literature[23]; however, on the basis of the results of biocompatibility testing of many redox mediators only three of them were further investigated here: hexaammineruthenium(III) chloride $[Ru(NH_3)_6]Cl_3$, ferrocenemethanol [FcMeOH] and potassium haxacyanoferrate(III) $[K_3(Fc(CN)_6]$.

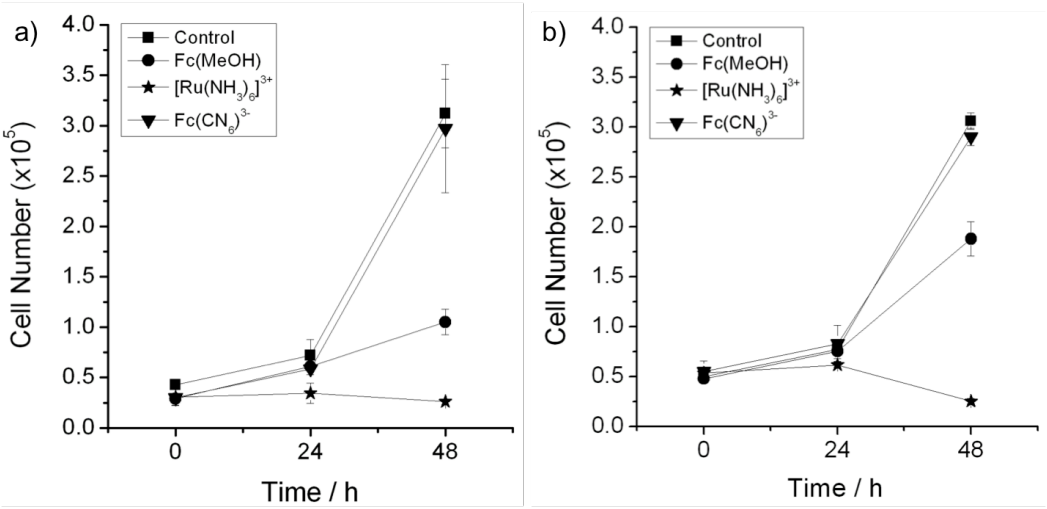

Figure 6. Cell viability of (a) RasV12 and (b) pBabe MCF10A cells, measured using trypan blue exclusion method after treatment with 1 mM of each redox mediator.

The selected mediators exhibit completely different behaviours on RasV12 and pBabe cells. In fact, in literature there are evidences that the cellular membrane in cancer cells should be more permeable than in normal ones, therefore the redox mediator can easily interact, influencing the viability of living systems[24]. In our experimental system $[(Fc(CN)_6]^{3-}$ does not show any negative effect on cellular growth, FcMeOH reduces cell growth particularly in RasV12 expressing cells, and $[Ru(NH_3)_6]^{3+}$ causes high mortality within 24/48h, and the cells began to appear unhealthy and exhibit changes in morphology already after 3 hours of treatment, that is however the time required for a complete SECM analysis. Moreover, the redox potentials of these possible mediators are: +0.4 V, +0.43 V, and -0.3 V vs Ag/AgCl 3M KCl for FcMeOH, $[(Fc(CN)_6]^{3-}$

$[Ru(NH_3)_6]^{3+}$

and $[Ru(NH_3)_6]^{3+}$, respectively. Considering that the redox potential of H_2O_2 detection (our biosensor's electroactive molecule) is +0.65 V, the first two mediators strongly influence the metabolites' analysis. Therefore, for monitoring the cell topography, we have decided to use $[Ru(NH_3)_6]^{3+}$, as the most suitable mediator, and to limit and avoid viability concerns, its concentration was decreased from 1 mM to 500 μM and every experiment was stopped after 2h of exposure.

Furthermore, we have performed MTT cell viability assay to verify that in our conditions (500 μM $[Ru(NH_3)_6]^{3+}$ - RPMI medium) both RasV12 and pBabe MCF10A cells were metabolically active.

9.2.2 MTT Test

The MTT assay is a colorimetric assay for assessing cell viability and proliferation (for details on protocol see Appendix #4). The reduction of tetrazolium salts is widely accepted as a reliable way to examine cell viability. Briefly, the yellow tetrazolium MTT, (3-(4,5-dimethylthiazolyl-2)-2,5-diphenyltetrazolium bromide), is reduced by metabolically active cells, in part by the action of dehydrogenase enzymes, to generate reducing equivalents such as NADH and NADPH. The resulting intracellular purple formazan can be solubilized and quantified by spectrophotometric means at a certain wavelength (usually between 500 and 600 nm). Figure 7 shows the results on cell viability after 3 h of treatment with: *1)* simply medium, used as control, *2)* medium with 500 μM $[Ru(NH_3)_6]^{3+}$, to assess the effect of the mediator on cells, *3)* RPMI medium and *4)* 500 μM $[Ru(NH_3)_6]^{3+}$ in RPMI medium.

The MTT cell viability assay determines the cell proliferation rate and conversely, when metabolic events lead to apoptosis or necrosis and the rate of cells death. From this analysis, we can conclude that 500 μM $[Ru(NH_3)_6]^{3+}$ in RPMI medium is slightly cytotoxic compared to a standard system. It is still the best solution found for investigations on cellular topographic contribution and electrochemical fluxes investigations, adopting a voltage-switching mode and using the same enzymatic probe.

It is very important to asses all of these parameters, we want to study the metabolic alterations on single living cells in physiological environment in order to evaluate the metabolism in standard conditions without, at the same time, loose the sensitivity of our enzyme-based UME biosensors.

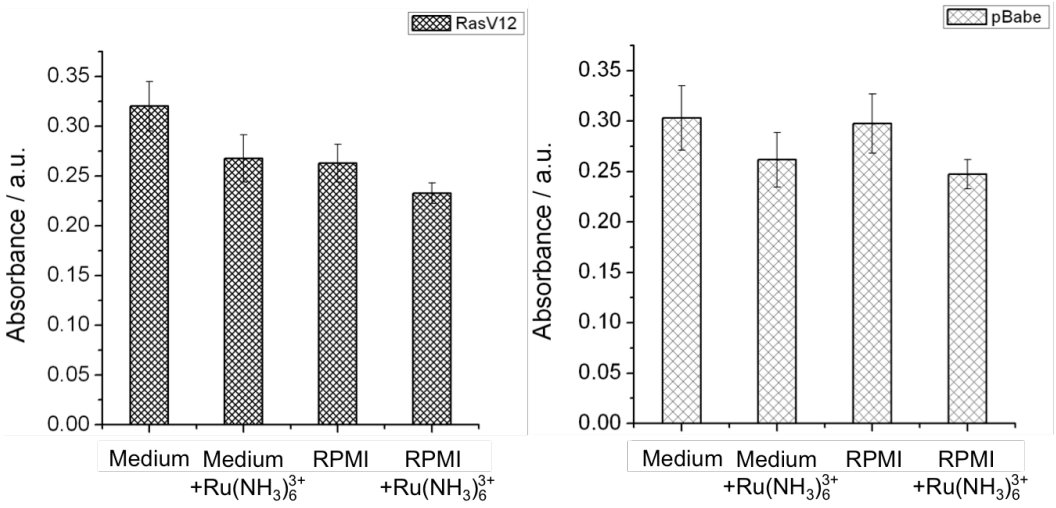

Figure 7. MTT Test for detecting cell viability of RasV12 and pBabe MCF10A cells for 3 h of treatment with *1)* simply medium, used as control, *2)* 500 μM $[Ru(NH_3)_6]^{3+}$ in medium, *3)* RPMI and *4)* 500 μM $[Ru(NH_3)_6]^{3+}$ in RPMI. Absorbance measured at 570 nm.

References

[1] Kueng A, Kranz C, Lugstein A, Bertagnolli E, Mizaikoff B, Integrated AFM-SECM in tapping mode: simultaneous topographical and electrochemical imaging of enzyme activity. *Angew. Chem. Int. Ed. Engl*. 42, pp. 3238-3240 (2003)

[2] Ueda A, Niwa O, Maruyama K, Shindo Y, Oka K, Suzuki K, Neurite imaging of living PC12 cells with scanning electrochemical/near field optical/atomic force microscopy. *Angew. Chem. Int. Ed. Engl*. 46, pp. 8238-8241 (2003)

[3] Mcpherson JV, Unwin PR, Combined scanning electrochemical microscopy. *Anal. Chem*. 72, pp. 276-285 (2000)

[4] Lee Y, Ding ZF, Bard AJ, Combined scanned electrochemical microscopy with shear force and current feedback. *Anal. Chem*. 73, pp. 3634-3643 (2002)

[5] Hengstenberg A, Blochi A, Dietzel ID, Schuhmann W, Spatially resolved detection of neurotransmitter secretion from individual cells by means of scanning electrochemical microscopy. *Angew Chem*. 81, pp. 9674-9681 (2001)

[6] Takahashi Y, Shiku H, Murata T, Yasukawa T, Matsue T, Transfected single-cell imaging by scanning electrochemical optical microscopy with shear force feedback regulation. Anal. Chem. 81, pp. 9674-9681 (2009)

[7] Schulte A, Nebel M, Schuhmann W, Single live cell topography and activity imaging with the shear-force-based constant-distance scanning electrochemical microscope (Chapter 12). *Methods in Enzymology*. Vol. 504, ©Elsevier Inc. (2012)

[8] Kurulugama RT, Wipf DO, Takacs SA, Pongmayteegul S, Garris PA, Baur JE, Scanning electrochemical microscopy of model neurons: constant distance imaging. *Anal. Chem*. 77, pp. 1111-1117 (2005)

[9] Osborn DM, Sanger RH, Smith PJS, Determination of single-cell oxygen consumption with impedance feedback for control of sample-probe separation. *Anal. Chem*. 77, pp. 6999-7004 (2005)

[10] Ding ZF, Zhao XC, Diakowski PM, Deconvoluting topography and spatial physiological activity of live macrophage cells by scanning electrochemical microscopy in constant-distance mode. *Anal. Chem*. 82, pp. 8371-8373 (2010)

[11] Schuhmann W, Pahler M, Santana JJ, Souto RM, Application of AC-SECM in corrosion science: local visualization of inhibitor films on active metals for corrosion protection. Chem. Eur. 17, pp. 905-911 (2010)

[12] Laforge FO, Velmurugan J, Wang YX, Mirkin MV, Nanoscale imaging of surface topography and reactivity with the scanning electrochemical microscope. *Anal. Chem*. 81, pp. 3143-3150 (2009)

[13] Fan FRF, Bard AJ, Imaging of biological macromolecules on mica in humid air by scanning electrochemical microscopy. *PNAS* USA. 96, pp. 14222-14227 (1999)

[14] Takahashi Y, Shevchuk AI, Novak P, Murakami Y, Shiku H, Korchev YE, Matsue T, Simultaneous noncontact topography and electrochemical imaging by SECM/SICM featuring ion current feedback regulation. *J. Am. Chem. Soc*. 132, pp. 10118-10126 (2010)

[15] Comstock DJ, Elam JW, Pellin MJ, Hersam MC, Integrated ultramicroelectrode-nanopipet probe for concurrent scanning electrochemical microscopy and scanning ionic conductance microscopy. *Anal. Chem*. 82, pp. 1270-1276 (2010)

[16] Takahashi Y, Shevchuk AL, Novak P, Zhang Y, Ebejer N, Macpherson JV, Unwin PR, Pollard AJ, Roy D, Clifford CA, Shiku H, Matsue T, Klenerman D, Korchev YE, Multifunctional nanoprobes for nanoscale chemical imaging and localized chemical delivery at surfaces and interfaces. *Angew. Chem. Int. Ed*. Engl. 50, pp. 9638-9642 (2011)

[17] Williams CG, Edwards JW, Colley AL, Macpherson JV, Unwin PR, Scanning micro-pipet contact method for high-resolution imaging of electrode surface redox activity. *Anal. Chem*. 81, pp. 2486-2495 (2009)

[18] McKelvey K, Snowden ME, Peruffo M, Unwin PR, Quantitative visualization of molecular transport through porous membranes: enhanced resolution and contrast using intermittent contact-scanning electrochemical microscopy. *Anal. Chem*. 83, pp. 6447-6454 (2011)

[19] Ebejer N, Schnippering M, Colburn AW, Edwards MA, Unwin PR, Localized high resolution electrochemistry and multifunctional imaging: scanning electrochemical cell microscopy. *Anal. Chem*. 82, pp. 9141-9145 (2010)

[20] Takahashi Y, Shevchuck AI, Novak P, Babakinejad B, Macpherson J, Unwin PR, Shiku H, Gorelik J, Klenerman D, Korchev YE, Matsue T, Topographical and electrochemical nanoscale imaging of living cells using voltage-switching mode scanning electrochemical microscopy. *PNAS*. 109:29, pp. 11540-11545 (2012)

[21] Nebel M, Grützke S, Diab N, Schulte A, Schuhmann W, Visualization of oxygen consumption of single living cells by scanning electrochemical microscopy: the influence of the faradic tip reaction. *Angew. Chem*. 52, pp. 6335-6338 (2013).

[22] Nebel M, Grützke S, Diab N, Schulte A, Schuhmann W, Microelectrochemical visualization of oxygen consumption of single living cells. *Faraday Discussion*. 164:19, pp. 19-32 (2013)

[23] Liebetrau JM, Miller HM, Baur JE, Scanning electrochemical microscopy of model neurons:imaging and real-time detection of morphological changes, *Anal. Chem*. 75, pp. 563-571 (2003)

[24] (a) Anghilieri LJ, Crone-Escanye MC, Thouvenot P, Brunotte F, Robert J, Mechanism of Gaffium-67 accumulation by tumors: role of cell membrane permeability. J. Nucl. Med. 29, pp. 663-668 (1988) (b) Li MS, Filice FP, Ding Z, A time course study of cadmium effect on membrane permeability of single human bladder cancer cells using scanning electrochemical microscopy. J. Inorg. Biochem. 136, pp. 177-183 (2014)

Chapter 10

Investigation of L-Lactate Release on Breast Cancer and Normal Human Cells

Abstract

A very sensitive and stable lactate biosensor able to provide detailed information on location and stage of cancer cells by monitoring lactate release was developed. The method is based on electrochemical measurements using *ad hoc* LOx-based UMEs in conjunction with Scanning Electrochemical Microscopy (SECM). This system allows the cell metabolism investigation with high sensitivity, spatial and time resolutions, since it can resolve the electrochemical activity across the entire surface of a single cell and it can dynamically record metabolic changes in time. Using this set up, the lactate release of both breast cancer and normal epithelial human (MCF10A) cells was monitored, proving evidence about the glycolytic switching present in tumors. Moreover, this application can be very useful and powerful for studying the kinetics of the oncogene expression during carcinogenesis and for monitoring the efficacy of metabolic anticancer drugs. Levels of lactate release were investigated also in other cancer cell lines, such as A549, HeLa and HepG2.

Key words LOx, lactate biosensors, SECM, *Warburg Effect*, RasV12, pBabe, anticancer drugs, kinetics of cancer

10.1 Drop-cast 10µm Pt LOx-UME Biosensors

10.1.1 Introduction

As already mentioned in previous chapters, most invasive tumor phenotypes show a metabolic switching from oxidative phosphorylation to an increased rate of glycolysis[1]. This switch ensures a sufficient energy supply from glucose and thus high viability, even in hypoxic environments[2-3]. This metabolic situation is accompanied by: *i)* ***higher consumption of glucose***, due to the lower efficiency in energy production by glycolysis and *ii)* increased

extracellular acidosis because of the ***high production of lactate*** and other acidic species[3]. Monitoring the level of these two molecules can give peculiar information about the location, the characteristics and the stage of tumors. Moreover, it may possible to take advantage of this peculiar metabolic feature of cancer cells for selective anticancer therapies[4].

In this project drop-casting method for the realization of LOx-based UME biosensors was optimized, achieving a very sensitive, reproducible and precise procedure in order to monitor the level of lactate released from one single cell (Figure 1a). These drop-cast LOx sensors were employed as probes of our BioSECM apparatus, measuring lactate release profiles on cancer and normal epithelial human breast MCF10A cells. As a reminder, MCF10A cells were infected either by a pBabe empty retroviral vector, used as control, and by vector expressing the oncogene RasV12, an oncogene successfully used in *in vitro* model.

In lactate detection, the sensitivity is the most critical parameter, because the physiological range for single cell lactate release is very low (in the range of μM); for this reason a high sensitive electrode is needed. The electropolymerized biosensor for lactate analysis manufactured and characterized in this work seems to lack this property, while the drop-cast one is very sensitive and the protocol was deeply optimized in order to increase as much as possible the spatial resolution. To confirm the capability of our system, the results were compared, in term of analysis, with the lactate concentrations obtained with a classical colorimetric assay.

10.1.2 Comparison with the EnzyChrom BioAssay Kit

In general, lactate is generated by lactate dehydrogenase (LDH) under hypoxic or anaerobic conditions. Therefore, monitoring lactate level is a good indicator of the balance between tissue oxygen demand and utilization and is useful when studying cellular and animal physiology. Nowadays, one of the most common way to measure lactate level is a simple, direct and automation-ready procedure based on colorimetric determination. Briefly, the lactate dehydrogenase catalyzes the oxidation of lactate to pyruvate; the reaction is accompanied by the reduction NAD^+ to NADH, which consequently reduces a formazan (MTT) reagent, which turns its colour from yellow to purple. The intensity of the product colour, measured at 565 nm, is proportionate to the

lactate concetration in the sample (for more details see Appendix #5).

The EnzyChrom™ L-Lactate Assay Kit (ECLC-100) for the colorimetric analysis was used as a control in this work. The concentration of lactate in the culture media of both RasV12 and pBabe cells in function of time were measured using the assay and our drop-cast LOx sensors (Figure 1). The comparison and analysis of the results showed that: *i)* the biosensor results are found to tally closely with those measured by colorimetric assay and *ii)* RasV12 cells produce more lactate than pBabe ones, as we expected. This difference in lactate levels is visible even after 6h of monitoring; underlining the glycolytic switching that characterizes cancer cells.

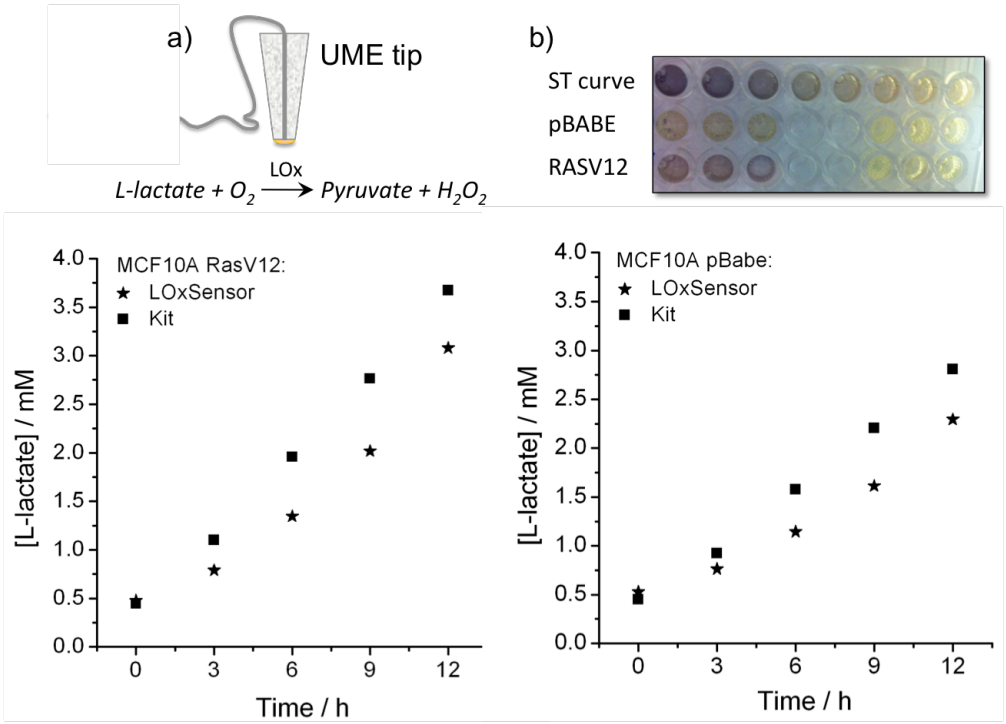

Figure 1. Diagrams of L-lactate concentrations as function of time. The concetration are measured in the same medium by using the drop-cast LOx UME biosensor (a) and the colorimetric bioassay kit (b), for RasV12 and pBabe MCF10A cells, after 3- 6- 9 and 12 h.

10.1.3 Approach Curves

To study the lactate release at single cell level, the drop-cast LOx UME biosensors were used as probes of our BioSECM apparatus. As for GOx biosensors, the electrode tip was positioned at a known distance from the plastic bottom Petri dish by using approaches curves. However, the concentration of lactate in the extracellular solution is insufficient to allow ACs curves; hence, a known amount of L-lactate (100 μM) was added in

solution and the hindered diffusion of this molecule to the sensor was followed while the probe is approaching the surface (Figure 2).

It is worth to underline that also in this case the classical ACs representation (I_T vs $L = d/a$) cannot be used because the exact radius of the active part of the electrode is difficult determined due to the presence of the enzymatic coating. Furthermore, the shape of ACs for enzyme-coated UMEs does not obey to the classical SECM feedback theory, pointing to the fact that the processes occurring at the UME are very complex.

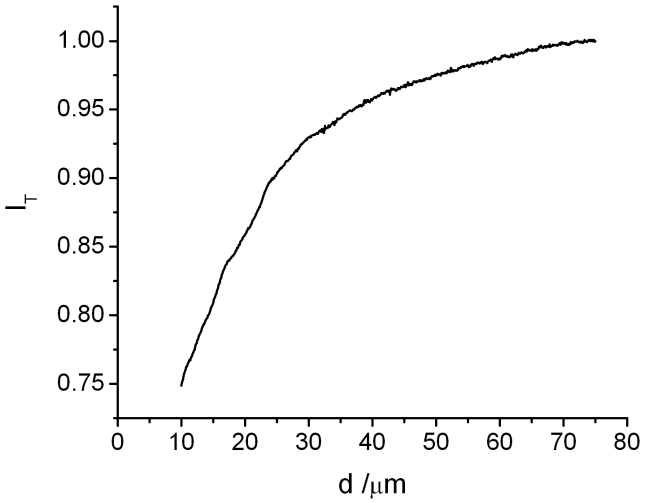

Figure 2. Typical approach curve of a drop-cast LOx 10μm Pt UME biosensor to the Petri dish in 0.1 mM lactate /RPMI medium. E = +0.65 V vs Ag/AgCl, 3M KCl. The current has been normalized respect to the steady-state bulk current value. During ACs experiments the current is blocked at 75% of the total steady-state current value, to avoid sensor damaging.

10.1.4 Lactate Release Profiles

After the approach curve, the lactate previously added was removed, in order to avoid interferences during analysis, then, the tip is retracted at the desired distance and it is moved along x or y above the live cell to get the metabolic profiles of lactate release. Even in this case SECM is used in constant height mode. The tip-substrate separation distance is very accurately controlled by piezoelectric and stepper motors, and the tip movement along axes is monitored through the optical inverted microscope to minimize the risk of damaging the enzymatic film of the biosensor during the experiment. The microscope is also useful to check the morphology of the scanned cells and the scan area. It is possible that the hydrogel matrix would be damaged during ACs, therefore it is mandatory to perform calibration experiments prior and after any SECM applications.

The amperometric current recorded at the UME probe is directly correlated with the concentration of the metabolite at a certain distance from the cell. For lactate investigation the current above single cell is higher because the cell is releasing lactate and its concentration locally increases with respect to the background solution that contains no lactate (Figure 3).

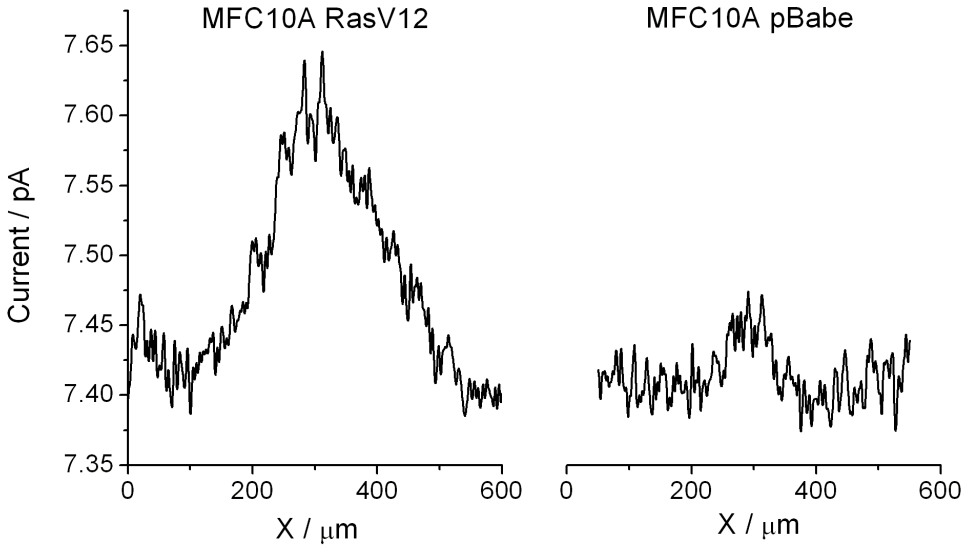

Figure 3. Representative SECM measurements of lactate release profiles of single RasV12 (cancer) and pBabe (control) MCF10A cells, obtained by using a single drop-cast (10 min deposition) LOx-based UME biosensor in RPMI medium. E = +0.65 V vs Ag/AgCl 3M KCl. Scan speed 3 μm/s.

In order to obtain the concentration values of glucose uptake for every single cell, the response current of each scan is normalized by the response current of the post-calibrations curves, in which we add 100 μM of lactate. Usually, the sensitivity slightly decreases comparing to calibrations done before SECM experiments. Upon performing several measurements on pBabe and RasV12 MCF10A cells, belonging to different culturing dishes, we have demonstrated for the first time at this high spatial resolution, that lactate release is statistically higher for cancer cells than in normal ones, proving exactly the Warburg observations[1] (Figure 4).

For statistical analysis, different drop-cast electrodes were employed, which are prepared with the same experimental protocol but changing enzymatic solutions. Even here, the error bar of transformed cells is larger likely because of the heterogeneity of the Ras vector infection entity.

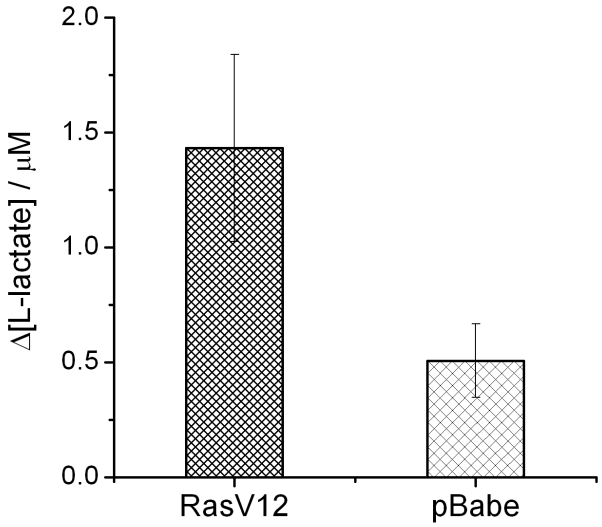

Figure 4. Statistical diagram that compares the lactate concentrations locally released at single cell level. The lactate release for cancer (RasV12) MCF10A cells is estimated to be 1.43 ± 0.41 μM upon **20** experiments, while for normal (pBabe) MCF10A cells is estimated to be 0.51 ± 0.16 μM upon **27** experiments.

Although the sensitivity is very high, this specific drop-cast procedure (with 10 minutes of hydrogel deposition) lacks in term of spatial resolution. Therefore, in order to increase this feature, the time of UME immersion in the enzymatic solution was decreased and optimized. In this way the width range of the current peak was reduced from 350 μm to 70 μm maintaining a great sensitivity (Figure 5).

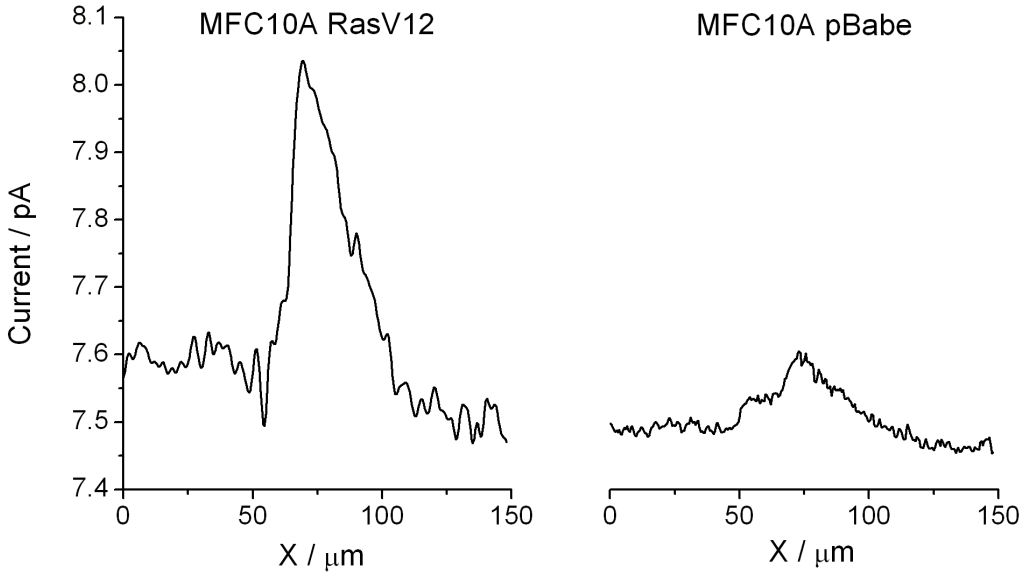

Figure 5. Representative SECM scans of lactate release of single RasV12 and pBabe MCF10A cells, obtained by using two different drop-cast LOx-based UMEs biosensors in RPMI medium. *E* = +0.65 V vs Ag/AgCl 3M KCl. Scan speed 3 μm/s.

Even in lactate monitoring the electrode-sample separation distance takes a role, however the topographical contribution analysis of pBabe and RasV12 cells were carried out, as reported in *Chapter 11*, and the results showed that the cell topographies are not statistically different. Therefore, this contribution does not affect the calculated difference of lactate release between normal and transformed MCF10A cells.

10.2 Application #1:

Kinetic Study on Oncogene Expression Monitoring Lactate Release

10.2.1 Experimental Strategy

The aim of this application is to study the kinetics of the expression and oncogene-induced metabolic changes during carcinogenesis. With our set up (BioSECM and LOx UME biosensors), the *glycolytic switching* (or the *Warburg effect*) as function of time can be monitored, by measuring the lactate production in time after microinjection of an oncogene vector, such as RasV12, in the cellular nucleus of normal MCF10A cells.

In detail, the experimental strategy was the following (Figure 6):

- MCF10A cells were plated at a proper confluence on a glass coverslips located in appropriated Petri dishes, equipped with a labelled grid on the bottom.
- Few μL of a solution containing 80 ng of DNA RasV12 (oncogene) vector plus 10 ng of Red Fluorescent Protein (RFP) vector were injected in the nucleus of some cells, and few μL of a solution containing 80 ng of DNA pBabe (control) vector plus 10 ng of Green Fluorescent Protein (GFP) vector in the nucleus of other cells. The location of the injected cells is exactly known thanks to the grid on the bottom.
- After 6h of incubation the cells started to express the fluorescent proteins and both red and green fluorescence was observed. Therefore, one could suppose that even the oncogene vector (RasV12) might be expressed, and the control pBabe as well. One sample was also incubated for 24 h after injection for further investigations.
- SECM analysis were performed with drop-cast LOx UME biosensors on both injected RasV12 and pBabe cells in order to monitor if the *Warburg*

effect was already detectable (see next section, Figure 7).

- To confirm SECM results, immunofluorescence analysis of the same scanned cells was performed (for the details see *Chapter 7.1.6*).

  This technique is commonly used in biology for visualizing the distribution of target molecules, such as proteins, through the sample. The method uses the specificity of antibodies to their relative antigens to monitor fluorescent dyes bound to specific biomolecules, used as targets, within a cell. Immunofluorescence can be also used in combination with non-antibody methods of fluorescent staining, for example by employing DAPI (4,6-diamidino-2-phenylindole) to label nuclear DNA allowing identification of the cells. A specific anti-RasV12 antibody that binds a particular peptide, mapping at the C-terminus of Ras protein vector of human origin was employed in this analysis (Figure 8).

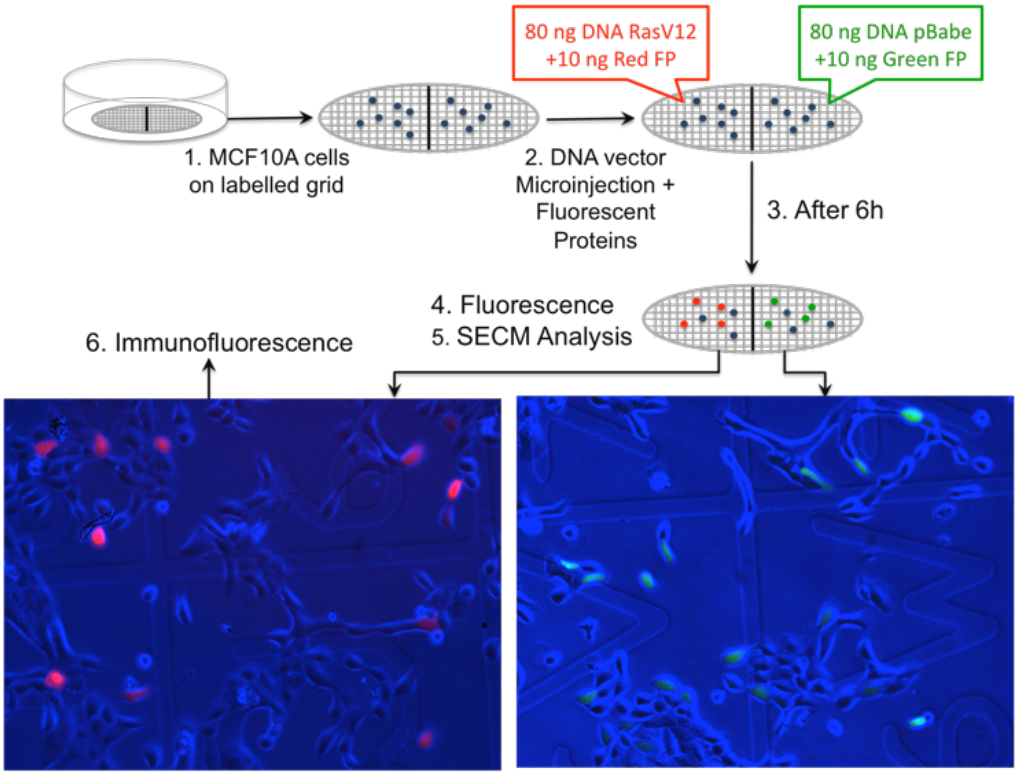

Figure 7. Experimental strategy scheme for the study of the kinetics of the oncogene (RasV12) expression during carcinogenesis. The fluorescent red cells tag the cells injected with the oncogene vector RasV12, while the green ones tag the cells injected with the empty vector (pBabe), used as control. At the bottom of the Petri dish containing the coverslip there is a grid that allowed us to perform the analysis on the same cells using SECM.

10.2.2 Preliminary Results

Preliminary SECM results show that after 6h of injection there was no difference in lactate production among MCF10A cells, MCF10A cells with RasV12 vector and MCF10A cells with pBabe vector. After the post-calibration of the electrode the local concentration of lactate for the analyzed cells was estimated to be equal to 1.5 μM. As it is shown in Figure 8, the three current peaks relative to lactate release from the three cells injected and non-injected are really similar from each other, meaning that 6h after oncogene microinjection were not enough to achieve the *glycolytic switching*. This observation was confirmed by the immunofluorescence analysis (Figure 9); indeed, after 6h the fluorescence (white) signal, relative to the Ras expression, was very weak. In order to appreciate an increased expression of the oncogene vector by immunofluorescence 24h would be required. We expect to measure also an increased amount of lactate release for cancer cells at the same time.

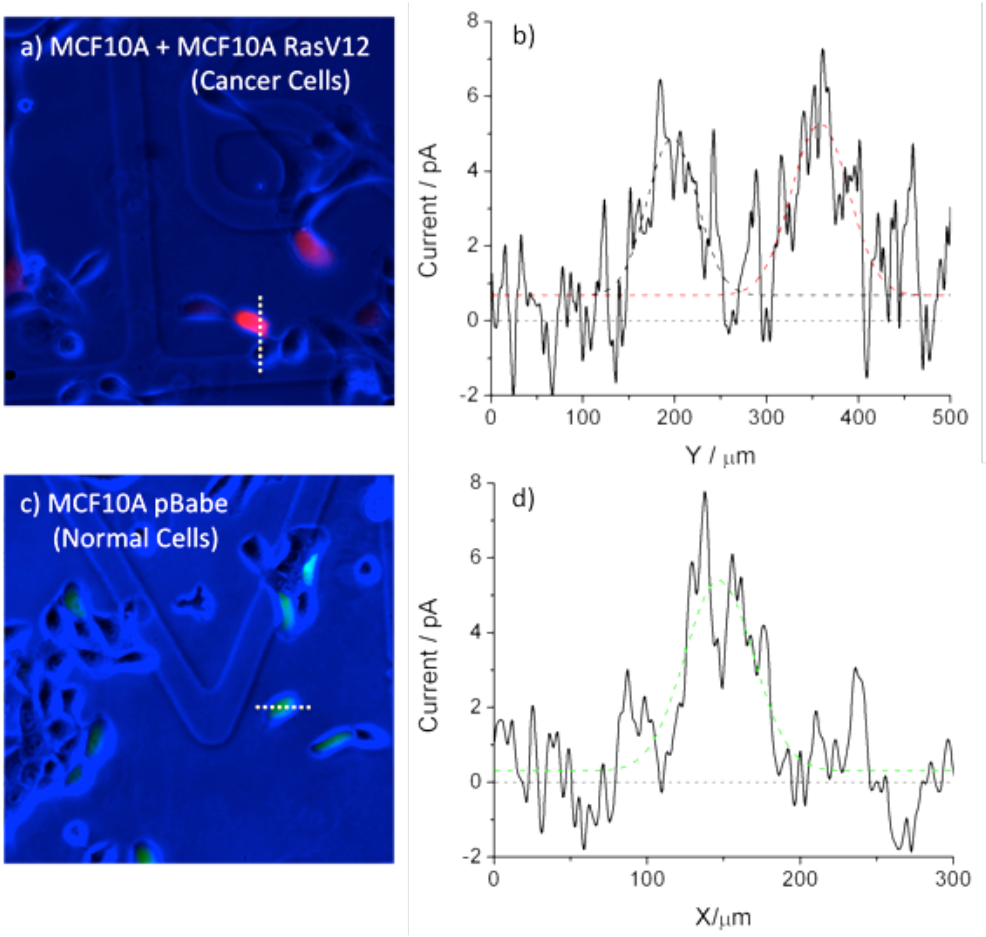

Figure 8. On the right are reported the fluorescent images of the analyzed cells: (a) no-injected (blue) and RasV12-injected (red) MCF10A cells (c) pBabe-injected (green) MCF10A cells. On the left the corresponding SECM measurements monitoring lactate release of (b) non injected and RasV12-injected MCF10A and (d) pBabe-injected MCF10A cells.

10.2.3 Immuno-fluorescence

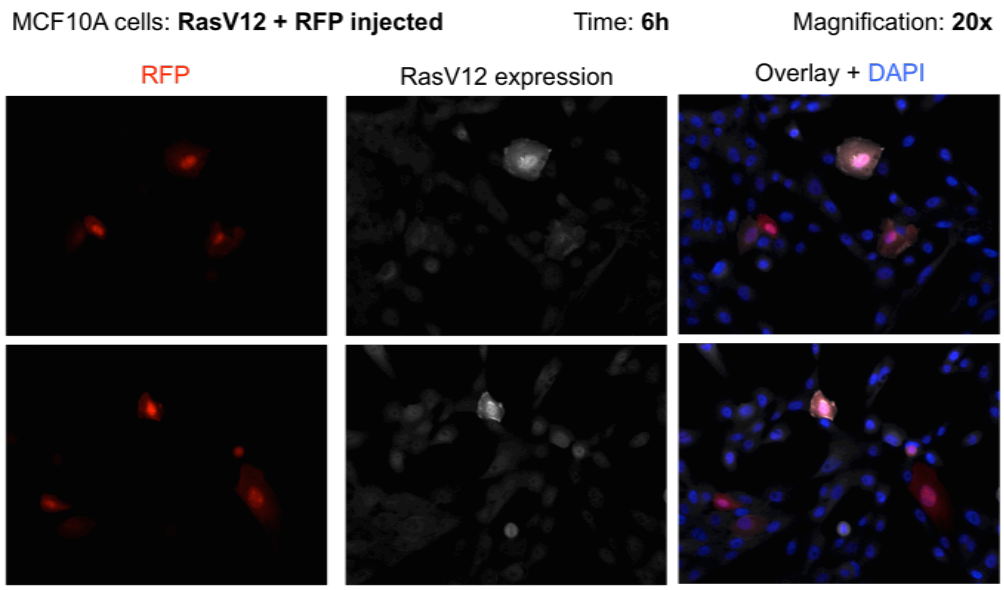

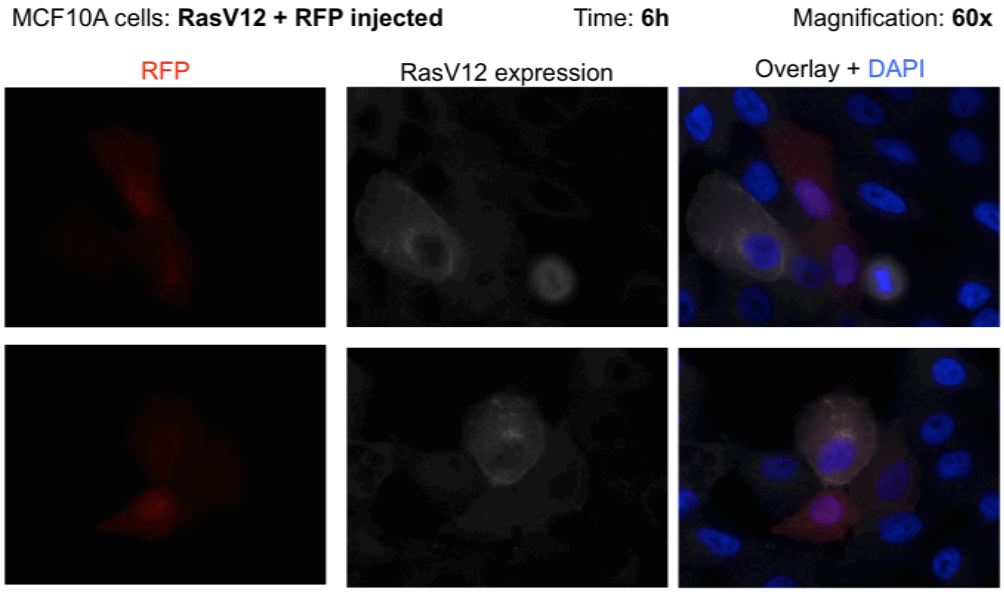

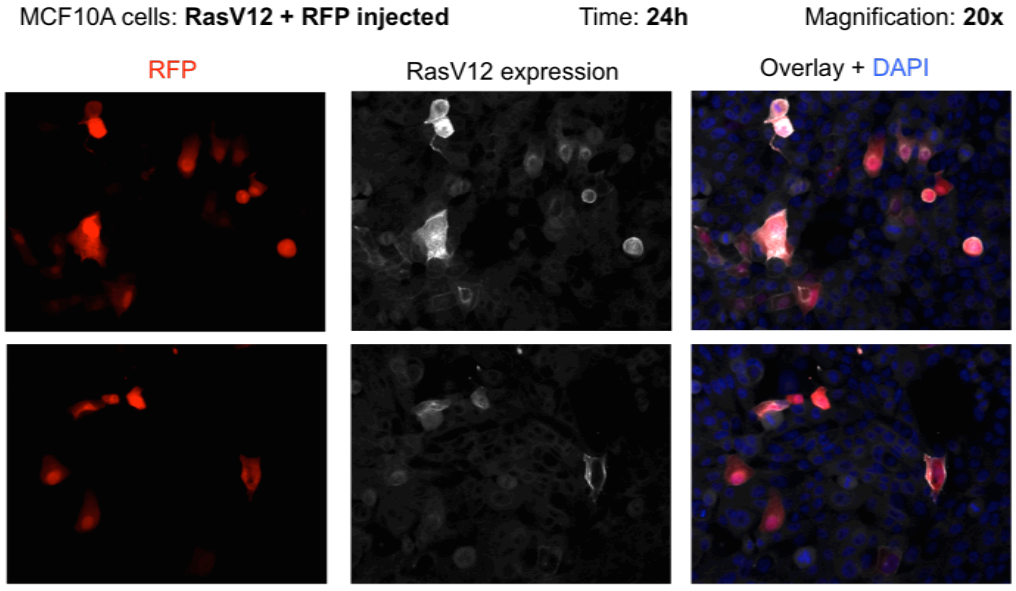

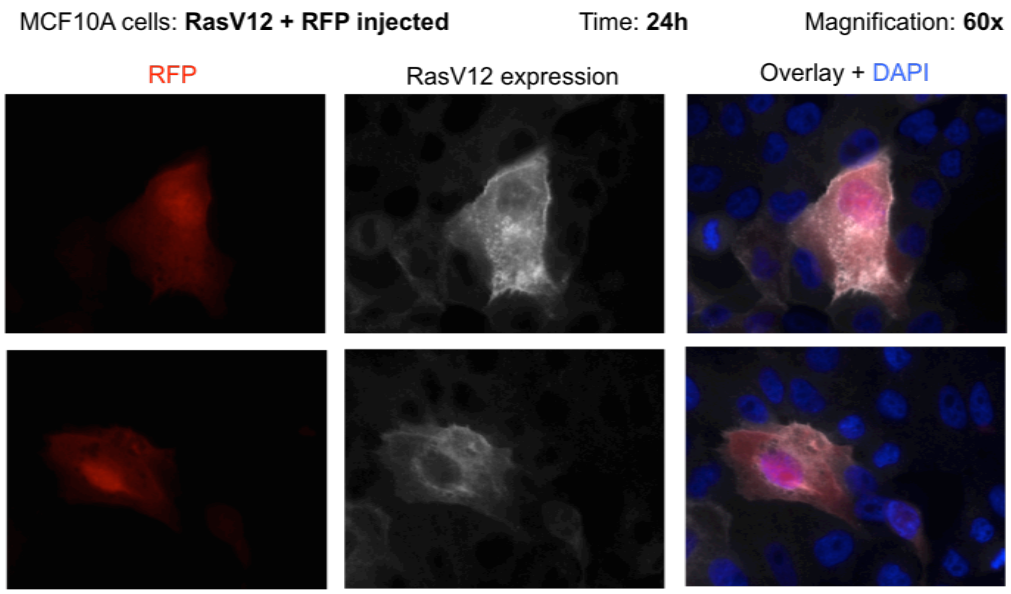

Figure 9. Immunofluorescence images of our samples, from 6h to 24h of incubation after RasV12 + RFP injection (magnification 20x and 60x). The first series of images (RFP) show the expression of the red fluorescent protein on the injected cells: the intensity is much higher after 24h than 6h. The second series of images is related to the expression of RasV12 as oncogene vector: also in this case the expression is higher after 24h, both in term of intensity and number. The last series overlay the RFP and RasV12 expression signals with DAPI signal, which tag the nuclear DNA present in the all cells.

In conclusion, is evident that after 6 hour the onceogene expression of RasV12 signal is very weak. At this time point also the lactate analyses performed with SECM and UME biosensors did not show an increased amount of lactate released in cancer model due to the *glycolytic switching*. However, for the first time with a BioSECM apparatus the kinetics of oncogenic expression during carcinogenesis was mapped with a high spatial resolution. This finding could be very useful in future in order to study the metabolic behaviour of cancer cells and metabolic anticancer drugs efficacy.

10.3 Application #2:

Efficacy of Anticancer Drugs on Lactate Release Inhibition

10.3.1 Overview on Analyzed Drugs

Drop-cast 10 µm Pt LOx-based UME biosensors coupled with BioSECM apparatus is a suitable device for monitoring the efficacy and the kinetics of experimental anticancer drugs on single cancer cells.

Regarding metabolic anticancer drugs, there are only few molecules in preclinical studies or clinical trials that are known to exploit, or interfere with, the increased glycolytic process of invasive tumors[4]. However, lactate dehydrogenase (LDH) is considered one of the major check-point for the switch from aerobic to anaerobic glycolysis by catalyzing the reduction of pyruvate into lactate. There are two types of LDH subunits: LDH-A and LDH-B, which differ from each other by the location in the living systems. The combination of them gives the structure of the five tetrameric LDH isoforms present in human. LDH-A_4 has been found to be over-expressed in several highly invasive and hypoxic carcinomas. This factor, together with the overexpression of the main glucose transporter, further promotes glycolysis and it was found as a common feature in several tumor lines[4]. For this reason, LDH-A was recently proposed as one of the most promising tumor targets[4]. Indeed, repression of its expression reduces the invasiveness of cancer cell lines. Compounds able to inhibit LDH-A enzymatic activity may constitute safe agents able to interfere with tumor growth and progression. There are just few LDH-A inhibitors already reported in literature, but there are many under study[4]. We have deeply investigated the effects of a series of compounds (Figure 9) based on the same N-hydroxyindole structural motif, with the difference on aromatic ring substituents. We examined them looking for a satisfactory level of LDH-A inhibition within this chemical class.

For all of them we measured the concetration of lactate released in the culture medium and the cell viability upon treatment, changing several parameters, such as drug concentration (from 10 μM to 100 μM) and time exposure (from 15 minutes to 6 hours).
As cell line models we used A549 (human lung carcinoma) known to have a very fast metabolism, causing ***high levels of lactate released*** and MCF10A (RasV12 and pBabe).

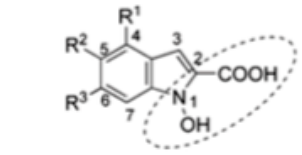

1a-k

compound	R^1	R^2	R^3
1a	H	H	H
1b	CH_3	H	H
1c	CF_3	H	H
1d	Cl	H	H
1e	Br	H	H
1f	H	H	Br
1g	C_6H_5	H	H
1h	H	C_6H_5	H
1i	H	H	C_6H_5
1j	CF_3	H	C_6H_5
1k	H	H	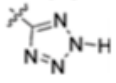

Figure 9. N-Hydroxyindoles designed as LDH-A inhibitors[4].

The aim of this analysis was to find the best condition for studying the efficacy and the kinetics of a metabolic anticancer drug by SECM analysis monitoring the level of lactate released at single cell level.

Unfortunately, the majority of these compounds have been found highly toxic on our cell line models; only compounds *1i* and *1j* seem to block effectively LDH-A, reducing the lactate amount in the culture medium (Figure 10). The best performance is achieved after 15 min of treatment with a drug concentration equal to 100 μM. In particular *1j* is more active in both cancer cell lines (A549 and RasV12), while it has not any effect on normal cells.

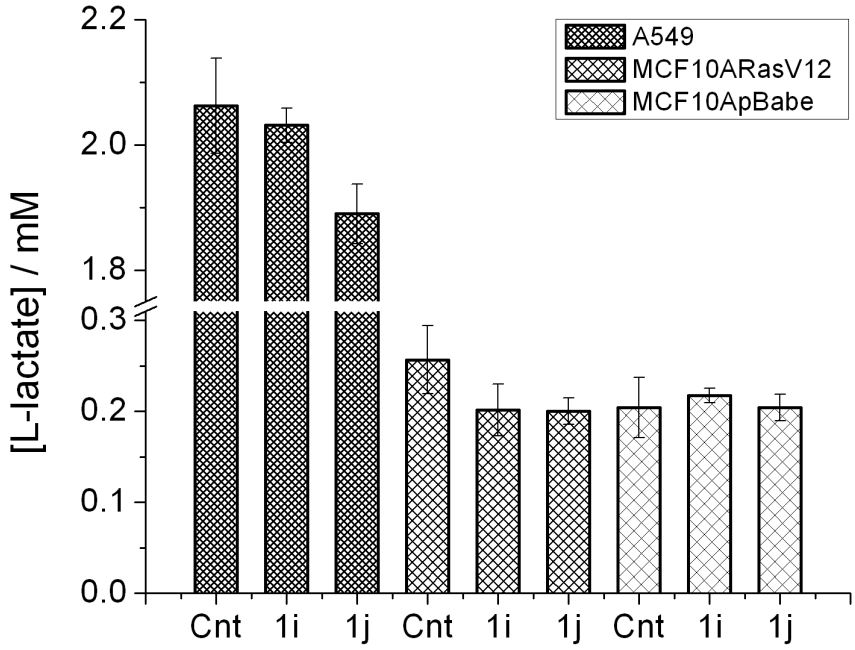

Figure 10. Colorimetric measurement (Bio-assay kit) of LDH-A inhibition analyzed on A549 and MCF10A cell lines. Normal (pBabe) cells do not affect the drug administration, while both cancer cells (A549 and RasV12) decrease their amount of lactate production.

10.3.2 Results and Discussion

From the diagrams of Figure 10 one can affirm that: *i)* A549 cell line effectively produces a higher concentration of lactate, compared to that produced by MCF10A, *ii)* already after 15 minutes of treatment with these drugs the amount of lactate for A549 and RasV12 is slightly decreased (the effect seems to be greater for *1j* than for *1i*, and *iii)* there is no visible mortality. Therefore, upon these observations, we decided to employ ***1j*** as the most suitable drug in order to monitor the kinetics of lactate release inhibition at single cell level. We employed our drop-cast LOx-based UME biosensors coupled with the BioSECM apparatus. The probe, after the first scan above the

cells (two RasV12 MCF10A) performed at high constant mode, was accurately retracted at the fixed starting point. Then, the scan was consecutively repositioned several times after 1, 3, 5 and 10 minutes of drug administration (Figure 11). It is worth to underline that this kind of analysis is possible mainly because the UME movement is very accurately controlled by piezo and stepper motors, and it can be monitored with the cell morphologies through the optical microscope.

As conclusion, these measurements demonstrated that the RasV12 cells stopped to produce lactate already after 5 minutes upon drug injection. The biological mechanism behind this inhibition is not exactly known, but with this approach the efficacy and the kinetics of a metabolic anticancer drug can be evaluated by studying the lactate release at single cell level. Moreover, the non-invasive nature of the SECM measurements opens up the possibility of continuously monitoring the effect of a drug dose response. This paves the way for choosing the most effective drug and concentration for treating an individual patient's condition (personalized therapies applications).

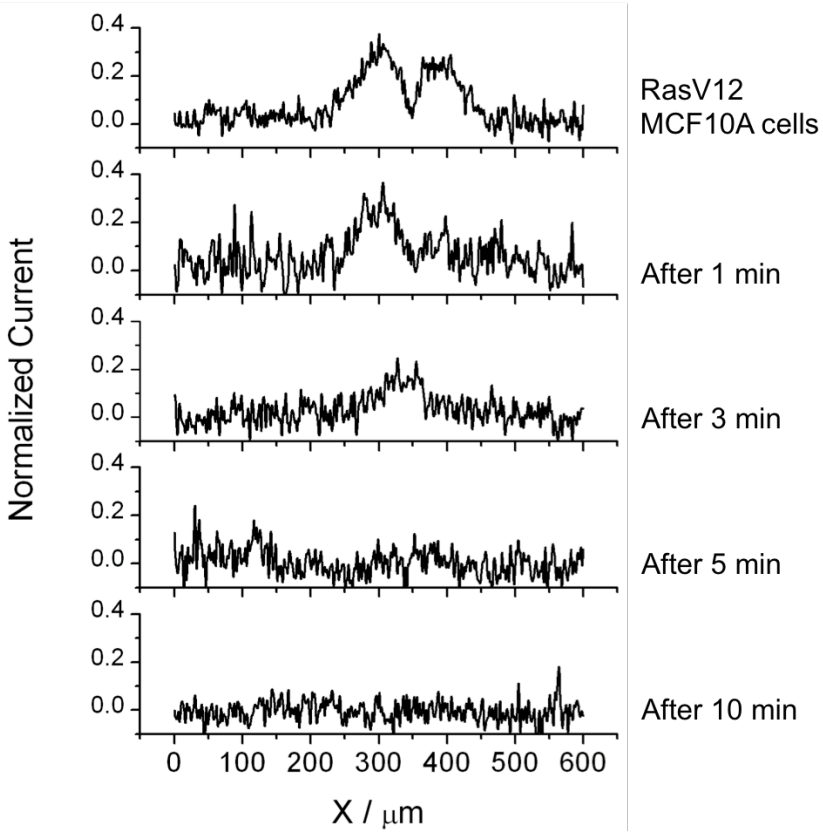

Figure 11. SECM measurements of a metabolic anticancer drug (*1j*) efficacy and kinetics on two Rasv12 MCF10A cells, using a drop-cast LOx UME biosensor. Drug concetration: 100μM in RPMI medium. E = +0.65 V vs Ag/AgCl 3M KCl. Scan speed 3 μm/s.

10.4 Application #3:

Monitoring L-Lactate Level on Other Cancer Cell Lines

10.4.1 HeLa and HepG2 cells Lactate Production

Drop-cast LOx UME biosensors have been also demonstrated to be suitable devices for measuring lactate concentrations directly in cell culture medium, without any kind of pre-treatment, which is usually required in the colorimetric assay. Using our LOx biosensors, lactate release of other two cancer cell line models has been investigated in function of time:

- *HeLa* cells (*Chapter 7.2.2*) are known to have a slow metabolism comparing to other cancer cells, but still higher than normal ones. In fact, as shown in Figure 11, the level of lactate released is not so high and it starts to slightly increase only after 48 hours of incubation.

- *HepG2* cells are very particular because they recycle the lactate released from anaerobic glycolysis in order to support their high proliferation. In fact, from Figure 11 it is evident that the amount of lactate in the first 24 hours decreases instead to increase to fulfil cell's nutrients demand.

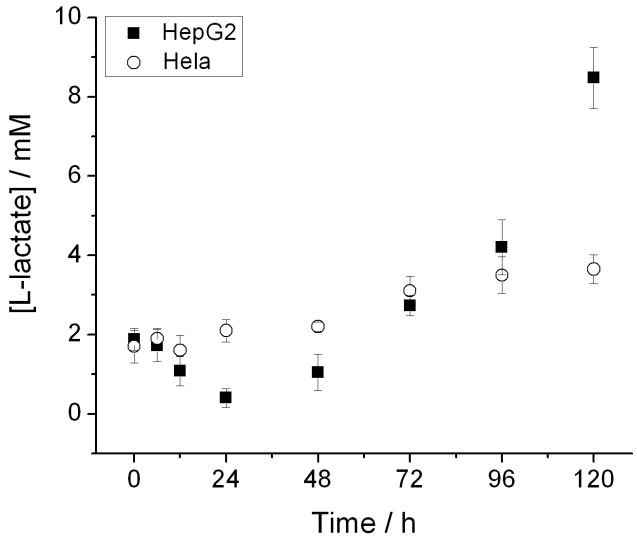

Figure 11. Lactate concetration released in HeLa and HepG2 culture media, measured in function of time with a drop-cast LOx UME biosensors at E = 0.65V Vs Ag/AgCl.

References

[1] Warburg O, On the origin of cancer cells. *Science*. 123, pp. 309-314 (1956)

[2] Gatenby RA, Gillies RJ, Why do cancers have high aerobic glycolysis? *Nature Reviews Cancer*. 4, pp. 891-899 (2004)

[3] Vander Heiden MG, Understanding the Warburg effect: the metabolic requirements of cell proliferation. *Science.* 324:5930, pp. 1029-1033 (2009)

[4] Granchi C, Roy S, Giacomelli C, Macchia M, Tuccinardi T, Martinelli A, Lanza M, Betti L, Giaccini G, Lucacchini A, Funel N, Lèon LG, Giovannetti E, Peters GJ, Palchaudhuri R, Calvaresi EC, Hergenrother PJ, Minutolo F, Discovery of n-hydroxyindole-based inhibitors of human lactate dehydrogenase isoform A (LDH-A) as starvation agents against cancer cells. *J. Med. Chem*. 54, pp. 1599-1612 (2011)

[5] Cairns RA, Harris IS, Mak TW, Regulation of cancer cell metabolism. *Nature Reviews Cancer*. 11, pp. 85-95 (2011)

[6] Vander Heiden MG, Targeting cancer metabolism: a therapeutic window opens. *Nature Reviews Cancer*. 10, pp. 671-684 (2011)

Chapter 11

Investigation on Breast Cancer Human Cells Oxygen Consumption

Abstract

The detection of cellular respiration activity is important for the assessment of the metabolic status of a biological cell. Due to its non-invasive character and high spatial resolution SECM is a powerful tool for single cell measurements. A flexible potential pulse profile with a time-dependent data acquisition is adopted in order to overcome some common limitations of single cell respiration studies performed by SECM. Differential pulse amperometry measurements were recorded while the tip was scanning the cells in a constant height mode. In order to investigate the respiration capability of cancer and normal cells a pool of drugs able to interact with the mitochondrial respiration chain were used.

Key words Oxygen consumption, pBabe and RasV12 MCF10A cells, FCCP, Rotenone, uncoupling respiration

11.1 Flexible Potential Pulse Profile

11.1.1 Introduction

Cellular respiration is an indicator of the metabolic activity of living cells. Beyond glucose and lactate levels, monitoring the local concentration of oxygen gives important information about the cell status[1].

The first attempt for visualizing the oxygen consumption rate of single living cells by mean SECM was described by Matsue et al.[2] in 1998, however, evaluation of the respiratory activity of individual cells remains challenging and complex. In particular, the dimensions and the morphology irregularity of living cells, used as sample, lead to limitations of using the conventional constant-height mode for SECM investigations.

Recently, many strategy were developed to overcome these restrictions by positioning the tip at a distance outside the feedback range, embedding cells

into cavities or subtracting the topographic contribution after cell death. To efficiently control the tip-sample separation researcher coupled SECM with other scanning probe techniques, such as AFM[3], scanning ion conductance microscopy (SICM)[4], shear-force[5-6] and impendence-based[7] methods.
Although SECM distance control systems are available, the detection of the respiration activity of single living cells remains challenging, owing also to the small rate of oxygen consumption by a single cell. Indeed, only small current variations on the top of the cell can be measured.

11.1.2 Technique

Herein, an efficient experimental strategy was employed, this approach is based on the use of a second potentiostat to record a flexible potential pulse profile with time-dependent data acquisition during SECM scan at constant height mode[8-9]. This implementation enables the measurement of the O_2 consumption avoiding artifacts due to oxygen depletion inside the gap between the SECM tip and a living cell, caused by the UME reaction. The oxygen consumption and the topographic contribution of RasV12 and pBabe MCF10A cells, using 100μM of $[Ru(NH_3)_6]Cl_3$ in the culture medium (without serum) (see *Chapter 7.1.3*), were simultaneously measured.
All experiments were carried out directly in a 3.5 cm Petri dish located on the inverted microscope plate holder and constituting the electrochemical chamber by itself, and by mean of a 10 μm Pt UME without any coating. The flexible potential pulse cycle used was: a first pulse of -0.3 V kept for 1s and a second pulse of -0.7 V kept for 1s. This sequence was repeated for all the scan curve duration. Data were sampled in the second part of both first and second pulses, the difference between the two signals is directly reported by the program. However, the two separated data sets related to the first and second pulses are also available. The time step is chosen in order to have a good compromise between *i)* longer sample intervals with better signal averages and decreased noises and *ii)* less oxygen depletion due to the UME reaction for shorter time steps. In order to investigate the respiration capability of cancer and normal cells we used a pool of drugs able to interact with the mitochondrial respiration chain.

11.2 O_2 uptake upon drug administration on MCF10A pBabe cells

11.2.1 Results on pBabe O_2 Consumption

The signals, related to the basal MCF10A pBabe cells O_2 consumption and the relative topographic contribution, were measured directly in the cell culture medium (Figure 1a and 1b, black lines, respectively). Then, the cells were stimulated with p-trifluoromethoxycarbonylcyanidephenylhydrazone (FCCP), an uncoupling agent of the electron transport chain (ETC), which dissipates the proton gradient across the mitochondrial inner membrane, and maximize mitochondrial respiration (uncoupled state), see Scheme 1. Addiction of 1 µM FCCP, just after few minutes, maximizes the respiration rate and generated a decrease of current signal due to an increase of O_2 consumption from cells and a consequent reduction of local oxygen concentration. Instead, the signal at -0.3 V, which is due to the topographical contribution, only slightly changes (Figure 1a and 1b, green lines) upon FCCP administration. Successively, 1 µM rotenone was added, this drug interferes with the electron transport chain in mitochondria. It inhibits the transfer of electrons from iron-sulfur centres in complex I to ubiquinone (see Scheme 1). After rotenone administration the measurements show that the MCF10A O_2 consumption decreases, (Figure 1a and 1b, red lines), while the current due to the cell topography is almost identical to the basal level.

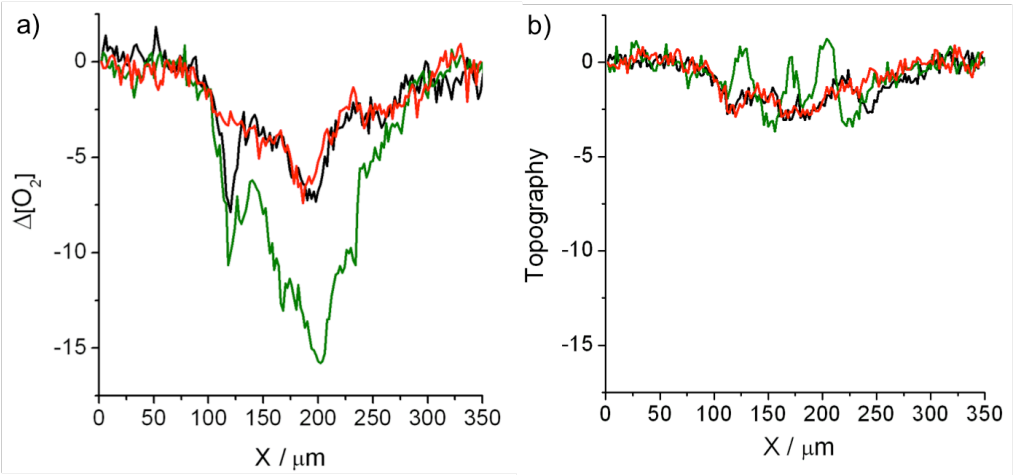

Figure 1. (a) O_2 consumption of pBabe MCF10A cells. Profiles measured at E = -0.7V. (b) Cellular topographic contribution owing to the negative feedback of the redox mediator (100µM of $[Ru(NH_3)_6]Cl_3$) recorded simultaneously at E = -0.3V. Black lines correspond to the basal levels, green lines after FCCP addition, and red lines after rotenone addition.

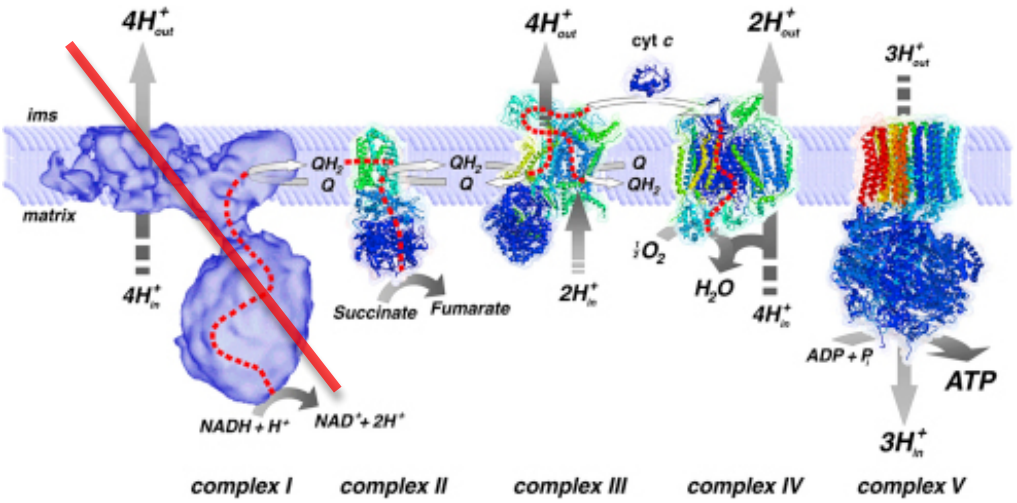

FCCP causes uncoupling of ETC → Increasing of the respiratory rate ↑

Rotenone causes inhibition of Complex I → Reduction of the respiratory rate ↓

Scheme 1. Mitochondrial respiratory chain or electrons transfer chain (ETC) where oxidative phosphorylation takes place. The process is an oxygen-dependent transmission of electrons down the chain, which maximize the production of ATP.

The chain consists of five multimeric enzyme complexes (Complex I, II, III, IV and V) positioned along the mitochondrial membrane. FCCP is an uncoupling agent; it disrupts ATP synthesis by transporting hydrogen ions through a cell membrane before they can used to provide the energy for oxidative phosphorylation. At the beginning the cell increase the respiration rate, then the cell dies. Rotenone is a drug that inhibits the transfer of electrons from iron-sulfur centres in complex I to ubiquinone. This interferes with NADH during the creation of ATP. Complex I is unable to pass off its electron to CoQ, creating a back-up of electrons within the mitochondrial matrix. [*reproduced with permission from Nijtmans et al., 2004*][10].

The comparison of the respiration activities at basal level, upon the FCCP (uncoupled respiration) and upon rotenone administration (inhibited respiration) is commonly used to assess the overall respiration capability of the mitochondria[11]. The present approach allows a study of the respiration activities of intact cells and single cell level. Moreover, the cells are kept in their adhesion state and in their original culture medium avoiding stressing procedures. To better compare the O_2 consumption and the relative topographic contribution in the analysed respiratory states, the differences of the oxygen current signals obtained upon drug administrations in respect to the basal level signals (Figure 2a and 2c), and the corresponding differences obtained for the signals at -0.3 V were plotted (Figure 2b and 2d).

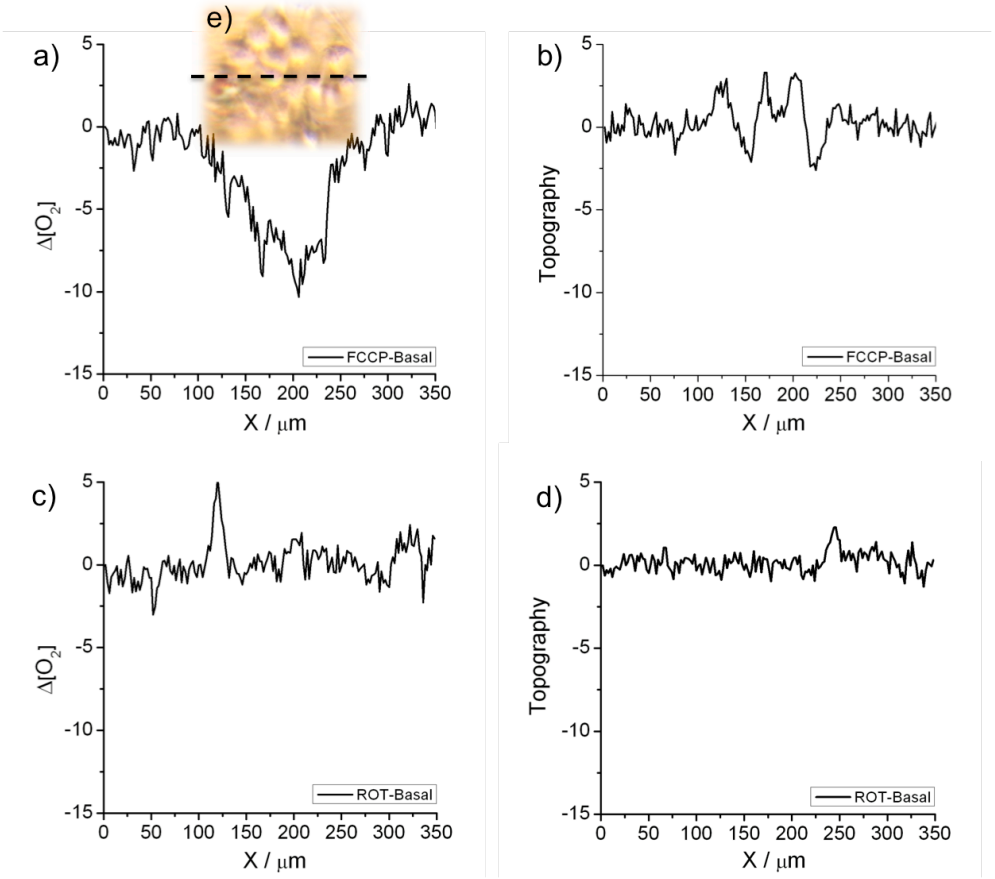

Figure 2. Differences on *oxygen current signals* obtained upon subtracting drug administration signals from the basal level signals: (a) FCCP-Basal and (c) Rotenone-Basal. Differences on the *topographic current signals* obtained upon subtracting drug administration signals from the basal level signals: (b) FCCP-Basal and (d) Rotenone-Basal. (e) optical image of the investigated cell area.

11.3 O_2 uptake upon drug administration on MCF10A RasV12 cells

11.3.1 Results on RasV12 O_2 Consumption

The O_2 consumption signals and the cell topography of MCF10A RasV12 cells at basal level were measured (Figure 3a and 3b, black lines). As for normal cells, the cancer cells were stimulated, firstly, with 1μM of FCCP and, then with 1μM of rotenone in order to measure the relative oxygen consumption and their cell topography. On the contrary of previous data the oxygen consumption does not increase after FCCP injection (Figure 3a and 3b, green lines). While, the O_2 current increases comparing to the currents recorded at basal level, consistently with a decrease of O_2 consumption when rotenone is added (Figure 3a and 3b, red lines). The current due to the cell topography at basal level and after rotenone injection is almost identical.

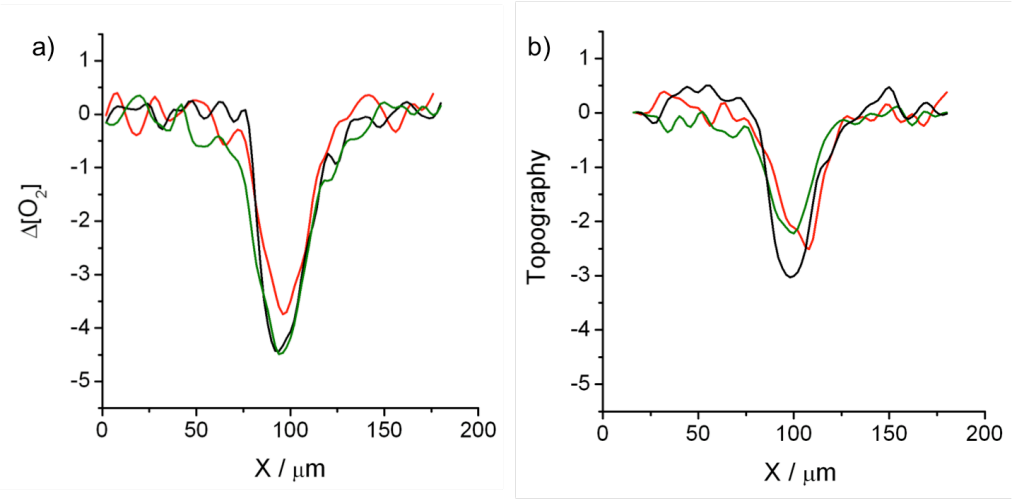

Figure 3. (a) O_2 consumption of a single RasV12 MCF10A cell. Profiles measured at E = -0.7V. (b) Cellular topographic contribution owing to the negative feedback of the redox mediator (100μM of $[Ru(NH_3)_6]Cl_3$) recorded at E = -0.3V. Black lines correspond to the basal levels, green lines after FCCP addition, and red lines after rotenone addition.

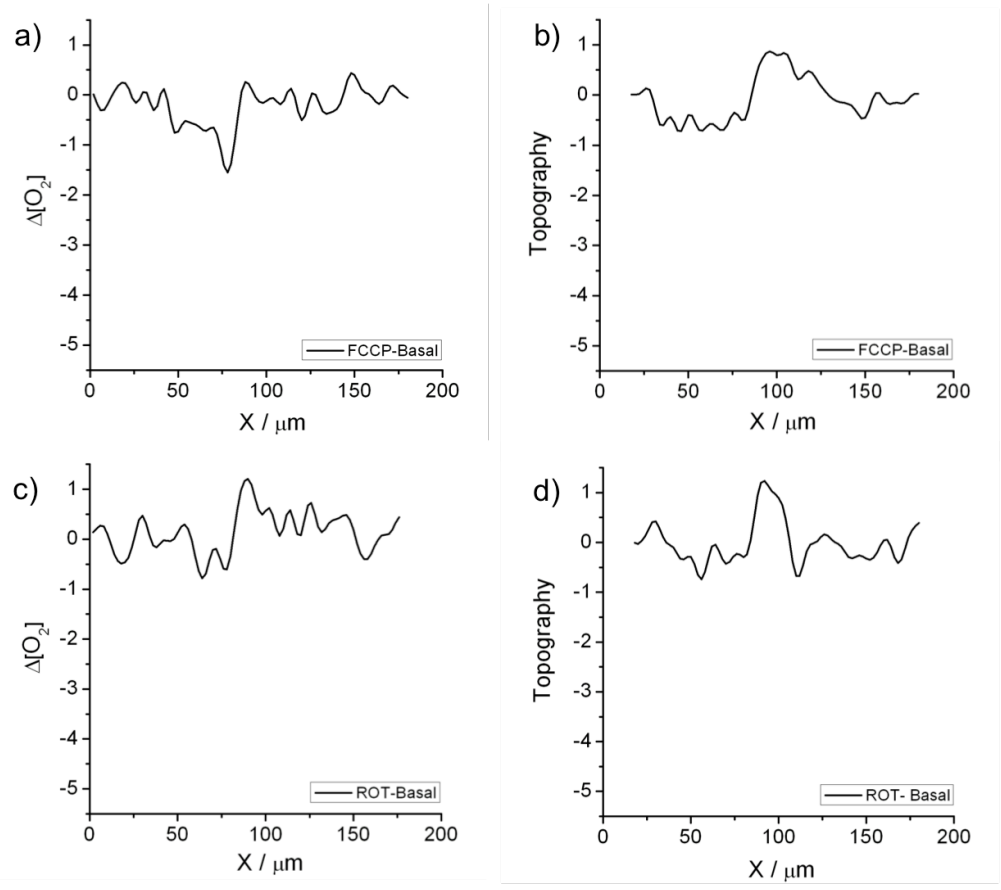

Figure 4. Differences on *oxygen current signals* on a single RasV12 cell, obtained upon subtracting drug administration signals from the basal level signals: (a) FCCP-Basal and (c) Rotenone-Basal. Differences on the *topographic current signals* obtained upon subtracting drug administration signals from the basal level signals: (b) FCCP-Basal and (d) Rotenone-Basal.

To better compare the O_2 consumption and the relative topographic contribution in the analysed respiratory states, the differences of the oxygen current signals obtained upon drug administrations in respect to the basal level signals (Figure 4a and 4c), and the corresponding differences obtained for the signals at -0.3 V were plotted (Figure 4b and 4d). In this case the differences are not evident due to the very weak and noisy signals. More experiments are planned in future in order to increase the statistics.

11.4 Final Remarks

11.4.1 RasV12 and pBabe Cell Topography

Regarding RasV12 and pBabe MCF10A cell topographical contributions, the signal obtained at -0.3V was ***statistically*** further analyzed. The results demonstrated that RasV12 transformed cells and pBabe cells are not significantly different: the mean average of the obtained values and the relative standard deviations are reported in Figure 5.

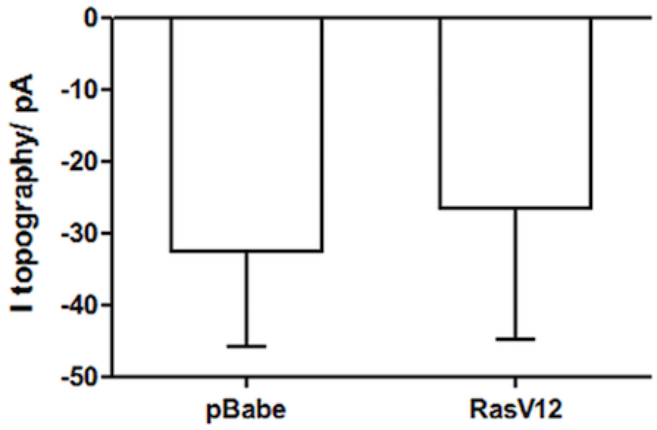

Figure 5. Cell topography characterisation by SECM. Average values ± SD of negative feedback currents, calculated as the difference between the currents on the top of the cells and the background currents, recorded by SECM scans in 500μM of $[Ru(NH_3)_6]Cl_3$ of control or RasV12 transformed cells, the t-test gave a value of $p>0.05$ and assessed that the contributions are not significantly different.

11.4.2 Conclusions

In conclusion, the FCCP uncoupling agent increases the respiration rate of normal cells and does not affect the cancer cell respiration, confirming that mitochondria in cancer cells are already uncoupled in their basic state[11].

Mitochondrial uncoupling results in a metabolic switching from the

oxidative phosphorylation of pyruvate to the uncoupled oxidation of glutamine or other fatty acids to maintain mitochondrial function. This task highlights two critical concepts: first, glycolysis remains the critical pathway by which cancer cells meet their energy demands. Indeed, the shift is required by cancer cells because of the inability of uncoupled mitochondria to generate ATP. Second, the continued reduction of oxygen, in the absence of pyruvate oxidation, suggest that reactions from non-glucose carbon sources must be reorganized and involved in order to support the oxidation of fatty acids or glutamine.

References

[1] Land SC, Porterfield DM, Sanger RH, Smith PJ, The self-referencing oxygen-selective microelectrode: detection of transmembrane oxygen flux from single cells. *J Exp. Biol*. 202, pp. 211-218 (1999)

[2] Yasukawa T, Kondo Y, Uchida I, Matsue T, Imaging of cellular activity of single cells by scanning electrochemical microscopy. *Chem. Lett*. pp 767-768 (1998)

[3] Macpherson JV, Unwin PR, Hillier AC, Bard AJ, In-situ imaging of ionic crystal dissolution using an integrated electrochemical/AFM probe. *J. Am. Chem. Soc*. 118, pp. 6445-6452 (1996).

[4] Comstock DJ, Elam JW, Pellin MJ, Hersam MC, Integrated ultramicroelectrode-nanopipet probe for concurrent scanning electrochemical microscopy and scanning ion conductance microscopy. *Anal. Chem*. 82, pp. 1270-1276 (2010).

[5] Ludwig M, Kranz C, Schuhmann W, Gaub HE, Electrochemical microscope based on hydrodynamic forces between tip and sample. *Rev. Sci. Instr*. 66, pp. 2857-2560 (1995)

[6] Ballesteros Katemann B, Schulte A, Schuhmann W, Constant-distance mode scanning electrochemical microscopy. Part I: adaptation of a non-optical shear-force based positioning mode for SECM tips. *Chem. Eur. J*. 9, pp. 2015-1033 (2003)

[7] Alpuche-Aviles MA, Wipf DO, Impedance feedback control for scanning electrochemical microscopy. *Anal. Chem*. 73, pp. 4873-4881 (2001)

[8] Nebel M, Grützke S, Diab N, Schulte A, Schuhmann W, Microelectrochemical visualization of oxygen consumption of single living cells. *Faraday Discussion*. 164:19, pp. 19-32 (2013)

[9] Nebel M, Grützke S, Diab N, Schulte A, Schuhmann W, Visualization of oxygen consumption of single living cells by scanning electrochemical microscopy: the influence of the faraic tip reaction. *Angew. Chem*. 52, pp. 6335-6338 (2013)

[10] Nijtmans LGJ, Ugalde C, Van Den Heuvel LP, Smitink JAM, Function and dysfunction of the oxidative phosphorylation system. *Mitochondrial Function and Biogenesis*. 8, pp. 149-176 (2004)

[11] Marcu R, Rapino S, Trinei M, Valenti G, Marcaccio M, Pelicci PG, Paolucci F, Giorgio M, Electrochemical study of hydrogen peroxide formation in isolated mitochondria, *Bioelectrochemistry*. 85, pp.21-28 (2012)

PART III

CONCLUSIONS & FUTURE DIRECTIONS

Chapter 12

Concluding Remarks

12.1 Main Advantages and Disadvantages

12.1.1 Innovations of our system

The aim of this PhD thesis project was to study the metabolism of living cells with high spatial and time resolutions by monitoring mainly two important metabolites, such as glucose and lactate, in order to provide a better insight in cancer metabolism. In fact, most tumors are characterized by metabolic alterations, involving a shift in ATP generation from oxidative phosphorylation to aerobic glycolysis, also known as *Warburg effect*. As a consequence, cancer tissues metabolize approximately tenfold more glucose to lactate in a given time and the amount of lactate released from cancer tissues is much greater than from normal ones. Therefore, the investigation of the above metabolic changes between normal and transformed cells may represent an important contribution in cancer research with great potential impact in clinical applications.

We used a set up based on amperometric measurements using *ad hoc* modified GOx- and LOx-based ultramicroelectrodes biosensors used as probes of Scanning Electrochemical Microscopy (SECM). Enzyme-based amperometric biosensors coupled with SECM technique is an irreplaceable analytical method for the non-invasive study of metabolism at single cell level for several reasons.

Among the advantages of using ***SECM*** compared to other techniques:

- It can detect electrochemical activities across the entire surface of single cells with high spatial resolution;
- It dynamically records the metabolic changes and fluxes with high temporal resolution**;**

- It can be used under physiological conditions; such as in cell culture medium, at room or physiological temperature and under atmospheric condition (no vacuum or inert systems required).

As already mentioned in *Chapter 6*, the use of ***UME***s has several advantages, such as:

- The response current is immune to convective effects due to the fact that diffusive fluxes to the small electrode disk are quite large;
- Currents reach steady state values in relatively short times, fractions of a second (SECM probe can be treated as a steady-state system);
- The ohmic potential drops in solution and in double-layer charging current are negligible due to the small currents that characterize most SECM experiments with UME probe (generally nA to pA);
- They have very small size allowing experiments in microscopic domains, like living cell systems (typical cell dimensions are 20 ÷ 100 μm).

Moreover, real-time quantitative measurements on living cells are feasible through the application of ***enzyme-based biosensors*** by virtue of their:

- High selectivity toward a single analyte;
- Possibility to improve sensitivity, time scale and information content;
- High specificity on the recognition of particular analytes, such as glucose and lactate, based on their structural complementarity.

Upon reviewing some of the major enzymatic immobilization procedures available in the field of enzyme-based UME biosensors to be coupled with SECM, one of the goals of this work was to optimize the micro-biosensor performances and to provide the relative experimental protocols in detail. The ensuing full characterization of UME biosensors was then aimed at identifying the most efficient ones for the metabolic studies of single living cells.

In this regard, covalent immobilization with GDA displays suitable properties, such as:

- Easy and cheap manufacturing procedure. The reagents are commercially available and enzyme immobilization does not require a customized chemical synthesis;
- High sensitivity to the analyte of interest. With the optimized protocol, the drop-cast enzyme-based UMEs biosensors reach a detection limit of metabolites concentration in the order of 1 μM;

- Fast response. Indeed, we can measure differences in current response in the order of less than one second. Note that the response time given in chapter 6 is defined for variations of concentrations much larger then the one explored in a SECM analysis of a single cell; for the typical variation of concentration in a cell scan the response time is much faster then a second. Therefore, we are able to map metabolic variations directly when the tip is moving during the SECM scanning, also thanks to the fast enzymatic kinetics;
- High spatial resolution. The optimized protocol gives us the opportunity to control almost perfectly the thickness of the enzymatic matrix. This parameter is indispensable in SECM imaging;
- High reproducibility;
- Physical and enzymatic stability (storage for 2 weeks at room temperature). The hydrogel matrix is not degraded by the solutions utilized during the measurements of living cells, even if cell media are often very complex;
- Good permeability and selectivity for the analytes of interest.

Thanks to the above described features of the manufactured electrochemical biosensors optimized in this work, it was possible to quantify with great precision and in a very reproducible way the glucose uptake and lactate release - at the single cell level - of either cancer or normal breast epithelial human cells, thus assessing the *Warburg effect*.

A voltage-switching mode strategy was employed, in which the enzyme-based UMEs biosensors were used as probes to acquire, subsequently, high quality images of cell topography and molecular fluxes of living cells. By switching the applied potential it was in fact possible to measure alternatively *i)* the faradaic current generated by a redox mediator that does not interact with cells, suitable for distance control and topographical imaging of cell surface, and *ii)* the electrochemical fluxes of the metabolites of interest, such as glucose and lactate.

The above method proved to be also very powerful, due to its ability of recording little analytic gradients, for studying the kinetics of the oncogene expression, and for monitoring the efficacy of metabolic anticancer drugs at

single cell level. Indeed, the procedure and protocol herein developed can be employed for validating the efficacy of an anticancer drug and determining its optimal dose by measuring the specific metabolic response upon treatment.

12.1.2 Limitations However, besides all the advantages mentioned before, which make drop-casting method suitable for biosensor applications, and considering all the operational parameters of the several tested biosensors, it is difficult to identify a single specific immobilization procedure with overall optimal biosensor performance. For example, GDA is slightly toxic; therefore it might present some limitations *in vivo* applications. Moreover, procedures based on GDA lack of the electrochemical control over membrane growth that is instead available with sol-gel or electropolymerization method. More efforts should be made to single out a method for enzyme immobilization that would satisfy all the criteria of low toxicity, easy manufacturing, stability, sensitivity, fast kinetic parameters, and precise control of membrane deposition. As biosensor technology continues to develop and spread among different laboratories worldwide, one may however expects that such an ideal biosensing device will emerge in the near future.

12.2 Future Tasks

12.2.1 Technology Upgrades Cancer cell metabolism can be identified by the simultaneous increase of glucose uptake and release of lactate in the presence of normal oxygen levels. Definitely, monitoring simultaneously glucose uptake, lactate release and oxygen consumption with the same probe would be more effective and informative.

Dual Electrode With this purpose, the next upgrade of the developed system will be the encapsulation of two 10 μm Pt wires in a double glass capillary in order to obtain a dual ultramicroelectrode system. One Pt wire will be activated with glucose oxidase and the other with lactate oxidase to measure the concentration gradients of glucose and lactate. The probe would also allow the investigation of the cell topography.

in vivo Application For the *in vivo* measurements, a sensor provides a reliable detection of the analyte concentration in the surrounding tissues and the mutual interactions

with the biological medium must not influence the results. However, often the implanted device perturbs the environment and initiates a response.

Therefore, for *in vivo* application, it is necessary to minimize the interference of the environment on sensor performance. Despite the use of specific molecular recognition elements to detect analytes, the sensors are susceptible to also detect endogenous electroactive molecules present in tissues such as uric acid, dopamine and ascorbate. Adsorption of such biomolecules and biofouling would decrease the sensitivity when the sensor is initially implanted[1]. The reduction of biofouling has predominantly been accomplished by developing particular permselective coatings on the outermost membrane surface, which minimally comprises the enzymatic matrix and inhibits protein adhesion to the surface. In literature, hydrogels[1], flow-based systems, Nafion™ [5], surfactants, *o*-phenylendiamine[5], cellulose acetate[6], polyester sulfonic acid and other methods have been employed with varying degrees of effectiveness. However, some acidic anions, such as pyruvate and lactate, are challenging because traditional anionic barriers, e.g. Nafion™, will also exclude the access of the analyte of interest[1]. Alumina sol-gel have also proven to be an effective material for enzyme immobilization as well as to provide permselectivity and stability over extended periods of time and response times lower than 10 s[1]. Moreover, there are several patents that describe protocols to prevent biofouling[5].

One of these methods can be implemented in the enzyme immobilization protocol of this work to prevent protein penetration through the matrix and biofouling of the electroactive biosensor surface for real *in vivo* applications.

12.2.2 Biological Claims

By using the herein implemented setup, new biological claims could be investigated: a step forward might be the study of the transcriptional regulation of the *Warburg effect*.

One well-defined mechanism by which numerous tumors establish the aerobic glycolysis, involves the transcriptional upregulation of glucose transporters and glycolytic enzymes that would strongly contribute to tumor progression. With enzyme-based UME biosensors coupled with the BioSECM apparatus, effects of MYC overexpression and p53 suppression could be investigated. Briefly, MYC is an oncogene that upregulates several glucose transporters and

glycolytic enzymes, such as PDK1 and lactate deydrogenase A. These molecules enhance the *Warburg effect* by increasing flux of glucose through the glycolytic pathway and by attenuating entry of pyruvate into the Krebs cycle[2-3]. While loss of p53 causes: *i)* down-regulation of TP53-induced glycolysis and TIGAR (apoptosis regulator); *ii)* blockage of Cyt C oxidase-2. Such factors enhance the Warburg effect by simultaneously increasing flux through glycolysis and by decreasing oxidative phosphorylation[3-4]. Monitoring these phenomena and how they are influenced by other factors would represent an important contribution to cancer research also from a therapeutic point of view.

References

[1] Wilson GS, Gifford R, Biosensors for real-time in vivo measurements. *Biosensors and Bioelectronics*. 20, pp. 2388-2403 (2005)

[2] Dang CH, MYC, metabolism, cell growth and tumorigenesis. *Cold Spring Harb Perspect Med* (2013)

[3] Zhang C, Liu J, Liang Y, Wu R, Zhao Y, Hong X, Lin M, Yu H, Liu L, Levine AJ, Hu W, Feng Z, Tumor-associated mutant p53 drives the Warburg effect. *Nat Commun*. 4, pp. 2935-2951 (2013)

[4] Zawacka J, Grinkevich VV, Hunten S, Nijulenkov F, Gluch A, Li H, Enge M, Kel A, Targeting Warburg effect to fight cancer. *J. Biol. Chem*. 286, pp. 41600-41615 (2011)

[5] Hascup KN, Hascup ER, Littrell M, Hinzman JM, Werner CE, Davis VA, Burmeister JJ, Pomerleau F, Quintero JE, Huettl P, Gerhardt GA, Microelectrode array fabrication and optimization for selective neurochemicals detection (Chapter 2). *Microelectrode Biosensors*. Marinesco S, Dale N. (Eds.), Humana Press c/o Springer Science (2013)

[6] (a) Dale N, Hatz S, Tian F, Laludet E, Listening to the brain: microelectrode biosensors for neurochemicals. *Trends in Biotechonology*. 23, pp. 420-428 (2005) (b) Dale NE, Llaudet E, Droniou M, Coating WO2004048603 A2.

APPENDIX

Appendix 1. AFM Setup and Technique Principles

Setup. Tapping Mode AFM imaging and analysis were performed using a Digital NanoScope IIID Multimode (Veeco, USA), instrument operated in tapping mode and in air (resonance frequency around 360 kHz). Images were recorded on different sample areas to check the surface homogeneity. The protein (GOx) was immobilized following protocol #4 on platinum supports consisting of glass substrates (11 x 11 mm^2) covered with a chromium under-layer (1 ÷ 4 nm thick) on which a platinum layer (200 ÷ 300 nm thick) was deposited (Arrandee™, Germany). NanoScope 6.14r1 software was used for data elaboration.

Technique principles. AFM is a scanning probe technique based on the use of a cantilever as probe, which is used to scan the investigated surfaces. In the proximity of the substrate, there is a deflection of the cantilever, due to the forces generated from the interactions between the tip and the sample, such as Van der Waals forces, capillary forces, chemical bonding, electrostatic and magnetic forces. Typically the cantilever deflection is measured by using a laser spot, which is reflected from the top surface of the cantilever into an array of phodiodes. AFM can operate in three imaging modes: contact mode, tapping mode and non-contact mode. Tapping mode is the most suitable approach when soft, fragile or sticky samples have to be analyzed, because it achieves high-resolution topographic images, preventing the risk of sample damaging.

The cantilever is driven to oscillate near the surface until it begins to slightly touch or tap the surface at its resonance frequency, which is controlled by a small piezoelectric element mounted in the AFM tip holder. Selection of the optimal oscillation frequency is software-assisted. The oscillation amplitude depends on the forces acting on the cantilever when the tip comes close to the surface. This amplitude variation is used as a feedback signal to measure topographic changes of the sample substrate. Phase imaging is a powerful extension of tapping mode AFM, which goes beyond simple topographical mapping in order to detect variations in homogeneity, composition, adhesion, friction, viscoelasticity and other properties. Phase imaging can also act as a real-time contrast enhancement technique, because highlights the edges, providing clearer observation of fine features, which can be obscured by rough topography (height images).

Appendix 2. Protocol for Cell Counting Using Trypan Blue

Trypan Blue is one of several stains recommended for use in dye exclusion procedures for viable cell counting. This method is based on the principle that live (viable) cells do not take up certain dyes, whereas dead (non-viable) cells do. Staining facilitates the visualization of cell morphology. The used protocol is:

1. Prepare a cell suspension in a balanced salt solution (PBS);
2. Transfer 0.4% of Trypan Blue solution (w/v) to a 96-well plate. Add 10 μL of the cell suspension previously diluted in PBS (x 2) and mix thoroughly;
3. Allow to stand a couple of minutes. NOTE: If cells are exposed to Trypan Blue for extended periods of time, viable cells, as well as non-viable cells, may begin to take up dye;
4. Use a pipette to transfer 10 μL of Trypan Blue-cell suspension mixture to one of the hemocytometer chambers. Carefully touch the edge of the chamber with the pipette tip and allow each chamber to fill by capillary action. Do not overfill or under-fill the chamber;
5. Start to count all the cells in the 1 mm center square and four 1 mm corner squares for chamber 1. Non-viable cells will stain blue. NOTE: Count cells on top and left touching middle line of the perimeter of each square. Do not count cells touching the middle line at bottom and right sides;
6. Repeat this procedure for chamber 2. NOTE: If greater than 10% of the cells appear clustered, repeat entire procedure making sure the cells are dispersed by vigorous pipetting in the original cell suspension as well as the Trypan Blue-cell suspension mixture. If less than 200 or greater than 500 cells (i.e., 20-50 cells/square) are observed in the 10 squares, repeat the procedure adjusting to an appropriate dilution factor;
7. Withdraw a second sample and repeat count procedure to ensure accuracy;
8. CELL COUNTS: each square represents a total Vol of 0.1 mm^3 or $10^{-4}cm^3$. Since 1 cm ≈ 1 mL, the subsequent cell concentration per mL (and the total number of cells) will be determined using the following calculations:

   Cells per mL *= the average count per square x dilution factor x* 10^4

   Total cells *= Cells per mL x the original volume of cell suspension (from which cell sample was removed).*

Appendix 3. Cell Cycle Analysis by Flow Cytometry

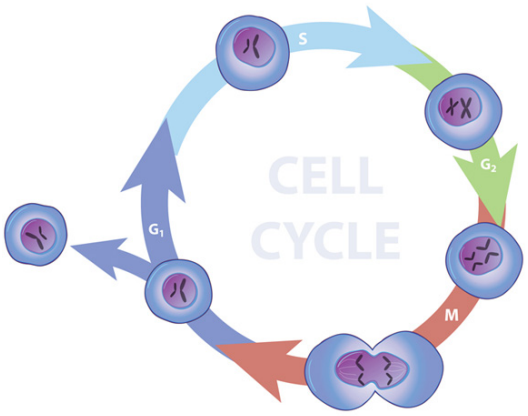

In cell biology *Cell Cycle Analysis* by Flow Cytometry (FACS) is a method to distinguish cells into the different cell cycle phases. The first step in preparing cells for cell-cycle analysis, which is the permeabilization of the cellular plasma membranes. Then, the cells are treated with a fluorescent dye that stains DNA quantitatively, usually Propidium iodide (PI). They are fixed in ethanol, but prior or during the staining step, the cells are commonly treated also with RNase A in order to remove RNAs from cells, which one would create artefacts in the results. The fluorescence intensity of the stained cells at certain wavelengths is correlated with the amount of DNA they contain. As the DNA content of cells duplicates during S phase of the cell cycle, the relative amount of cells in G_0/G_1, S or G_2/M phases can be determined, as the fluorescence of cells in G_2/M phase will be twice as high as that of cells in G_0/G_1.

The used protocol of PI staining is the following:

1. Use 10^6 cells per sample;
2. Wash cells once with PBS in 1.5mL Eppendorf tubes (spin down cells at 5000rpm for 4 min);
3. Re-suspend the obtained cells' pellet in 300 µL of cold PBS in order to obtain a mono-dispersed cell suspension, with minimal cell aggregation;
4. Fix cells by adding 300 µL of pure cold ethanol (-20°C) dropwise while gently vortexing;
5. Leave cells in fixative for at least 30 min on ice (fixed cells can be kept at 4°C for several weeks);
6. Wash once with 1% BSA/PBS;
7. Re-suspend pellet in 1 mL of PI (50 µg/mL) and RNase (250 µg/mL) and incubate for 1h at room temperature, light protected;
8. Keep stained cells at 4°C until FACS analysis.

Transfer sample to the flow cytometer and measure cell fluorescence. Maximum excitation of PI bound to DNA is at 536 nm and emission is at 617 nm. Blue (488 nm) or green light lines of lasers are optimal for excitation of PI fluorescence.

Instrumentation. FACScalibur (Beckton Dickinson) equipped with 488nm and 633nm lasers. Cellquest PRO software was used for acquisition and analysis and Modfit LT3 software was used for elaboration data.

Appendix 4. Cell Viability MTT Test

Description. MTT (3-[4,5-dimethylthiazol-2-yl]-2,5- diphenyltetrazolium bromide; thiazolyl blue) is a water soluble tetrazolium salt yielding a yellowish solution when prepared in media or salt solutions lacking phenol red. Dissolved MTT is converted to an insoluble purple formazan by cleavage of the tetrazolium ring by dehydrogenase enzymes. This water insoluble formazan can be solubilized using isopropanol and the dissolved material is measured spectrophotometrically yielding absorbance as a function of concentration of converted dye. Active mitochondrial dehydrogenases of living cells will cause this conversion. Dead cells do not cause this change.

Procedure. MTT (5 mg/mL) is dissolved in RPMI-1640 without phenol red. The solution is filtered through a 0.2 μm filter and can be stored at 2–8°C for short period. MTT solution is added to each culture being assayed to equal one-tenth the original culture volume and incubated for 4h. At the end of the incubation period the medium is removed and the converted dye *crystals are* solubilized with acidic isopropanol (0.04 - 0.1N HCl in absolute isopropanol).

Measurement method. Absorbance of converted dye is measured at a wavelength of 570 nm with background subtraction at 630 - 690 nm.

The MTT cell viability assay determines the cell proliferation rate and conversely, when metabolic events lead to apoptosis or necrosis and the rate of cells death.

(From www.sigmaaldrich.com/technical-documents/articles/biofiles/cell-viability)

Appendix 5. Protocol for EnzyChrom L-Lactate BioAssay Kit

Description. Lactate is generated by lactate dehydrogenase (LDH) under hypoxic or anaerobic conditions. Monitoring lactate levels is, therefore, a good indicator of the balance between tissue oxygen demand and utilization and is useful when studying cellular and animal physiology. L-lactate is produced in only minor quantities in animals and measuring for L-lactate in animal samples is a means to determine the presence of bacterial infection.

Simple, direct and automation-ready procedures for measuring lactate concentration are very desirable. BioAssay Systems EnzyChrom™ lactate assay kit is based on lactate dehydrogenase catalyzed oxidation of lactate, in which the formed NADH reduces a formazan (MTT) Reagent. The intensity of the product color, measured at 565 nm, is proportional to the lactate concentration in samples.

Sensitivity. Detection limit of 0.1 mM and linearity up to 1 mM L-lactate in 96-well plate assay for cell culture samples containing red phenol.

Measurement method. The procedure involves adding a single working reagent and reading the optical density (absorbance at 565 nm) at time 0 and after 20 min.

Components. Assay Buffer [BSA/Tris(hydroxymethyl)aminomethane], Enzyme A [Lactate deydrogenase], Enzyme B [Diaphorase], NAD solution [b-nicotinamide adenine dinucleotide], MTT solution [Thiazolyl Blue Tetrazolium Bromide] and Standard [Lithium Lactate].

Procedure.

1. Standard curve preparation: prepare 1 mL 1.0 mM L-lactate Premix by mixing 50 µL of 20 mM Standard Reagent and 950 µL culture medium *without serum*. Dilute standard as explained in the following table.

N°	Premix + Medium	Vol (µL)	L-lactate (mM)
1	100 µL + 0 µL	100	2.0 or 1.0
2	80 µL + 20 µL	100	1.6 or 0.8
3	60 µL + 40 µL	100	1.2 or 0.6
4	40 µL + 60 µL	100	0.8 or 0.4
5	30 µL + 70 µL	100	0.6 or 0.3
6	20 µL + 80 µL	100	0.4 or 0.2
7	10 µL + 90 µL	100	0.2 or 0.1
8	0 µL + 100 µL	100	0

Transfer 20 µL standards into wells of a clear bottom 96-well plate. For samples

with potential endogenous enzyme activity (i.e. serum) two reactions should be run: one reaction with Enzyme A added and a No Enzyme A control. Serum and plasma should be diluted at least 2x with dH_2O prior to assay. Transfer 20 µL sample per well in separate wells.

2. Reagent Preparation: For each sample and standard well, prepare Working Reagent by mixing 60 µL Assay Buffer, 1 µL Enzyme A, 1 µL Enzyme B, 10 µL NAD and 14 µL MTT. For the No Enzyme A control, the Working Reagent includes 60 µL Assay Buffer, 1 µL Enzyme B, 10 µL NAD and 14 µL MTT.

3. Reaction. Add 80 µL Working Reagent per reaction well quickly. Tap plate to mix briefly and thoroughly.

4. Read optical density for time "zero" (OD_0) at 565nm (520-600nm) and OD_{20} after a 20min incubation at room temperature.

5. Calculation. Subtract OD_0 from OD_{20} for the standard and sample wells. Use the ΔOD values to determine the sample L-lactate concentration from the standard curve. For samples requiring a No Enzyme A control, subtract the ΔOD (no-enzyme) value from the ΔOD (sample) and use this ΔΔOD value to determine the sample L-lactate concentration from the standard curve. Note: if the sample OD value is higher than OD for 2 mM L-lactate standard, dilute sample in water and repeat the assay. Multiply the results by the dilution factor.

General Consideration. The following substances interfere and should be avoided in sample preparation: ascorbic acid, SDS (>0.2%), sodium azide, NP-40 (>1%) and Tween-20 (>1%).

(*From EnzyChromTM L-Lactate Assay Kit (ECLC-100) product document*)

Appendix 6. Microinjection Setup

DNA Microinjection was performed by mean of Zeiss Axiovert S100 Microscope equipped with a fully motorized micro injector (AIS2) and a Femtojet pump (Eppendorf). Time of injection 0.2 sec with a pressure equal to 150-200hPa.

The cells were cultured in gridded 35mm Ø glass bottom uncoated coverslips (P35G-2-14-CGRD Case purchased from MatTek Corporation) which permit to have cells and grid on the same focal plane.

A 10x UPlanFL 10x NA 0.30 Olympus Microscope was used to monitor the fluorescence, with an exposure time equal to 600 ms and a binning value of 2.